The H. Niewodniczański Institute of Nuclear Physics
Polish Academy of Sciences

Neutrino beam simulations and background studies for the SUNLAB location in Poland

Małgorzata Harańczyk

Doctoral dissertation

Supervisor: prof. Agnieszka Zalewska

Kraków, 2016

Instytut Fizyki Jądrowej im. Henryka Niewodniczańskiego
Polskiej Akademii Nauk

Symulacje wiązki i tła dla badań oscylacji neutrin w laboratorium SUNLAB

Małgorzata Harańczyk

Rozprawa Doktorska

Promotor: prof. dr hab. Agnieszka Zalewska

Kraków, 2016

Contents

Introduction

The main purpose of this thesis is to explore the opportunities which would be provided by the Sieroszowice Underground Laboratory SUNLAB, located in the Polkowice-Sieroszowice mine in the Lower Silesia province in Poland, to discover the CP violation in the neutrino sector. This discovery would be a milestone on the road to understanding the observed dominance of matter over antimatter in the Universe, which is one of the fundamental questions of contemporary science.The motivation for the presented study is the current very exciting situation in neutrino physics. According to many physicists, the discovery of neutrino oscillations in the years 1998-2002 and their interpretation within the framework of three neutrino flavour mixing, awarded the 2015 Nobel Prize in physics, provides firm evidence for new physics beyond the Standard Model. Recently, the θ_{13} mixing angle has been determined to be moderately large. This makes it possible to use conventional high power neutrino beams in accelerator long baseline experiments to answer the remaining questions in neutrino oscillations, which are the neutrino mass hierarchy and the measurement of the CP-violating phase.

At present, the most important accelerator-based long baseline oscillation experiments are the T2K experiment in Japan and the NOvA experiment in the USA. If the CP violation is close to maximal, these two experiments should be able to determine it with a significance of three standard deviations within a decade. The determination of the neutrino mass hierarchy should be possible with a similar precision and on a similar time-scale providing that the T2K and NOvA results are supplemented by the results of the future atmospheric experiment PINGU and the future reactor experiment JUNO. Reaching the discovery level of five standard deviations together with covering a larger region of the parameter space for the CP violation will require neutrino beams of much higher intensities and much larger and more precise detectors. Currently there are only two such projects in the world which are eligible: the LBNF-DUNE project at Fermilab in the USA, based on the liquid Argon detector technology, and the HyperKamiokande giant Water Cherenkov detector project, coupled with a beam from JPARC in Japan.

Feasibility studies of the future large underground laboratory in Europe, hosting huge detectors with a vast research programme including the accelerator long baseline oscillation studies, were performed within the EU LAGUNA project (2008-2011), followed by the EU LAGUNA-LBNO project (2011-2013). SUNLAB was one of seven locations considered by LAGUNA. Long baseline oscillation studies of the CP violation discovery potential, with a neutrino beam from CERN and a huge liquid Argon time projection chamber (LAr-TPC) located at SUNLAB, presented in this thesis, have been partially funded by the NCN grant *Preludium* UMO-2011/03/N/ST2/01971 .

This thesis consists of nine chapters. Chapter 1 gives basic information about neutrinos, with special emphasis on the phenomenology and experimental results concerning the neutrino oscillations. Chapter 2 addresses the unknowns in the neutrino oscillation physics, which are the neutrino mass hierarchy and CP-violating phase, while Chapter 3 presents the current and planned neutrino oscillation experiments and projects aimed at their determination. Chapter 4 contains the presentation of the SUNLAB location and the results of various studies and measurements which have already been performed for SUNLAB. Chapter 5 describes the computer software used to perform the simulations and calculations presented in the following chapters. Chapters 6, 7 and 8 present the results of studies for SUNLAB as a host laboratory of a far detector of the long baseline neutrino oscillation experiment aimed at the CP violation discovery. The simulations of the neutrino beam from CERN, optimised for the 950 km CERN-SUNLAB baseline, are described in Chapter 6. The parametrisation used to reproduce the Liquid Argon TPC detector performance is presented in Chapter 7. The determination of the sensitivity to the discovery of the CP violation, which is the main result of this thesis, is described in Chapter 8. The sensitivity calculations have been performed using the GLoBES software and assuming two phases of the experiment: the initial phase of ten years of data taking with a 20 kton LAr-TPC detector and the final phase of additional ten years of running with a giant 100 kton detector. To make the study complete, the influence of the background due to the natural radioactivity of the surrounding rocks and the cosmic radiation is shortly discussed in Chapter 9. The Summary contains the main conclusions of the presented study. The results of simulations and calculations, presented in Chapters 6-8, are obtained by the author of this thesis, except where explicitly stated otherwise.

The results of this thesis were presented at international conferences Neutrino2014, Boston USA [1]and NNN15 (Next Generation Nucleon Decay and Neutrino Detectors) Stony Brook, USA [2] as well as at the YRM 2015, GSSI Italy [3] and 'Astrophysics in Poland' conferences in Krakow 2013 and Warsaw 2015.

Chapter 1

Neutrino properties and oscillations.

The neutrino, as a new particle, was hypothesized in 1930 by Wolfgang Pauli in order to explain the measured continuous energy spectra of electrons from nuclear β-decays, despite the observation of only two decay products: an electron and a final state nucleus. The emission of the third particle, neutral and escaping the detection because of its very weak interaction with matter, made it possible to maintain the integrity of the conservation laws. The concept of this ghostly particle was used by Enrico Fermi to formulate in 1932. A quantitative theory of nuclear beta decay. The theory was successfully applied to the measurement results, strengthening the arguments in favour of the neutrino existence. In 1956 Clyde Cowan and Frederick Reines observed a neutrino, and more precisely, antineutrino interactions in the underground experiment near the reactor, directly proving their existence. Since then, neutrinos have been constantly studied, e.g. leading to observations of the other two types of neutrinos, ν_μ in 1962 and ν_τ in 2000. The discovery of the neutrino oscillation phenomenon by the SuperKamiokande experiment in 1998, confirmed by several other experiments in following years, opened a new chapter in these studies. The fact that neutrinos oscillate is considered to be the first evidence for physics outside the Standard Model of particle physics. In this chapter basic neutrino characteristics are presented (Section 1.1), a description of neutrino origin and sources is given (Section 1.2), the theory of neutrino oscillation phenomenon (Section 1.3) is introduced and experimental results obtained by oscillation neutrino experiments are shortly summarized (Section 1.4).

1.1. Neutrino characteristics

In the Standard Model of particle physics (SM) neutrinos belong to fundamental constituents of matter and are neutral, massless leptons. This causes that they can interact only weakly. Neutrinos come in three flavours, as it was proven by the studies of Z boson decay in e^+e^- collisions in the experiments at the LEP

accelerator at CERN [4]. They are neutral partners of three charged leptons, i.e. electron, muon and taon, and are referred to as electron neutrino ν_e, muon neutrino ν_μ, or tau neutrino ν_τ. The three kinds of neutrinos are complemented with their antiparticles, called electron, muon and tau anti-neutrinos. In its original form the SM foresees neutrino masses as being equal to zero. Currently, after neutrino oscillations have been experimentally proven and well described (Section 1.3), it is known that neutrinos are massive. However, the absolute values of their masses are so small that they have not been measured yet and only the mass upper limits are known.

A natural way to measure the masses of the three types of neutrinos involves studying well-known, weak decays of particles with neutrinos among the decay products and applying the energy-momentum conservation law. Currently, the best accuracy is obtained for the ν_e mass determination, based on the Tritium β-decay process. The upper limit for ν_e mass, set this way, is $2\,eV$ [5]. The latest Tritium based experiment KATRIN - a large, high resolution spectrometer is about to start taking data [6]. KATRIN will either measure the actual mass, if it is larger than $0.35\ eV/c^2$, or improve the current limit by one order of magnitude down to $0.2\ eV/c^2$. The measurement of ν_μ and ν_τ masses are are far less accurate. The charged pion decay $\pi^+ \rightarrow \nu_\mu + \mu^+$ is used for the ν_μ mass determination, while high multiplicity τ lepton decays, e.g. $\tau \rightarrow \nu_\tau + 5\pi^\pm$, are used for the ν_τ mass determination.

Moreover, the information about neutrino masses comes also from cosmological measurements, such as those provided by PLANCK. Here, the sum of the masses of three neutrino flavours is determined and currently is $\sum_{i=e,\mu,\tau} m_{\nu_i} = 0.23\ eV$ [7]. Additionally, the double-beta decay process with the emission of two electron neutrinos is allowed within the standard theory. Ettore Majorana hypothesized that a neutrino can be identical with its antineutrino, and in this case the neutrinoless double beta decay ($\beta\beta0\nu$) process would be possible. Several experiments and R&D projects are focused on $\beta\beta0\nu$ process searches for various nuclei, but with no definite result for now. The observation of this process is fundamental not only to neutrino mass measurement, but to understanding the nature of neutrino, i.e. whether they are Dirac particles like other fermions of matter or Majorana particles, i.e. identical with antineutrinos. A more detailed discussion of the neutrino mass phenomenon goes beyond this thesis, as the paper focuses on neutrino long baseline oscillation studies.

1.2. Neutrino sources

Neutrinos are the second, after photons, most abundant particles in the Universe. Because of their extremely small interaction cross sections ($\sigma_{CC} \sim 10^{-38}\ cm^2\ per\ nucleon$ for $E_\nu \sim 1\ GeV$ [5]), they travel practically undisturbed through the cosmic space conveying information about their origin. There are various natural sources of neutrinos. Starting from the relic neutrinos originated in the Big Bang, through neutrinos coming from thermonuclear fusion reactions in star cores, in particular in the Sun and from Supernova bursts, neutrinos coming from nuclear fissions in the Earth, called geoneutrinos, neutrinos related to the cosmic ray interactions in the Earth's atmosphere, and ending with very high energy neutrinos from hypothetical cosmogenic sources.

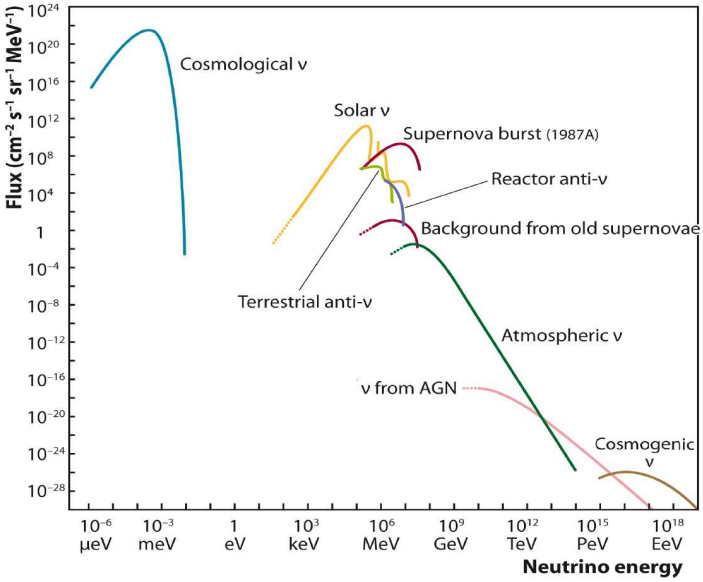

Figure 1.1. A compilation of the measured and expected fluxes of natural and reactor neutrinos [8].

For initial oscillation studies the solar and atmospheric neutrinos have been especially important. These studies have been supplemented with measurements using neutrinos from human-made sources, namely accelerator neutrino beams and reactor neutrinos. The energy spectra of accelerator neutrinos correspond to atmospheric neutrinos while reactor neutrinos have energies similar to solar neutrinos. A big advantage of these artificially produced neutrinos is that their systematic effects are much better controlled than those for neutrinos from natural sources, and this is why the majority of current and future oscillation experiments are based on the accelerator and reactor neutrinos.

1.2.1. Solar neutrinos

The Sun is a very strong source of electron neutrinos with energies predominantly below 0.4 MeV, but extending up to 20 MeV. They are produced in thermonuclear fusion reactions, mainly from the *pp* chain (eq. (1.1)), with a small contribution from the CNO cycle (eq. (1.2)). The neutrino energy spectra from particular reactions predicted by the Standard Solar Model (SSM) [9] [10] are presented in Figure 1.2.

$$\begin{aligned} p + p &\rightarrow {}^2H + e^+ + \nu_e \quad (pp) \\ p + e^- + p &\rightarrow {}^2H + \nu_e \quad (pep) \\ {}^3He + p &\rightarrow {}^4He + e^+ + \nu_e \quad (hep) \\ {}^7Be + e^- &\rightarrow {}^7Li + \nu_e \quad ({}^7Be) \\ {}^8B &\rightarrow {}^8Be + e^+ + \nu_e \quad ({}^8B), \end{aligned} \tag{1.1}$$

$${}^{13}N \rightarrow {}^{13}C + e^+ + \nu_e;\ {}^{15}O \rightarrow {}^{15}N + e^+ + \nu_e. \tag{1.2}$$

The total solar neutrino flux on the Earth is around $6 \times 10^{10} cm^{-2} s^{-1}$ [11]. Despite the fact that this flux is very large, the detection of solar neutrinos is difficult because of very low cross sections for neutrino interactions with matter at such low energies. Starting from the late sixties, underground radiochemical experiments such as the pioneer chlorine Davis's experiment at Homestake and later the Gallium detectors GALLEX, GNO and SAGE have measured a strong deficit in the solar electron neutrino flux with respect to the prediction of the Standard Solar Model (SSM). This was known as the solar neutrino puzzle, farther confirmed by the Kamiokande and SuperKamiokande experiments. The puzzle was finally explained by neutrino oscillations in the SNO experiment in Canada . More information about these measurements is given in Section 1.4.

1.2.2. Atmospheric neutrinos

Atmospheric neutrinos are related to the interactions of primary cosmic rays with nuclei in the atmosphere. These interactions are at the origin of the so called atmospheric cascades, resulting from several secondary interactions and containing various hadrons, in particular pions and kaons. These mesons decay into muons and muon neutrinos according to the equations (1.3) and (1.4). Additionally, before hitting the ground, some muons decay into electrons, electron neutrinos and muon neutrinos, as given by eq. (1.5).

$$\pi^+ \rightarrow \mu^+ + \nu_\mu,\ \pi^- \rightarrow \mu^- + \bar{\nu}_\mu \tag{1.3}$$

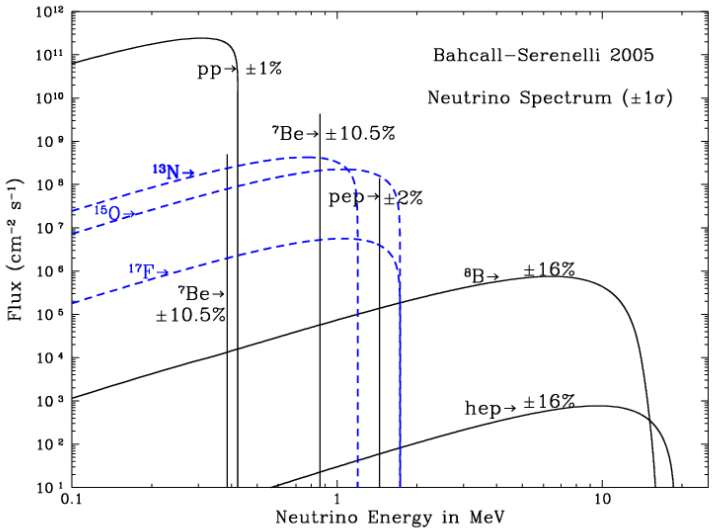

Figure 1.2. Solar neutrino spectra and fluxes on Earth as predicted by the SSM. Black lines correspond to neutrinos from the pp fusion chain, while blue-dashed lines correspond to the CNO cycle. Graph taken from [10].

$$K^+ \to \mu^+ + \nu_\mu,\ K^- \to \mu^- + \bar{\nu}_\mu \tag{1.4}$$

$$\mu^+ \to e^+ \nu_e + \bar{\nu}_\mu,\ \mu^- \to e^- + \bar{\nu}_e + \nu_\mu \tag{1.5}$$

Combining the reactions (1.3) and (1.4) one can see that for muons decaying in the atmosphere (with energies below 2 GeV) the ratio of the number of muon neutrinos to the number of electron neutrinos should be equal two.

$$\frac{N_{\nu_\mu} + N_{\bar{\nu}_\mu}}{N_{\nu_e} + N_{\bar{\nu}_e}} \simeq 2 \tag{1.6}$$

For muons with higher energies this ratio increases with muon energy, because more and more muons decay below the Earth's surface. In the late eighties and the early nineties several experiments measured this ratio, giving ambiguous results. In particular, the Kamiokande and IMB experiments obtained the value of the order of 1 instead of 2. This so called atmospheric anomaly has been

explained by neutrino oscillations by the SuperKamiokande experiment in 1998. More information about these measurements is given in Section 1.4.

1.2.3. Reactor neutrinos

Contemporary nuclear reactors are very strong sources of electron antineutrinos coming from β-decays of unstable neutron rich products of Uranium and Plutonium fission. Their average yield is about six $\bar{\nu}_e$ per fission. The reactor electron antineutrino flux seen by the detector has its maximum around 2-3 MeV and extends up to about 8 MeV. Reactor experiments have a long and rich history in neutrino studies, starting from the first observation of electron neutrino interactions by F.Reines and C.L.Cowan in 1956 [12]. In 2002, the KamLAND reactor experiment in Japan confirmed the SNO discovery of the solar neutrino oscillations. The results of this experiment are presented in Section 1.4.

1.2.4. Accelerator neutrinos

High-energy proton accelerators offer the possibilities to make a reaction chain similar to the one which is the source of neutrinos in the Earth's atmosphere, but in better controlled conditions. Protons with well known energy hit the target and produce mesons which undergo the decays (1.3), (1.4), (1.5) with neutrinos among their decay products. Positive mesons produce neutrinos, negative mesons produce antineutrinos. In the case of high intensity beams, the neutrino event rates can be relatively high. For example, the PS and then SPS-based neutrino beams had been used at CERN in 1960s- 1980s by pioneer experiments studying neutrino interactions and properties. The well-focused neutrino beams can be coupled with detectors placed at long and suitably chosen distances from the interaction targets to study neutrino oscillations in the long baseline oscillation experiments. The results obtained in such experiments are presented in Section 1.4.

1.3. Neutrino oscillations

The concept of neutrino oscillations was introduced by Bruno Pontecorvo in 1957 [13] and was further developed by Maki, Nakagawa and Sakata [14]. In this subsection one can find a brief description of this phenomenon, which, as will be shown, is possible only for neutrinos with non-zero masses.

1.3.1. Oscillations formalism for propagation in vacuum

Neutrino oscillation is a quantum mechanical phenomenon in which a neutrino changes its flavour as it travels. Three flavour neutrinos (ν_e, ν_μ, ν_τ) are produced and observed via weak interactions and therefore are referred to as weak eigenstate neutrinos. Oscillation can arise on condition that neutrinos have non-zero masses. In such a case there are mass eigenstates, which are not mandatory identical to the weak (flavour) eigenstates. In other words, mass-matrix of neutrinos written in a weak basis is not diagonal. For three active neutrinos we have:

$$|\nu_\alpha\rangle = \sum_{i=1}^{3} U^*_{\alpha i}|\nu_i\rangle; \quad \begin{pmatrix} \nu_e \\ \nu_\mu \\ \nu_\tau \end{pmatrix} = \begin{pmatrix} U_{e1} & U_{e2} & U_{e3} \\ U_{\mu 1} & U_{\mu 2} & U_{\mu 3} \\ U_{\tau 1} & U_{\tau 2} & U_{\tau 3} \end{pmatrix} \begin{pmatrix} \nu_1 \\ \nu_2 \\ \nu_3 \end{pmatrix} \tag{1.7}$$

where α stands for a flavour (e, μ, τ), i stands for a mass state (1, 2, 3) and **U** is a unitary leptonic mixing matrix also known as the PMNS (Pontecorvo-Maki-Nakagawa-Sakata) matrix. This is matrix analogous to the CKM matrix known from the quark sector.

The PMNS matrix **U** is usually expressed by three rotation matrices using three mixing angles θ_{ij} between the mass eigenstates i and j, and one Dirac-type CP phase δ_{CP} (eq. (1.8)), where $c_{ij} = cos\theta_{ij}$ and $s_{ij} = sin\theta_{ij}$. There are two additional Majorana phases, if neutrinos are Majorana particles, but even in such a case oscillations are not sensitive to these phases, so they could be ignored. The first matrix is related to the solar or 12-sector, the second one to the 13-sector, and the third one to the atmospheric or 23-sector. The 13-sector is responsible for the connection between the solar and atmospheric regimes, and can be used to determine δ_{CP} related to the CP conservation or violation for neutrinos. When multiplied, the PMNS matrix has the form given by equation (1.9).

$$\mathbf{U} = \begin{pmatrix} 1 & 0 & 0 \\ 0 & c_{23} & s_{23} \\ 0 & -s_{23} & c_{23} \end{pmatrix} \begin{pmatrix} c_{13} & 0 & s_{13}e^{-i\delta_{CP}} \\ 0 & 1 & 0 \\ -s_{13}e^{i\delta_{CP}} & 0 & c_{13} \end{pmatrix} \begin{pmatrix} c_{12} & s_{12} & 0 \\ -s_{12} & c_{12} & 0 \\ 0 & 0 & 1 \end{pmatrix} \tag{1.8}$$

$$\mathbf{U} = \begin{pmatrix} c_{12}c_{13} & s_{12}c_{13} & s_{13}e^{-i\delta_{CP}} \\ -s_{12}c_{23} - c_{12}s_{23}s_{13}e^{-i\delta_{CP}} & c_{12}c_{23} - s_{12}s_{13}s_{23}e^{-i\delta_{CP}} & c_{13}s_{23} \\ s_{12}s_{23} - c_{12}s_{13}c_{23}e^{-i\delta_{CP}} & -c_{12}s_{23} - s_{12}s_{13}c_{23}e^{-i\delta_{CP}} & c_{13}c_{23} \end{pmatrix} \tag{1.9}$$

The probability of a transition of the initial neutrino with α-flavour and energy E into the final β-favour after travelling a distance L in vacuum is given by :

$$P(\nu_\alpha \to \nu_\beta) = P_{\alpha\beta} = \left| \sum_j U_{\beta j}\, e^{\frac{-i\, m_j^2 L}{2E}} U^*_{\alpha j} \right|^2 , \tag{1.10}$$

$$\begin{aligned} P_{\alpha\beta} = \delta_{\alpha\beta} - 4 \sum_{i>j} \mathrm{Re}(U^*_{\alpha i} U_{\beta i} U_{\alpha j} U^*_{\beta j}) \sin^2(\Delta m^2_{ij} \frac{L}{4E}) \\ +2 \sum_{i>j} \mathrm{Im}(U^*_{\alpha i} U_{\beta i} U_{\alpha j} U^*_{\beta j}) \sin(\Delta m^2_{ij} \frac{L}{2E}) \, . \end{aligned} \tag{1.11}$$

The $\Delta m^2_{ij} = m^2_i - m^2_j$ parameter is a mass splitting of two mass eigenstates i and j, and neutrino oscillations are sensitive to this mass-squared difference but not to the absolute neutrino masses. The oscillatory behaviour of the transition probability is clearly visible in equation (1.11). Since oscillations can occur only if at least one mass-squared difference does not vanish, an observation of this phenomenon gives a proof that at least two neutrinos have non-zero masses.

It is important to point out that the last term in equation (1.11) contains the CP violating part. This means that the measurement of δ_{CP} can be performed only in the so called appearance experiment ($\alpha \neq \beta$), since for the disappearance experiment ($\alpha = \beta$) this term becomes zero ($\mathrm{Im}(\|U_{\alpha i}\|^2 \|U_{\alpha j}\|^2) = 0$). This observation is crucial for the studies performed within the framework of this thesis.

1.3.2. Two flavour approximation

Thanks to the smallness of $\sin\theta_{13}$ and thus of U_{e3}, the formalism of two flavour oscillations has been a reasonably good approximation to determine oscillation parameters based on the results of the initial oscillation experiments for the atmospheric, solar, accelerator and reactor neutrinos. The simplified formula for the oscillation probability in vacuum for only two flavours comes from the original one by assuming no CP violation ($\delta_{CP} = 0$) and θ_{13} equal zero. Then the oscillation probability depends on the ratio of the distance between the neutrino source and the detector (L) over the neutrino energy (E_ν), the difference between the mass squares of the two mass states (Δm^2) and their mixing angle θ. The formula (1.11) becomes:

$$P_{\alpha\beta} = \sin^2 2\theta \sin^2 \frac{\Delta m^2 L}{4E_\nu} \tag{1.12}$$

for the appearance of the neutrinos with flavour β among the initial neutrinos of flavour α. At the same time the probability describing the disappearance of neutrinos with flavour α is given by the formula:

$$P(\nu_\alpha \to \nu_\alpha) = P_{\alpha\alpha} = 1 - P_{\alpha\beta} \tag{1.13}$$

1.3.3. Neutrino oscillations in matter

Oscillation probability changes significantly when a neutrino passes through dense matter. This is caused by the weak interaction which couples the neutrinos with ordinary matter (i.e. electrons, protons and neutrons). Neutrinos of all flavours interact with matter through the neutral current interaction mediated by the Z^0 boson. These contributions are the same for neutrinos of the three flavours, leading to the overall phase which can be subtracted. The ordinary matter contains electrons, but no muons and tau leptons. This gives an additional contribution to electron neutrinos because of their charge current (CC) interactions with electrons, mediated by $W^\pm$ exchange. The additional matter-related potential is given by the formula:

$$A = \pm 2\sqrt{2} G_F N_e E \tag{1.14}$$

where G_F is the Fermi coupling constant, N_e is the electron density (for example inside the Earth or the Sun) and E is the neutrino energy; the positive sign is for neutrinos and the negative one - for antineutrinos. This affects oscillation probabilities heavily and gives additional interesting effects such as "Mikheyev Smirnov Wolfenstein (MSW)-resonance" and neutrino-antineutrino asymmetry, sometimes called "fake CP asymmetry" [15].

The approximate analytic expression for the $P_{\mu e}$ probabillity, with terms up to the second order in θ_{13}, is given by the following equasion and then used in Chapter 8 describing the simulation of neutrino oscillations in GLoBES.

$$\begin{aligned} P_{\mu e} \simeq & \underbrace{\sin^2\theta_{23}\sin^2 2\theta_{13}\frac{sin^2[(1-\hat{A})\Delta]}{(1-\hat{A})^2}}_{C_0} + \underbrace{\alpha^2\cos^2\theta_{23}\sin^2 2\theta_{12}\frac{sin^2(\hat{A}\Delta)}{\hat{A}^2}}_{C1} \\ & \underbrace{\mp\alpha\sin 2\theta_{13}\cos\theta_{13}\sin 2\theta_{12}\sin(\Delta)\frac{\sin(\hat{A}\Delta)}{\hat{A}}\frac{sin[(1-\hat{A})\Delta]}{(1-\hat{A})}}_{C_-}\sin\delta_{CP} \\ & \underbrace{+\alpha\sin 2\theta_{13}\cos\theta_{13}\sin 2\theta_{12}\cos(\Delta)\frac{\sin(\hat{A}\Delta)}{\hat{A}}\frac{sin[(1-\hat{A})\Delta]}{(1-\hat{A})}}_{C_+}\cos\delta_{CP}, \end{aligned} \tag{1.15}$$

where

$$\alpha \equiv \Delta m^2_{21}/\Delta m^2_{31},\ \Delta \equiv \frac{\Delta m^2_{31} L}{4E},\ \hat{A} \equiv \frac{A}{\Delta m^2_{31}}.$$

Figure 1.3 shows the calculated probability using the eq. (1.15) for the electron neutrino appearance after travelling a distance of 950 km through the Earth for two mass hierarchies: Normal and Inverted, for δ_{CP} values from the full range i.e., from -180 to 180 degrees. Each thin line represents a different value of δ_{CP}. The matter effects increase the probability of $\nu_\mu \rightarrow \nu_e$ transition for Normal Hierarchy and decreases for Inverted Hierarchy. For baseline 950 km the matter effects are big enough to slightly separate the red and blue bands in the region between the first and second oscillation maxima.

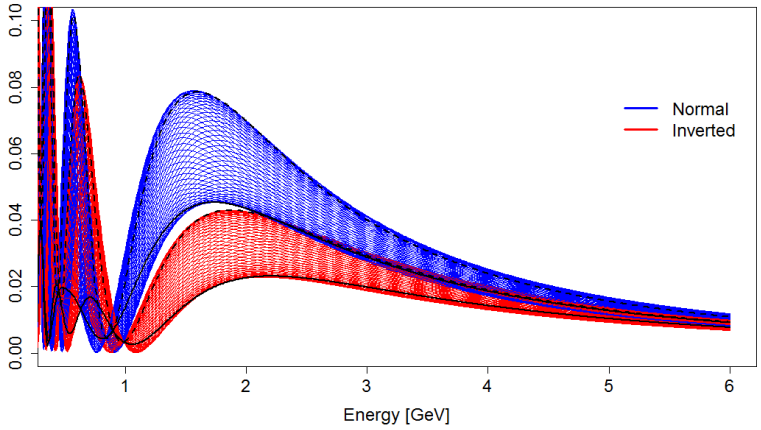

Figure 1.3. The ν_e appearance probability $P_{\mu e}$ calculated as a function of the neutrino energy for 950 km distance and $\delta_{CP} \in (-\pi,\ \pi)$, with a step of 5°; Normal mass hierarchy - blue, Inverted mass hierarchy - red; $\delta_{CP} = \pi/2$ black solid line, $\delta_{CP} = -\pi/2$ black dashed line.

1.3.4. Summary of the oscillation parameters

In summary, the oscillation formalism for three neutrino flavour and three neutrino mass states requires six independent parameters: three mixing angles θ_{12}, θ_{23}, θ_{13} and the CP phase δ_{CP} relating to the $\mathbf{U}_{PMNS}$ mixing matrix, and two independent mass square differences Δm^2_{21}, Δm^2_{32}, the third one Δm^2_{31} being expressed by the first two. The values of these theoretical parameters have to be determined experimentally.

The Δm^2_{ij} parameters give the information about relative values of neutrino masses, but not about the neutrino mass scale and hence their mass values. Both the value and sign of Δm^2_{21} are known from the measurements of solar neutrinos owing to their propagation through a dense matter in the Sun. In the case of Δm^2_{32}, only its absolute value $|\Delta m^2_{32}|$ has been determined so far because of inad-

equate experimental conditions to include interactions with matter, necessary for the determination of the sign. This gives the possibility of two hierarchies of the neutrino mass ordering: the so called Normal Hierarchy (NH) for $sgn\ \Delta m^2_{32} = +1$ and Inverted Hierarchy (IH) for $sgn\ \Delta m^2_{32} = -1$. The determination of the neutrino mass hierarchy is, apart from the determination od δ_{CP}, a topical question for the current and future long baseline oscillation experiments.

The accelerator long baseline oscillation experiments are crucial for further studies of the oscillation parameters. The possibility of tuning the beam parameters and neutrino energies to reach interesting ranges of these parameters is applied to both types of the dedicated oscillation experiments: the appearance experiments (for example OPERA for $\nu_\mu \rightarrow \nu_\tau$, T2K for $\nu_\mu \rightarrow \nu_e$) and the disappearance experiments (for example K2K, MINOS, T2K for $\nu_\mu \rightarrow \nu_\mu$, reactor experiments for $\overline{\nu}_e \rightarrow \overline{\nu}_e$). Currently, the most interesting case is the ν_μ to ν_e transition probability $P(\nu_\mu \rightarrow \nu_e)$. This is the main appearance channel in superbeam experiments designed to explore the neutrino mass hierarchy and to measure δ_{CP}. It should be mentioned that modern long baseline oscillation experiments usually cover the analysis of both the appearance $\nu_\mu \rightarrow \nu_e$ and disappearance $\nu_\mu \rightarrow \nu_\mu$ channels. The procedure of the optimization of the conventional neutrino beam for oscillation studies is further described in Chapter 6 of this thesis.

Moreover, experimental anomalies, such as LSND anomaly, reactor ν flux anomaly or Gallium anomaly, observed in neutrino studies might suggest the existence of additional not active neutrinos, the so called sterile neutrinos. There are several new projects focused on the search for sterile neutrinos, in particular a short baseline neutrino programme with liquid Argon detectors at Fermilab designed to resolve the LSND anomaly. The oscillation formalisms, including the three active neutrinos and one or more sterile neutrinos, are more complex and speculative than those described above.

1.4. Determination of the oscillation parameters

Two types of the oscillation experiments, the disappearance ($\nu_\alpha \rightarrow \nu_\alpha$) and appearance ($\nu_\alpha \rightarrow \nu_\beta$) ones, have been performed to determine five out of six oscillation parameters: Δm^2_{21}, $|\Delta m^2_{32}|$ and three mixing angles θ_{12}, θ_{23} and θ_{13}. The sixth parameter, δ_{CP}, and the sign of $|\Delta m^2_{32}|$ remain to be measured. A short summary of the main results is given in this section.

1.4.1. Determination of Δm^2_{21} and θ_{12}

Parameters Δm^2_{21} and θ_{12} are responsible for neutrino oscillation in the solar sector and have been measured in experiments detecting neutrinos coming from the Sun and in experiments studying reactor antineutrinos. As it will be demonstrated, these two types of experiments give consistent and statistically significant, different from zero, values of Δm^2_{21} and θ_{12}, despite the fact that for solar neutrinos the flavour change is due to the weak interactions with the dense matter in the Sun while reactor antineutrinos propagate in vacuum. The parameters Δm^2_{21} and θ_{12}, determined using the two flavour approximation, are often called Δm^2_{solar} and θ_{solar}.

The Davis chlorine radiochemical experiment, which started in the late 1960s at Homestake, was the first one to successfully detect and count solar neutrinos [16], [17]. Testing the Standard Solar Model (SSM) using neutrinos from the solar fusion reactions was the original motivation for this experiment. However, a large discrepancy between the predicted and observed electron neutrino flux created the so called solar neutrino puzzle.

Following this first experiment, a few others were used to detect and investigate solar neutrinos and to solve the solar neutrino puzzle. The too small measured neutrino flux has been confirmed by the radiochemical experiments Gallex/GNO [18] at the LNGS laboratory in Italy and the SAGE [19] experiment at Baksan in Russia, all three using gallium instead of chlorine. The Kamiokande experiment in Japan, which had started data taking in 1987, gave a similar result, later confirmed by the SuperKamiokande experiment.

The radiochemical chlorine and gallium experiments are characterised by low energy thresholds for the detection of solar neutrinos (0.23 MeV for gallium and 0.81 MeV for chlorine), but they cannot give information about the interaction time, energy or direction of the neutrino. The Kamiokande and SuperKamiokande detectors, based on the detection of the Cherenkov radiation in water, provide real-time information on the energy and the direction of neutrinos. Unfortunately, for this detection technique the neutrino energy threshold is relatively high ($E_\nu \geq 5MeV$), and only a small, high energy part of the solar neutrino energy spectrum has been measured. Despite these differences, all these experiments have consistently observed a number of solar electron neutrinos between 0.3(Davis's experiment) and 0.5-0.6(all the other experiments) of the number expected in the

SSM.

It is worth adding that in 1989 the Kamiokande experiment demonstrated that the measured neutrinos definitely come from the Sun by taking the advantage of the directional correlation between the incoming solar neutrino and the measured recoiled electron in the neutrino scattering on electrons [20] (eq. (1.16)). This reaction is sensitive to all active neutrinos, but the ν_e component is dominating ($\nu_{\mu,\tau}\, e \approx 0.16\, \nu_e\, e$) , which is due to the charge current exchange possible only in the case of ν_e elastic scattering.

The solution to the puzzle was found by the SNO (Sudbury Neutrino Observatory) experiment in Canada [21] which has started observations in 1999 using a 1 kton heavy water Cherenkov detector. The neutrino flux was measured for two reactions on deuterium: the Charge Current (CC) neutrino interaction (eq. (1.17)) and the Neutral Current (NC) neutrino interaction (eq. (1.18)). This detector also registered the neutrino scattering on electrons, i.e. the same reaction as in the SuperKamiokande detector, so for this reaction the results from both experiments could have been combined, leading to the reduced measurement error. The main feature is that the CC reaction is only sensitive to electron neutrinos, while the NC reaction is sensitive to all three types of neutrinos that couple to the Z^0 boson with the same coupling. So if the flux deficit is caused by the flavour transitions $\nu_e \rightarrow \nu_{\mu,\tau}$ due to neutrino oscillations, the NC flux should agree with SSM predictions while the CC flux should be significantly smaller. The results obtained by SNO are presented in Table 1.1 and show that the oscillation hypothesis is clearly confirmed.

$$\nu_x + e^- \rightarrow \nu_x + e^- \quad (ES) \tag{1.16}$$

$$\nu_e + d \rightarrow e^- + p + p \quad (CC) \tag{1.17}$$

$$\nu_x + d \rightarrow \nu_x + n + p \quad (NC) \tag{1.18}$$

The SNO discovery was confirmed by the independent measurement of the Δm^2_{solar} and θ_{solar} parameters by the KamLAND (Kamioka Liquid scintillator AntiNeutrino Detector) experiment equipped with a one kiloton liquid scintillator detector located in Kamioka in Japan. It was a long baseline neutrino oscillation experiment using several nuclear reactors as $\overline{\nu}_e$ sources. The experiment observed the expected decrease on the neutrino flux [22] and in addition a clear periodic

	reaction	neutrino flux (^8B)
SSM prediction [5]	all reactions	$5.69(1.00 \pm 0.16)\ \times 10^6 \mathrm{cm}^{-2}\mathrm{s}^{-1}$
SNO Phase I+II+III	fit to all reactions	$5.25 \pm 0.16 \pm 0.13\ \times 10^6 \mathrm{cm}^{-2}\mathrm{s}^{-1}$
SNO Phase II	CC	$1.68 \pm 0.06 \pm 0.09\ \times 10^6 \mathrm{cm}^{-2}\mathrm{s}^{-1}$
SNO Phase II	NC	$4.94 \pm 0.21 \pm 0.38\ \times 10^6 \mathrm{cm}^{-2}\mathrm{s}^{-1}$
SNO Phase II	ES	$2.35 \pm 0.22 \pm 0.15\ \times 10^6 \mathrm{cm}^{-2}\mathrm{s}^{-1}$
Super-K Phase III	ES	$2.32 \pm 0.04 \pm 0.05\ \times 10^6 \mathrm{cm}^{-2}\mathrm{s}^{-1}$

Table 1.1. The results of ^8B neutrino flux measurement from the SNO and SuperKamiokande experiments.

behaviour of the $\overline{\nu}_e$ survival probability [23]. The observed antineutrino spectrum and related fit of the oscillation model is shown in Figure 1.4. The combined results of the solar and KamLAND analyses showed at a higher than 5σ confidence level that $\Delta m^2_{solar} \sim 7.5 \times 10^{-5}$ and $\tan^2\theta_{solar} \sim 0.45$. In addition, the so called Large Mixing Angle solution for solar neutrinos was chosen by the fit [24].

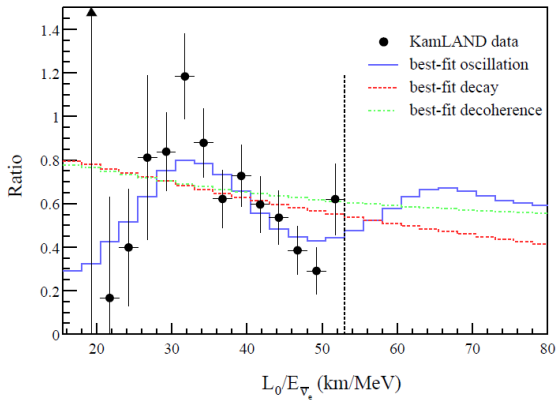

Figure 1.4. Ratio of the observed $\overline{\nu_e}$ spectrum to the expectation for no oscillation hypothesis as a function of versus L_0/E with $L_0 = 180\ km$ [23]. The blue curve shows the prediction of best fit for 3 flavour oscillation model. The dashed curves show the expectations for the best-fit decay and best-fit decoherence models.

The latest results of the observation of low energy solar neutrinos (down to 250 keV) come from a real time experiment - Borexino - equipped with a liquid scintillator detector placed in LNGS and characterized by the extremely low and well known background [25]. The long operation together with an excellent understanding of the detection technique, excellent energy resolution and control of the systematics allow Borexino to distinguish between different reactions in the Sun [26], [27], [28]. Figure 1.5 presents the combined Borexino results for

solar neutrino flux measurements presented as survival probabilities for electron neutrinos from *pp*, ^{7}Be, *pep* and ^{8}B reactions in the solar pp cycle. This way the door has been opened opened for studies of the Sun using neutrinos, according the original Davis's idea from 50 years ago.

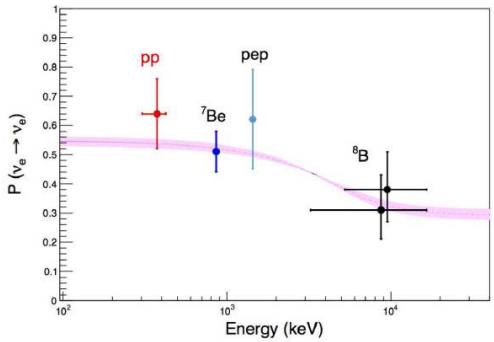

Figure 1.5. Survival probabilities for solar electron neutrinos (Borexino only data) as a function of energy [28].

1.4.2. Determination of Δm^2_{32} and θ_{23}

The parameters Δm^2_{32} and θ_{23} describe neutrino oscillations in the so called atmospheric sector. They have been first measured by experiments detecting neutrinos originated in the Earth's atmosphere. To make the phenomenon fully understood, a complimentary studies using data from the accelerator neutrino experiments have also been performed.

As was presented in Section 1.2.2, the expected ratio of the atmospheric muon and electron neutrino fluxes at low energies ($\lesssim 1GeV$) is approximately $(\phi_{\nu_\mu} + \phi_{\bar{\nu}_\mu}) : (\phi_{\nu_e} + \phi_{\bar{\nu}_e}) \simeq 2 : 1$. The experiments use to measure the so called double ratio:

$$R = \frac{(\phi_{\nu_\mu} + \phi_{\bar{\nu}_\mu})_{obs}}{(\phi_{\nu_\mu} + \phi_{\bar{\nu}_\mu})_{theor}} \Big/ \frac{(\phi_{\nu_e} + \phi_{\bar{\nu}_e})_{obs}}{(\phi_{\nu_e} + \phi_{\bar{\nu}_e})_{theor}} \tag{1.19}$$

with the measured fluxes of muon and electron neutrinos divided by their expected values obtained from the Monte Carlo simulations. In normal conditions R should equal 1.

The indication of deviation from one of the R values came from Water Cherenkov detectors operating in the 1980's. The IMB experiment in the USA measured $R = 0.69 \pm 0.10 \pm 0.09$ [29] and the Kamiokande detector in Japan

measured $R = 0.60 \pm 0.07 \pm 0.06$ [30] for > 0.1 GeV samples. This consistent preference of the measured neutrino flux values to be much lower than expected from the calculations was called the atmospheric neutrino puzzle. More detailed evidence of these phenomena was provided by the next generation experiments. The ratio measured by the SuperKamiokande collaboration in 1998 [31], based on total fluxes of muon and electron neutrinos, was statistically lower than its predicted value equalling one ($R = 0.638 \pm 0.017 \pm 0.050$ for sub-GeV sample). In addition, there was a clear increase in the deficit in the flux of muon neutrinos with the distance travelled by them through the Earth. A good measure of this distance is the so called zenith angle between the z axis of the Superkamiokande cylinder and the incoming neutrino direction. The zenith angle distribution for ν_e (e-like) and ν_μ (μ-like) events is shown in Figure 1.6 for sub-GeV and multi-GeV data sets. The sub-GeV data are shown separately for $p < 400\ MeV/c$ and $p > 400\ MeV/c$. The multi-GeV e-like distributions are shown for $p < 2.5\ GeV/c$ and $p > 2.5\ GeV/$c and the multi-GeV μ-like are shown separately for fully contained (muon stopping in the detector) and partially contained (muon leaving the detector) events. For upward going neutrinos cosine of the zenith angle is negative while for downward going neutrinos it is positive. In particular, for neutrinos travelling through the whole Earth (about 13 000 km), the cosine of the zenith angle equals -1. It can be seen that for e-like events the observed zenith angle distributions are consistent with no-oscillation model for all energy ranges. The distributions for μ-like events show a big discrepancy between the data and no-oscillation model for the upward going neutrinos which travelled through the Earth. This disappearance of the ν_μ flux and the unchanged, within errors, ν_e flux can be interpreted as the result of the oscillations between the muon and tau neutrinos. Because of the high energy threshold for the production of tau lepton, the tau neutrino interactions are rare in the SuperKamiokande experiment. In addition, they are difficult to analyse in the water Cherenkov detector, but the ν_τ appearance in the muon neutrino beam was directly observed by the dedicated OPERA experiment. A detailed description of the analysis performed by the SuperKamiokande collaboration based on the early data (SK-I) can be found in [32].

The complementary and more accurate information has come from the long baseline neutrino experiments. Thanks to the well understood neutrino flux and energy spectrum as well as an increasing intensity of neutrino beams resulting in a higher number of the detected neutrino interactions, values of the $|\Delta m^2_{32}|$ and of the mixing angle θ_{23} have been better determined.

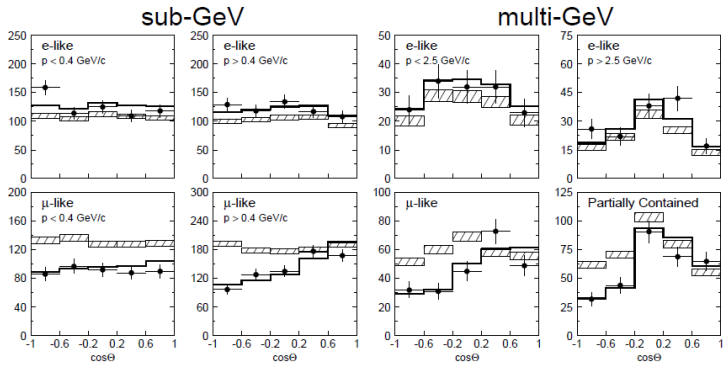

Figure 1.6. The zenith ange distributions of e-like and μ-like events for two energy regimes: Sub-GeV and multi-GeV [31]. The hatched boxes show the non-oscillated Monte Carlo events and the solid line corresponds to the best fit for two flavour $\nu_\mu \rightarrow \nu_\tau$ oscillations.

The K2K (KEK-to-Kamioka) long baseline neutrino oscillation experiment in Japan [33] was the first accelerator-based experiment studying the ν_μ disappearance channel. A horn-focused wide-band muon neutrino beam was produced at KEK-PS and directed to the Super-Kamiokande far detector. The neutrino path length was $L = 250\ km$, and mean neutrino energy value of $\langle E_\nu \rangle \sim 1.3\ GeV$. The spectrum and profile of the neutrino beam before oscillations were additionally measured by the near neutrino detector at KEK. This pioneering long baseline experiment showed the distorted neutrino energy spectrum measured in the far detector to be consistent with neutrino oscillation parameters measured by the SuperKamiokande detector for atmospheric neutrinos.

MINOS in the USA was the second long baseline neutrino oscillation experiment equipped with a near and a far detector. Neutrinos from the the NuMI (Neutrinos at the Main Injector) beam were registered by magnetized iron-scintillator tracking calorimeters, located at Fermilab (near detector) and in the Soudan mine (far detector). The baseline distance is 735 km. The NuMI beam is a magnetic horn - focused wide-band beam with the neutrino energy spectrum which can be varied by moving the target position relative to the first horn and changing the horn current. Most of the MINOS data were taken with the beam 'low-energy' option in order to be close to the first oscillation maximum for the $\nu_\mu \rightarrow \nu_\tau$ transition. The MINOS data clearly confirmed the ν_μ disappearance. In addition, MINOS was the first experiment to observe muon antineutrino disappearance with the NUMI beam line optimized for $\overline{\nu}_\mu$ production and the MINOS magnetic detector with a capability to partially separate neutrinos and antineutrinos. The results of the fit

within the two-neutrino oscillation framework, using the full MINOS data sample, are [34]: $|\Delta m^2_{32}| = 2.42^{+0.09}_{-0.10} \times 10^{-3} eV^2$, $sin^2 2\theta_{23} = 0.950^{+0.035}_{-0.036}$

The T2K (Tokai to Kamiokande) experiment in Japan is the first off-axis long baseline neutrino oscillation experiment. It stared taking data in 2010. The baseline distance between the J-PARC in Tokai and the SuperKamiokande detector is 295 km. A wide-band ν_μ beam produced using protons from the J-PARC Main Ring is 'kinematically focused' by placing one of two near and far detectors at 2.5 degree off-axis of the beam. With this configuration, the ν_μ beam is well tuned to the first oscillation maximum for the transitions $\nu_\mu \rightarrow \nu_\tau$ and $\nu_\mu \rightarrow \nu_e$, giving the best conditions for precise measurements. In 2014 the T2K collaboration published the results based on precise analysis in three neutrino flavour formalism for normal and inverted hierarchy giving: $\Delta m^2_{32} = 2.51 \pm 0.10 \times 10^{-3} eV^2$, $sin^2\theta_{23} = 0.514^{+0.055}_{-0.056}$ for normal hierarchy, and $\Delta m^2_{32} = 2.48 \pm 0.10 \times 10^{-3} eV^2$, $sin^2\theta_{23} = 0.511 \pm 0.055$ for inverted hierarchy.

The CERN Neutrino to Gran Sasso (CNGS) neutrino beam produced at CERN and directed towards Laboratori Nazionali del Gran Sasso laboratory (LNGS) in Italy started its operation in 2006 and finished it in December 2012 [35]. The beam was designed to produce the maximum number of CC ν_τ interactions in the detectors at the Gran Sasso laboratory. The distance between CERN and Gran Sasso is 730 km and the mean ν_μ beam energy was 17 GeV. In this facility the CERN SPS accelerator was used as a 400 GeV proton source with the nominal intensity of 2×10^{13} protons on target per 10.5 μs extraction, which gave 18.24×10^{19} protons on target during the total operation time. The physics goal was to directly confirm the $\nu_\mu \rightarrow \nu_\tau$ transition during the 730 km travel through the Earth. Two detectors in two different technologies were designed and operated in this task.

The OPERA detector using the nuclear emulsion detection technique took data on the CNGS beam in ν_{tau} appearance mode and in 2010 it observed the first ν_τ event [36], confirming the $\nu_\mu \leftrightarrow \nu_\tau$ oscillations. During five years of its operation, OPERA observed five tau neutrino appearance events in total, which allowed the $\nu_\mu \leftrightarrow \nu\tau$ oscillation at 5σ level to be confirmed.

The second detector installed in the LNGS hall, ICARUS T600, was built in the innovative Liquid Argon Time Projection Chamber technology, demonstrating its usefulness for the neutrino study [37], [38]. Because of the cost limitation,

the mass of the detector (600 ton) was too small to observe the ν_τ appearance. ICARUS brought interesting neutrino results, e.g. by narrowing the area of possible sterile neutrino existence [39] or the solution for super luminal neutrino anomaly by measuring the neutrino time of flight with good precision.

The NOvA experiment is the largest currently running neutrino project at Fermilab. It began taking data in 2013 with only a part of the far detector. The construction was completed in January 2014 and since then the expeirment with both near and far detectors has been successfully operating. The detectors are composed of plastic cells filled with liquid scintillator. The near detector of a mass of 330 tons is located at Fermilab at a distance of a few hundred metres from the target and the far detector in the Ash River, Minnesota, at a distance of 810 km from the target. The Nova experiment uses the NuMI (Neutrinos from Main Injector) beam with the Main Injector delivering 400 kW of power to this beam and with both detectors placed at 3.3 degrees off-axis. At this angle the maximal muon neutrino flux is at a neutrino energy of 2 GeV, corresponding to the first oscillation maximum for the $\nu_\mu \rightarrow \nu_e$ transition. In addition to the NOvA experiment, the MINOS+ experiment takes data with its detectors located on-axis of the beam at distances of 1 km and 730 km from the target. MINOS+, as the continuation of MINOS, will further exploit the NuMI beam potential, collecting high statistics neutrino data and testing the existence of non-standard neutrino interactions and sterile neutrinos so as to increase the precision of measurement of standard oscillation parameters.

1.4.3. Determination of θ_{13}

The θ_{13} angle was difficult to measure because of its relative smallness. As was shown in Section 1.4.2, the Superkamiokande measurements for atmospheric neutrinos, within experimental errors, did not require the $\nu_\mu \rightarrow \nu_e$ oscillations to explain a decrease in the ν_μ flux. In addition, θ_{13} connects the solar and atmospheric oscillation sectors, therefore a good knowledge of other oscillation parameters is very helpful in θ_{13} determination, especially for $\nu_\mu \leftrightarrow \nu_e$ oscillations. Two different oscillation channels have the θ_{13} dependency in it. First, the probability of electron antineutrino survival $P(\overline{\nu}_e \rightarrow \overline{\nu}_e)$ (equal to $P(\nu_e \rightarrow \nu_e)$) can be measured by reactor experiments at such distances to the detectors for which the matter effects are negligible owing to the smallness of Δm^2_{12}. The second one, the probability of electron neutrino appearance in the muon neutrino beam $P(\nu_\mu \rightarrow \nu_e)$ can be measured by accelerator long baseline experiments. In the case of the ν_e appearance experiment, the $\sin\theta_{13}$ parameter is connected with the δ_{CP}

phase, therefore the measurement depends on the δ_{CP} value.

The first experiment that in 2011 announced the suggestion of a non-zero, 'large' θ_{13}, was the long baseline experiment T2K searching for the ν_e appearance signal in the ν_μ beam [40]. However, the statistical significance was only 2.5σ, which was due to a small data sample collected before the earthquake in Japan in March 2011. After the reparation of damages, T2K continued successfully data taking and announced the observation of ν_e appearance where $\theta_{13} = 0$ hypothesis was excluded with a significance of 7.3σ [41].

In the same year the Double Chooz reactor experiment in France published an indication of reactor electron antineutrino disappearance consistent with neutrino oscillations which could be interpreted as a non-zero value of θ_{13} mixing angle with the best fit: $\sin^2 2\theta_{13} = 0.086 \pm 0.041$ (stat) ± 0.030 (syst) [42].

The Daya Bay reactor experiment was the first one to report in 2012 5.2σ evidence for a non-zero θ_{13} [43]. It measured $P(\overline{\nu}_e \rightarrow \overline{\nu}_e)$ using electron antineutrinos from the Daya Bay nuclear power plants in China with six identical detectors deployed in two near (470 m and 576 m) and one far (1648 m) underground pits. This setup allowed an extremely good understanding of the systematic errors. In 2015, based on the data sample coming from the experiment running for 404 days, the Daya Bay collaboration published the result of the oscillation analysis based both on the rates and shapes of spectra [44]. This analysis gave the most precise measurement of θ_{13}: $sin^2 2\theta_{13} = 0.084 \pm 0.005$.

The RENO experiment in Korea, using a set of two identical detectors located at 294 m and 1383 m from the reactor centre, also announced the result of θ_{13} measurement [45] in 2012 with in 229 days of running time. RENO reported $sin^2 2\theta_{13} = 0.113 \pm 0.013(stat) \ \pm 0.019(syst)$ obtained from a rate-only analysis, excluding the no-oscillation hypothesis at the 4.9 σ level.

1.4.4. Global fits

The consistent determination of the oscillation parameters within the three flavour neutrino oscillation model requires a global analysis of the results obtained by all oscillation experiments. A few phenomenological groups are systematically working on this task. In Table 1.2 recent results of the global fit to all available experimental data from [46] are presented.

The $sin^2\theta_{23}$ is large and the mixing in the atmospheric sector is almost maximal, but the uncertainties are relatively big (at 17% level), so the solution for the θ_{23} mixing angle is degenerated - this is the so called θ_{23}-octant degeneracy problem. The θ_{12} angle is also large. The third mixing angle θ_{13} is small, but significantly greater than zero and bigger than previously expected.

Fitting the Δm^2_{21}, Δm^2_{32}, Δm^2_{31} parameters requires an explanation. The three mass square differences are not independent:

$$\Delta m^2_{21} + \Delta m^2_{32} + \Delta m^2_{31} = 0 \; . \tag{1.20}$$

The relation between two mass square differences determined experimentally from the atmospheric and solar data, using two neutrino flavour oscillation model, is $\Delta m^2_{21}(\Delta m^2_{solar}) \ll \Delta m^2_{32}(\Delta m^2_{atmospheric})$. Thus, the implication for the third mass square difference from the three flavour model is:

$$|\Delta m^2_{31}| = |\Delta m^2_{32} + \Delta m^2_{21}| \sim |\Delta m^2_{32}| = |\Delta m^2_{atmospheric}| \; . \tag{1.21}$$

In the three neutrino flavour oscillation model the atmospheric measurement is not a pure Δm^2_{32} measurement, but $\Delta m^2_{atmospheric} \sim cos^2(\theta_{12})|\Delta m^2_{31}| + sin^2(\theta_{12})|\Delta m^2_{32}|$. However, the difference between the Δm^2_{32} and Δm^2_{31} is very small, around 3%, so it is very difficult to distinguish between them experimentally, and often the Δm^2_{31} value is used in global fits for normal hierarchy instead of Δm^2_{32}.

The last row of Table 1.2 contains the best fit value for δ_{CP}. The estimation is very rough and not significant. However, the solution of the non-zero value of δ_{CP} is preferred over the CP conservation scenario.

	Normal Ordering best fit point $\pm 1\sigma$	Inverted Ordering best fit point $\pm 1\sigma$
$sin^2\theta_{12}$	$0.304^{+0.013}_{-0.012}$	$0.304^{+0.013}_{-0.012}$
$sin^2\theta_{23}$	$0.452^{+0.052}_{-0.028}$	$0.579^{+0.025}_{-0.037}$
$sin^2\theta_{13}$	$0.0218^{+0.0010}_{-0.0010}$	$0.0219^{+0.0011}_{-0.0010}$
$\frac{\Delta m^2_{21}}{10^{-5}\ eV^2}$	$7.50^{+0.19}_{-0.17}$	$7.50^{+0.19}_{-0.17}$
$\frac{\Delta m^2_{3l}}{10^{-3}\ eV^2}$	$+2.457^{+0.047}_{-0.047}$	$-2.449^{+0.048}_{-0.047}$
$\delta_{CP}\ ^\circ$	306^{+39}_{-70}	254^{+63}_{-62}

Table 1.2. Results of the three flavour oscillation parameters fit to global data [46]. The second column contains values of parameters assuming the normal mass hierarchy ($\Delta m^2_{3l} \equiv \Delta m^2_{31} > 0$) and the third one - values of parameters assuming the inverted mass ordering ($\Delta m^2_{3l} \equiv \Delta m^2_{32} < 0$).

Chapter 2

Open questions in the oscillation neutrino physics

The neutrino oscillation phenomenon, especially within the framework of three active neutrinos, is now well understood but still not fully exploited, and several important measurements should be addressed in the near future. Assuming the three active neutrino framework, the mass hierarchy and the δ_{CP} parameter need to be determined. The already mentioned $sin^2\theta_{23}$ octant degeneracy also needs to be solved based on more precise measurements of the atmospheric neutrinos. The LSND effect as well as a too small flux of reactor neutrinos and the so called Gallium anomaly may be the signs of the oscillations between the known three neutrino flavours and sterile neutrinos. The SBN experiment at Fermilab in USA, several experiments with very strong radioactive sources and more precise measurements of the reactor neutrino flux are being prepared to answer the question concerning the existence of the sterile neutrinos.

This chapter is dedicated to the proposed next-generation long baseline neutrino and antineutrino oscillation experiments, i.e. the determination of the neutrino mass hierarchy and studies of the CP non-conservation in the leptonic sector.

2.1. Mass Hierarchy

The sign of the $|\Delta m^2_{31}|$ determines the neutrino mass hierarchy. The Normal Hierarchy is for $sign(\Delta m^2_{31}) = +1$ and the Inverted Hierarchy for $sign(\Delta m^2_{31}) = -1$. The fact whether the hierarchy is normal or inverted has a significant impact on other experimental observations. Firstly, an unknown hierarchy may lead to a reduced ability to observe CP violation in the leptonic sector. A measurement of the hierarchy will also be useful for the interpretation of results in the case of discovery of the neutrinoless double beta decay as well as for other new physics.

A natural way to determine $sign(\Delta m^2_{31})$ is to study either the atmospheric neutrino or the accelerator neutrino oscillations in the three flavour model. The matter effects during neutrino propagation change the sign of the weak potential depending on the MH, and if the sign of the matter effects can be measured, the mass hierarchy can be determined.

One way to measure this effect is to use a natural, wide range of energies and directions of the incoming atmospheric ν_μ's and to perform the ν_μ disappearance study by measuring the $P(\nu_\mu \rightarrow \nu_\mu)$. The neutrinos crossing the Earth Core experience different matter effects than those crossing only the atmosphere or Earth Mantle. The comparison of both leads to the mass hierarchy determination. The detector for such measurements should be large enough to provide a sufficient number of neutrino interactions with a good angular resolution for the precise determination of the neutrino path and hence a matter density profile. It should also have an excellent energy resolution for the precise determination of neutrino energy. Additionally, a good knowledge of the θ_{13} parameter is necessary. Atmospheric experiments such as ORCA (Mediterranean See) [47] and PINGU (South Pole, Antarctica) [48], which use natural water reservoirs or Antarctic ice as active targets, are currently under evaluation. The other two: INO - iron calorimeter in India [49], and water Cherenkov HyperKamiokande (Japan) [50], are also considered for the future.

An other way to determine the neutrino mass hierarchy to use an accelerator based long baseline neutrino experiment with a sufficiently long baseline and to perform the $\nu_\mu \rightarrow \nu_e$ appearance study. The longer baseline, the larger matter effects and the easier MH determination. An example of the matter effects influence on the ν_e appearance probability as a function of the baseline is presented in Figure 2.1. The baselines of T2K and NOvA, the two currently running accelerator experiments are depicted by vertical dotted lines. Vertical thin solid lines show the uncertainty coming from the θ_{23} octant degeneracy. Future long baseline experiments such as LBNF-DUNE will be able to clearly determine the neutrino mass ordering. However, the NOvA experiment can give a strong suggestion of the hierarchy in the relatively near future.

The third new idea of the MH determination, possible only thanks to a relatively large θ_{13}, is to use reactor neutrinos on a medium baseline and look for $P(\overline{\nu}_e \rightarrow \overline{\nu}_e)$ disappearance. A small, oscillation pattern coming from the difference between Δm^2_{31} and Δm^2_{32} will appear on the dominant solar term. The Fourier

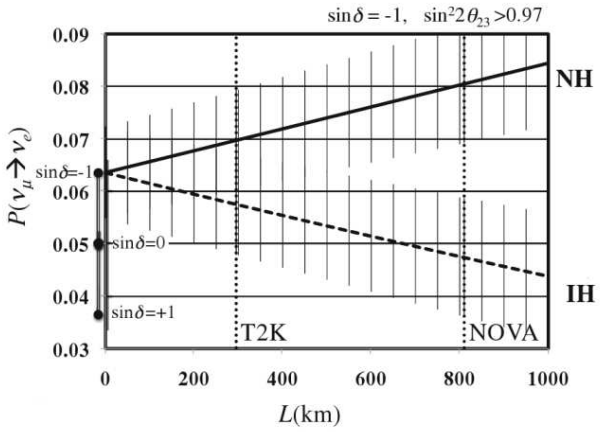

Figure 2.1. Baseline dependence of the $\nu_\mu \rightarrow \nu_e$ appearance probability. For the T2K and NOvA baselines vertical dotted lines are shown [51].

analysis of the interference effects between the solar and atmospheric oscillations gives the possibility to distinguish between the Δm^2_{31} and Δm^2_{32} components. The relation between them serves to determine the mass ordering: $|\Delta m^2_{31}| > |\Delta m^2_{32}|$ for the Normal Hierarchy, $|\Delta m^2_{31}| < |\Delta m^2_{32}|$ for the Inverted Hierarchy. However, the expected difference between the Δm^2_{31} and Δm^2_{32} parameters is of the 3% order, so the energy resolution of the detector must be extremely good, as well as its calibration and response function very well known. Two reactor experiments focused on this measurement are proposed, the JUNO (Jiangmen Underground Neutrino Observatory) experiment [52], the follower of the Daya Bay experiment in China with a 20 kton liquid scintillator detector and a 50 km baseline, and RENO50 [53], the follower of RENO in Korea.

2.2. Determination of δ_{CP}

The measurement of the CP violation in leptonic interactions may be crucial for the understanding of the origin of flavour mixing and its impact on our Universe. The CP violation effect is introduced in the neutrino oscillation formalism by the imaginary component of the U_{PMNS} mixing matrix, which is proportional to the δ_{CP} parameter.

The CP violation can be measured from the asymmetry between the neutrino and antineutrino ν_e ($\overline{\nu}e$) appearance probability around the first oscillation maximum.

$$A_{CP} = \frac{P_{\nu_\mu \to \nu_e} - P_{\overline{\nu}_\mu \to \overline{\nu}_e}}{P_{\nu_\mu \to \nu_e} + P_{\overline{\nu}_\mu \to \overline{\nu}_e}} \tag{2.1}$$

Using the equation (1.15) the CP asymmetry A_{CP} can be written as:

$$A_{CP} \simeq -\frac{\pi sin2\theta_{12}\Delta m^2_{21}}{tan\theta_{23}sin2\theta_{13}\Delta m^2_{31}}\ sin\delta_{CP} \pm 2\hat{A}\ \sim\ -0.27\ sin\delta_{CP} \pm 2\hat{A} \tag{2.2}$$

In the maximum region the δ_{CP} value has the strongest effect on the shape of $P_{\mu e}$, as wis shown in Figure 1.3. However, there is a difficulty in this measurement because of 'fake CP asymmetry' the already mentioned in Section (1.3.3) and caused by the matter effects. The matter effects come from the weak potential, so it generates the opposite sign for neutrinos and antineutrinos depending on the mass ordering. The problem with the matter effects in the $sin\delta_{CP}$ measurement can be handled in two different ways. The first one is to use a relatively short baseline so that the matter effects become irrelevant, e.g. in the proposed HyperKamiokande experiment with the far detector at a distance of 295 km from the ν_μ source at J-PARC. The second way is to use a very long baseline, for which the matter effects will be dominant, in order to measure the mass hierarchy first and then optimise the beam for the δ_{CP} measurement. This approach is proposed for the LBNF-DUNE project with a baseline of 1300 km, currently under evaluation in the USA. Experimental difficulties related to the δ_{CP} measurement in long baseline experiments are the relatively small probability of the $\nu_\mu \to \nu_e$ transition and small cross sections for neutrino interactions. Therefore, for the δ_{CP} measurement a long baseline experiment has to be well optimised w.r.t. the oscillation maxima, have intense neutrino and antineutrino beams, a large far detector with a good energy resolution and a long time of operation.

In summary, the determination of δ_{CP} at $\geqslant 5\sigma$ level will probably come from the future accelerator long baseline projects, such as HyperKamiokande in Japan and LBNF-DUNE in the USA. However, the present experiments, such as T2K and NOvA, should be able to provide us with the δ_{CP} measurement at the 3σ level in less than ten years.

Chapter 3

Future Long Baseline neutrino programme

The main components of a long baseline neutrino experiment are: the near and far detectors and the neutrino beam. In the following chapter the summary of the detector techniques planned for long baseline neutrino experiments together with a description of the production of the neutrino beam is presented in Section 3.1 and Section 3.2. The review of the neutrino long baseline programmes in Europe, the USA and Asia is shortly discussed in Sections 3.4, 3.5, 3.6.

3.1. Detector concepts

The near detectors are not necessary for the appearance oscillation study but they play an important role in long baseline experiments. As it is concluded from the currently operated long baseline experiments, the near detectors significantly reduce systematic errors from the neutrino beam extrapolation models by measuring the actual neutrino spectrum near their origin. The near detector made in the same technology as the far detector also helps to understand and control the far detector systematics owing to much better statistics near the neutrino source.

There are many interesting technologies serving neutrino far detectors in the present long baseline neutrino experiments for example: the Iron Calorimeter detector used by the MINOS experiment, plastic PVC filled with scintillator used by NOvA or lead interleaved with nuclear emulsion used by OPERA. The detectors for the future long baseline oscillation experiments have to be much larger and precise, so the easiness of detector mass scaling by at least a factor of ten and the precision of measurements of basic properties of particles produced in neutrino oscillations are the basic criteria for choosing the detector technology. The following three technologies based on liquids seem to be particularly promising from this point of view: a water Cherenkov detector used by the SuperKamiokande experiment, a liquid scintillator used by KamLAND and Borexino and a liquid Argon TPC used by ICARUS. In the following they are shortly presented.

3.1.1. Water Cherenkov

The Water Cherenkov (WCh) detector has the form of a large tank filled with ultra-clear water surrounded by photo-multiplier tubes (PMT). Charged particles produced in the neutrino interactions in water and passing the detectors with a velocity bigger than the light speed in water emit the Cherenkov photons along their trajectories. These photons form rings on the detector walls and are registered by PMTs. The quasi-elastic neutrino scattering reactions with a single charged lepton in the final state are the best suited neutrino interactions for the water Cherenkov detectors. The data analysis, based on the amplitudes and timing of the PMT signals, the ring opening angle and its shape, allows the determination of the neutrino interaction vertex, lepton direction, velocity energy and mass. The Cherenkov ring produced by a muon is characterised by a sharp external edge because the muon's interaction with matter is dominated by ionization. For electrons, which are much lighter than muons, the photon emission process leading to an electromagnetic cascade is very probable and the Cherenkov ring is fuzzy.

The analysis of the Cherenkov rings and the neutrino flavour determination based on quasi-elastic scattering is brought up to almost perfection by the long term operation of the SuperKamiokande experiment. However, it is important to notice that the performance of the WCh detectors for high energy multi-particle events is much poorer because of difficult analysis of multi-ring views. Neutrino interactions at energies over 1 GeV are dominated by processes leading to multi-ring events, limiting the use of the Water Cherenkov detectors to relatively short baselines with the energy of the first oscillation maximum below 1 GeV. For example, in the case of the T2K experiment the baseline of 295 km and the beam energy of 0.6 GeV correspond to the first oscillation maximum.

In addition, to achieve an improvement in the performance the newly proposed WCh detector would have to be considerably larger than the SuperKamiokande detector and therefore significantly more expensive and technologically challenging. Still, several studies have been performed proposing this detector technique with a detector mass of up to 1 Mton. The most advanced project of this kind is the Hyper-Kamiokande [50] detector in Japan with a target mass of 500 kton. In Europe, the LAGUNA study [54]has included the Water Cherenkov detector called MEMPHYS [55] placed in the Frejus laboratory in France at a distance of 130 km from CERN with a fiducial mass of around 440 kton. Also the LBNE design study in the USA [56] in its initial phase has been considering the WCh technology for the far detector in the long baseline experiment.

3.1.2. Liquid Scintillator

The Liquid scintillator (LSc) as an active target for neutrino detectors has been used for more than 60 years. The technique is well known and the successes of past experiments have encouraged further developments. Thanks to their very low energy threshold, excellent energy resolution and background discrimination capabilities, the liquid-scintillator detectors have proven to be valuable tools in the investigation of low energy neutrinos. The reactor neutrino oscillation experiments such as KamLAND and Daya Bay or the solar neutrino experiment Borexino which have made excellent measurements of the sub-MeV neutrinos, are very good illustrations of this technique.

The JUNO experiment in China [52] is currently the most advanced project of the large LSc detector. The ongoing construction concerns a 20 kton liquid scintillator detector placed 700 m underground and detecting reactor neutrinos from nuclear power plants at a distance of 53 km. As mentioned in the previous chapter, in order to distinguish between two mass hierarchies the technological goal is to achieve an extremely good energy resolution below 3%.

The other project LENA (Low Energy Neutrino Astronomy) [57], has been proposed as a next-generation low-energy neutrino observatory within the LAGUNA study. Based on a mineral oil liquid scintillator and the target mass of 50 ktons, LENA would provide excellent conditions for the observation of both astrophysical and terrestrial neutrinos. The long baseline accelerator experiment with LENA as a far detector placed in the Pyhäsalmi mine in Finland at a distance of 2300 km from CERN would be sensitive to the mass hierarchy and leptonic CP violation. However, as LAGUNA study concludes, in order to be fully exploited LENA would have to be located deep underground. The difficulty with the operation of the LENA type detector lies also in the construction of the tank that would hold such a big amount of mineral oil inside a water veto detector.

3.1.3. Liquid Argon TPC

The liquid Argon Time Projection Chamber (LAr TPC) is a new and very promising detector technique for neutrino physics. The LAr TPCs with a mass up to 100 kton are studied in the context of the next generation long baseline neutrino oscillation experiments searches for proton decay and neutrino astrophysics. Thanks to two kinds of signals from the ionization and scintillation processes induced by charged particles in Argon, this technique offers a very

fast trigger, excellent 3D event imaging and precise calorimetric measurements. Owing to a very good spacial resolution even high energy neutrino events can be registered and precisely measured. After the successful underground operation of the ICARUS T600 detector [38] at the Gran Sasso Underground Laboratory, this detector technique has become the main option for the future long baseline neutrino experiments. Currently some *R&D* studies at Fermilab and CERN are carried on in view of their application in the LBNF-DUNE and SBN experimental programmes at Fermilab.

There are two types of LArTPC detectors: single phase - ICARUS design [37] and double phase - GLACIER design [58], and both are under further development. The difference between those two techniques is in the ionisation signal treatment. In the single phase detector two or more planes of signal collection wires are immersed inside the liquid Argon volume to register the primary ionisation signal. This technique based on the ICARUS 600 ton detector [38], is being further developed under the WA104 (ICAR-US) programme at CERN, the MicroBOONE detector at Fermilab and in the LBNF-DUNE context. In the double phase detector primary ionisation electrons are extracted from the liquid to the gas phase, then multiplied by LEM (Large Electron Multiplier) devices and afterwards collected on the striped anode. The small setup for LEM - based charged readout R&D was assembled within the ArDM experiment at CERN [59]. The double-phase-GLACIER-design technique has not yet been demonstrated in a large scale by any experiment. The work on the first large scale prototype ($6m \times 6m \times 6m$) is ongoing at CERN under the WA105 (LBNO-DEMO) programme with the goal of its application to the DUNE detector as an alternative solution for one or more detector modules.

3.2. Conventional neutrino beams

This section gives a short introduction to the production of the accelerator based neutrino beams. The beams of neutrinos from π and K meson decays have been produced since the early sixties of the last century, e.g. at BNL and CERN. They are often named 'conventional' to be distinguished from some new concepts of accelerator neutrino beams. The long baseline neutrino experiments where neutrinos travel hundreds of kilometres to the far detector have special requirements, such as high intensity, good focusing and adjusted neutrino energy spectrum. The first long baseline accelerator neutrino experiment which used the conventional accelerator neutrino beam was the Japanese K2K experiment, later followed by

the MINOS and NOvA experiments on the NuMi beam in the USA, the OPERA and ICARUS experiments on the European CNGS neutrino beam, and the T2K experiment on the beam produced at J-PARK in Japan.

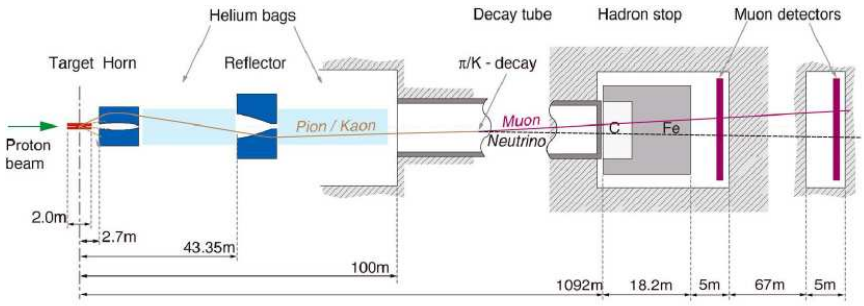

Figure 3.1. An example of neutrino beam production. Schematic representation of CNGS beam setup at CERN [60].

The conventional procedure to obtain a neutrino beam is as follows: a proton synchrotron delivers bunches of high-energy protons on a target, which results in proton-target interactions and the production of secondary particles, mainly pions and kaons. The intensity of the neutrino beam depends on the number of delivered protons, so the commonly used unit to describe the neutrino beam intensity is protons on target - p.o.t. Further, by using magnetic focusing devices, such as a set of two cylindrically symmetric magnets called a horn and reflector, mesons with a selected charge sign and momentum are focused into a decay tunnel. In the tunnel they decay mostly into a muon and muon neutrino:

$$\pi^+ \rightarrow \mu^+ + \nu_\mu \quad \text{branching ratio} \approx 100\% \tag{3.1}$$

$$\pi^- \rightarrow \mu^- + \bar{\nu}_\mu \tag{3.2}$$

$$K^+ \rightarrow \mu^+ + \nu_\mu \quad \text{branching ratio} \approx 63.5\% \tag{3.3}$$

$$K^+ \rightarrow \mu^- + \bar{\nu}_\mu \tag{3.4}$$

At the end of the decay tunnel muons are usually monitored using dedicated muon detectors which indirectly provide information about the directions of neutrinos. The length of the decay tunnel should be chosen such that most of the pions generating neutrinos will decay; however, the number of muon decays is kept low because among their decay products there are electron flavour neutrinos which are the main background for $\nu_\mu \leftrightarrow \nu_e$ oscillations.

$$\mu^+ \rightarrow e^+ \nu_e \, \bar{\nu}_\mu \tag{3.5}$$

The following relatively rare (branching ratio $\approx 4.8\%$) decay of K^+ is another source of the ν_e background.

$$K^+ \rightarrow \pi^0 e + \nu_e \tag{3.6}$$

As can be seen from decays (3.1) - (3.4), the produced beam is dominantly composed of ν_μ ($\bar{\nu}_\mu$) if positively (negatively) charged mesons are chosen and focused. However, the beam is polluted by other neutrino flavours like $\bar{\nu}_\mu$ (typically 1-7%), ν_e (usually $< 1\%$), $\bar{\nu}_e$ (usually $< 0.1\%$) coming from the muon decays (3.5), K_{e3} decays (3.6) and oppositely charged pions passing through the magnets. A good knowledge of the ν_e intrinsic beam contamination is crucial for studies of $\nu_\mu \leftrightarrow \nu_e$ oscillations. For low energy beams the ν_e is mostly due to muon decays, while the kaon decays become more important at higher energies. For example, at 4.5 GeV proton energy 10% of the total ν_e contamination comes from K_{e3} decays [61].

In the literature, one can often find a term 'superbeams'. These beams are simply the conventional neutrino beams, but with much higher intensities than those obtained up to now. This requires the design and construction of powerful proton drivers, dedicated focusing systems and targets that can survive very high energy deposits. In the ongoing studies around the world, several innovative ideas are considered, such as the usage of a multiple target instead of a single one or a closed horn scenario instead of the NuMi-like horn and reflector design.

3.3. Other concepts of neutrino beams

The current programme for the future long baseline neutrino experiments is based on the superbeam technology. However, a few years ago before the θ_{13} measurement, several new ideas of neutrino beam technologies had been developed for the case of very small values of θ_{13}, resulting in a very difficult measurement of δ_{CP}. These new concepts were neutrino factories providing neutrinos from the decays of accelerated muons and beta beams resulting from the decays of accelerated β-unstable isotopes.

3.3.1. Neutrino factories

The idea of the Neutrino Factory was born out of the Muon Collider proposal [62]. Various designs have been developed, but the basic idea is similar. The

principle is to extract muons produced in the pion and kaon decays and then cool, bunch and accelerate them. These muons are then injected into a storage ring, in which they decay in the long straight sections pointing towards far detectors. The high luminosity accelerated muons are the source of clean, intense and collimated beams of ν_e and $\overline{\nu}_\mu$ for accelerated μ^+ (or $\overline{\nu}_e$ and ν_μ for μ^-). Thus, for μ^+ mode the two oscillation channels will be simultaneously observed: the $\nu_e \rightarrow \nu_\mu$ which will be tagged by a μ^- in a far detector and $\overline{\nu}_\mu \rightarrow \overline{\nu}_\mu$ tagged by μ^+. The magnetised detector is necessary to distinguish between these two oscillation channels by the measurement of electric charges of the detected muons, .

3.3.2. Beta-beams

The Beta-beam idea was originally introduced as an adaptation of the muon storage ring idea to accelerated radioactive ions instead of accelerated muons [63]. The proposal was to produce $\overline{\nu}_e$ and ν_e beams from the beta decays of accelerated radioactive ions. Such a beam, consisting purely of electron neutrinos or electron anti-neutrinos, would be well collimated. The European EUROnu study assuming the use of the CERN accelerator has investigated the possibility of the high rate production, acceleration and formation of stable beams for the following isotopes being beta-emitters: ^6He, ^{18}Ne, ^8Li and ^8B [63].

3.4. Long baseline studies in Europe

The European experience in producing neutrino beams for a long baseline programme relies on the operation of the CNGS (CERN Neutrinos to Gran Sasso) ν_μ beam [35] mentioned in 1.4.2.

Since July 2008, for four years the LAGUNA (Large Apparatus studying Grand Unification and Neutrino Astrophysics) FP7 project had investigated seven European sites as the location for the future large underground laboratory to host one or more of the following detectors: Water Cherenkov with 1 Mtonne of water, Liquid Argon Glacier - type detector with 100 kton of Liquid Argon and Liquid Scintillator LENA detector with 50 kton of scintillator. Since September 2012 a new project LAGUNA-LBNO (Long Baseline Neutrino Oscillation experiment) [64], has been carried out with an extended programme of accelerator neutrino physics, focused on investigating the possibilities of the Pyhäsalmi mine in Finland as the site for the far detector in the long baseline experiment using two neutrino beam scenarios. At first, a neutrino beam based on the hypothetical High Power PS2 proton accelerator proposed as one of options for upgrading

the CERN accelerator complex, with 50 GeV protons and a very high repetition rate has been simulated. Secondly, the study was performed for the neutrino superbeam produced at CERN using 400 GeV protons from SPS. Additionally, the Russian accelerator complex Protvino has also been considered as a neutrino beam source based on the 70 GeV proton beam after the accelerator upgrade planned in the near future. The distance between CERN and Pyhäsalmi is 2300 km and the Protvino-Pyhäsalmi distance is 1160 km. The detailed simulations of both, CERN and Protvino based hypothetical neutrino beams, aiming Pyhäsalmi mine equipped with 20 kton in the initial phase and up to 100 kton LAr-TPC detector in the next phases, have been performed by the collaboration and the results can be found in the final report of the project [65].

The LAGUNA-LBNO project was not included into the "2013 European Strategy for Particle Physics" [66]. Instead, the CERN Neutrino Platform programme has been proposed and funded to support the participation of European neutrino physicists in the long baseline neutrino experiments in the US and Japan. In the near future none of the accelerator based neutrino experiments is foreseen to be performed in Europe.

3.5. Neutrino oscillation projects in the USA

The accelerator based neutrino studies have become the first priority for Fermilab, the largest particle physics laboratory in the USA. The NOvA experiment at the NuMI beam, mentioned in Chapter 1 is currently the largest neutrino experiment in the laboratory. Two new big neutrino oscillation experiments are under preparation: the SBN (Short Baseline Neutrino) experiment [67], with a time line of two years from now, LBNF-DUNE (Long Baseline Neutrino Facility - Deep Underground Neutrino Experiment) [68] with a realisation plan for 10-20 years from now. They are shortly introduced below.

3.5.1. SBN experiment

There is a proposal for the SBN experiment composed of three LAr-TPC detectors located on the Booster Neutrino Beam (BNB) at Fermilab [67]. The preparations are performed by three detector collaborations: the ICARUS-WA104 Collaboration; the LAr1-ND Collaboration and the MicroBooNE Collaboration.

This new SBN experiment is designed to resolve a class of experimental anomalies in neutrino physics, including the question concerning the existence of

sterile neutrinos at the eV mass-scale. The studies will be done for both appearance $\nu_\mu \rightarrow \nu_e$ and disappearance $\nu_\mu \rightarrow \nu_\mu$ oscillation channels for both neutrinos and antineutrinos. The SBN physics programme also includes the study of neutrino-Argon cross sections using the well characterized neutrino fluxes of the BNB beam. The SBN detectors will also have the possibility to record events from the off-axis NuMI beam with a energy spectrum different than that from BNB. Finally, the experiments on the short baseline offer the excellent opportunity to further develop the LAr-TPC technology and analysis methods for the future long baseline neutrino programme at Fermilab.

3.5.2. Long-Baseline Neutrino Facility (LBNF) and Deep Underground Neutrino Experiment (DUNE)

The programme is carried out as an international experiment for neutrino science and proton decay studies, named DUNE - the Deep Underground Neutrino Experiment. The facility required to support this experiment, the Long-Baseline Neutrino Facility (LBNF), is hosted by Fermilab. LBNF and DUNE will together prepare a new, high-intensity neutrino beam at Fermilab, a high-precision near detector on the Fermilab site and a massive liquid Argon TPC detector (ultimately 40 ktons of fiducial mass) as a far detector installed deep underground at the Sanford Underground Research Facility in South Dakota on the 1300 km baseline. The main physics goal is the precision of the study on neutrino oscillation phenomenon, including δ_{CP} measurement and mass hierarchy determination.

3.6. Neutrino oscillation projects in Asia

The T2K (Tokai to Kamiokande) experiment is currently the most important accelerator long baseline experiment in Asia. After successful operation in neutrino mode, studying both ν_μ disappearance and ν_e appearance channels, T2K is currently is operated in antineutrino mode. The main goals for the next seven years is the δ_{CP} determination at the 3 sigma level. In addition, the T2K baseline of 295 km is well complementary to the NOvA experiment with 810 km baseline in view of the common determination of the δ_{CP} and mass hierarchy.

HyperKamiokande is a water Cherenkov detector proposed as the successor of SuperKamiokande in Japan for neutrino study [50]. Its total mass will be at the order of 500 kton. If realised, it will be operating as a long baseline accelerator neutrino experiment at the same neutrino beam facility and configuration as T2K, i.e. at a distance of 295 km from J-PARK and 2.5° off-axis. The systematic errors

are already well understood based on the SuperKamiokande and T2K experience, but the big advantage will be high neutrino event statistics due to large fiducial mass. The physics goals of the long baseline accelerator neutrino configuration of the HyperKamiokande detector are the δ_{CP} measurement, MH determination and precision studies of neutrino oscillation parameters.

Also the next generation reactor neutrino experiments, JUNO in China and RENO50 in Korea, are proposed in a medium baseline configuration. The main purpose of those experiments is to precisely measure Δm^2_{12}, θ_{12} and θ_{13} and determine the mass hierarchy as described in Section 2.1.

The proposed India Neutrino Observatory (INO) in India project assumes the construction of the Iron Calorimeter type detector. It will be used for the atmospheric neutrino study but there were also ideas and theoretical studies of using it as a far detector for a long baseline neutrino experiment [49] with a neutrino beta beam produced at CERN. However, the θ_{13} mixing angle is relatively large and such an experiment is not needed for now.

Chapter 4

Studies for the SUNLAB location

The Sieroszowice UNderground LABoratory (SUNLAB) is a Polish R&D project for building an underground laboratory. The idea of such a laboratory was connected with the excitement caused by the discovery of neutrino oscillation at the beginning of this century and was related to the initiative of Antonio Ereditato and Andre Rubbia [58] to look for a possible location for a huge liquid Argon detector for studies of neutrino properties, neutrino astrophysics and proton decays. This initiative evolved into the European FP7 LAGUNA project, already mentioned in Chapter 3.

When LAGUNA started in 2008, the Polish site in the Polkowice - Sieroszowice mine, named SUNLAB, was one of the seven locations considered as future hosts for the large underground laboratory [69]. Geomechanical feasibility studies for the SUNALB laboratory, hosting a 100 kton liquid Argon GLACIER detector in anhydrite rock, were performed in the years 2008-2011 within LAGUNA and gave very positive results [70], [71]. The neutrino long baseline experiment coupled with the neutrino beam from CERN was the main motivation for LAGUNA and therefore the dedicated study for SUNLAB as a host of the far detector for the long baseline experiment was needed.

The study for SUNLAB as a site for such an experiment has been performed within the Polish National Science Centre (NCN) Preludium grant (UMO-2011/03/N/ST2/01971), in parallel to the LAGUNA-LBNO project focused on the Pyhäsalmi mine in Finland at a distance of 2300 km from CERN. The SUNLAB study is also the subject of the presented thesis.

Now, the status of neutrino long baseline physics is more clear. It is known that a new large underground laboratory in Europe will not be built in the near future, while the LBNF project in the USA has become a flagship of the research

programme at Fermilab.

However, the salt rock in Sieroszowice is characterised by an extremely low level of the natural radioactivity. Therefore the SUNLAB project of a small, low background laboratory is still under consideration and was placed on the Polish Roadmap for Research Infrastructures in 2011 and 2013.

In this chapter the SUNLAB location and results of the geomechanical studies of the large laboratory as well as measurements of the natural radioactivity performed in the Polkowice-Sieroszowice mine will be presented.

4.1. Characteristics of the Polkowice-Sieroszowice mine and the region

4.1.1. ZG Polkowice-Sieroszowice

The proposed host of the SUNLAB laboratory is the Polkowice-Sieroszowice mine (Zakład Górniczy Polkowice-Sieroszowice) [69], [72] . It is one of the divisions of the KGHM Polska Miedź S.A. holding of copper mines and metallurgic plants. It is located in Kaźmierzów, district Polkowice, province Lower Silesia in south-western Poland. The mine currently operates in three mining regions (Polkowice II, Radwanice Wschód and Sieroszowice I) with a total exploitation underground area of about 178 km^2. The Polkowice-Sieroszowice mine mines out copper ore and salt. It has been under continuous operation for more than 30 years and the mine development strategy assumes further lifetime to be no less than 40 years. The mine infrastructure includes a number of large shafts (up to 7.5 m in diameter - P7 shaft), an extended network of underground roads for a car transport, a very efficient ventilation system and machines for extraction work. For the SUNLAB location it is important that the Polkowice-Sieroszowice region is characterised by a tectonically stable and good quality hard rock (thick layers of dolomites and anhydrites) and locally saltrock. The depth of the existing and planned excavations varies from about 600 m to about 1500 m below the surface.

4.1.2. Geological conditions

The mine region geological structure and seismic behaviour is very well known thanks to constant monitoring and the fact that the mine has been operating for a long time. The Polkowice-Sieroszowice region lies within the monocline of the Sudetic Foreland. In a broad outline, this region is built of three main

rock formations. The rock bed is formed by crystalline and sedimentary rocks such as Red Sandstone from the Proterozoic and the Paleozoic periods. The Permian and Triassic sedimentary systems over them include copper-bearing shales, dolomite-anhydrite and saltrock. Finally, the Cenozoic cover deposits like clay and sands are from the Paleogene, Neogen, and Quaternary periods. A typical geological profile in the Polkowice-Sieroszowice mine region is presented in Figure 4.1.

The study of hydrogeological conditions [70] in the considered area shows that water-bearing deposits are in the shallow Cenozoic clay and sand layers and in the Permian limestone as well as Red Sandstone, i.e. in geologically different areas than anhydrite and salt strata. It means that thick anhydrite and salt layers are dry and this makes them very good candidates for the location of the detector caverns; the large ones for LAGUNA in anhydrite and the smaller ones for a smaller low background laboratory in salt.

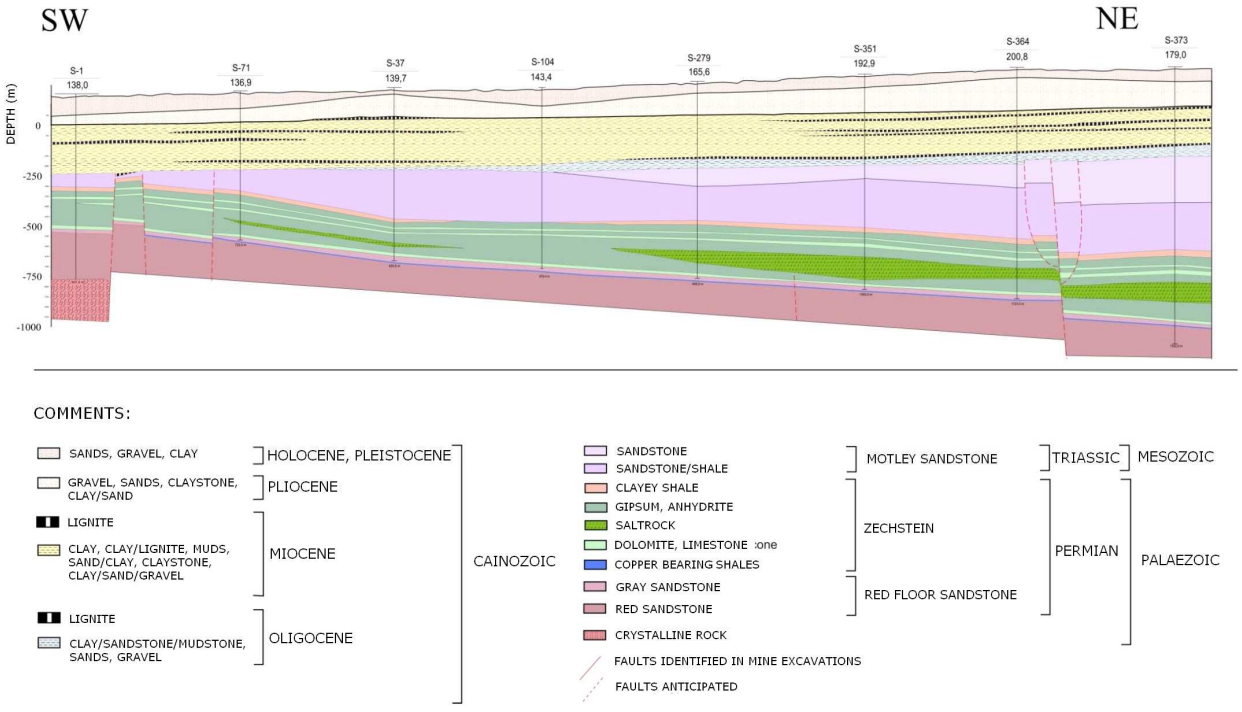

Figure 4.1. A typical geological cross-section in the Polkowice-Sieroszowice mine region.

4.2. Geomechanical studies and designs for underground laboratory location

The geomechanical study of the underground 100 kton detector's cavern was performed by KGHM Cuprum CBR in cooperation with the Mineral and Energy Economy Research Institute of the Polish Academy of Sciences (IGSiEM PAN) [70] [71]. The detector was foreseen to hold 100 kilotons of liquid Argon with some additional space for the gas phase and readout electronics at the top of the detector. The detector design assumed a cylindrical shape with an additional dome of the diameter $D = 70\ m$ and total height $H = 27.0\ m$. The main goal was to find the best underground location for the GLACIER detector. The geomechanical studies and simulations were performed based on three sources of the input information. Firstly, a great advantage for the study was the KGHM geological database developed over a the long period of underground extraction in the mine area considered for the GLACIER location. Secondly, it was the availability of the results of direct measurements of rock samples, which were performed by IGSiEM PAN and KGHM in their specialized laboratories. Within these measurements several rock properties were described, such as: strength, elastic properties (Young modules), rock mass mechanical properties and rheological properties of rock salt. The third source of the input information contained the time dependent movement of the salt rock coming from physical measurements performed in a large chamber (15 m wide, 18 m high, 100 m long, about 950 m underground), excavated in salt deposit and observed by KGHM for a period of a dozen or so years.

All rock mechanical parameters were prepared and properly scaled to design the parameters in the rock mass units. The design of the caverns' shape was consulted with the detector tank designer and the considered cavern shapes constituted generally a combined structure of different spherical surfaces to avoid sharp corners and flat planes. The numerical stability analyses were performed for the following three locations in anhydrite and one location in salt.

1. cavern in salt rock at a depth of 983 m below surface (b.s.),
2. cavern in lower anhydrite at a depth of 1112 m b.s.,
3. cavern in upper anhydrite at a depth of 617 m b.s.,
4. cavern in upper anhydrite at a depth of 639 m b.s.

The analyses were performed with different salt flow models, assuming standard expected seismic behaviour, elastic-plastic with a strain softening model for anhydrite and elastic-plastic model for the remaining rocks. The computer program FLAC3D based on the finite element approach was used. The results

were: stress and strain displacement contours, instantly after the excavation and after 40 years (for saltrock and anhydrite under the saltrock layer exclusively); locations of unstable parts of the surrounding rocks (the so called spalling). As an example, a result of the stress simulation for the GLACIER cavern in anhydrite, prepared by KGHM Cuprum, is presented in Figure 4.2.

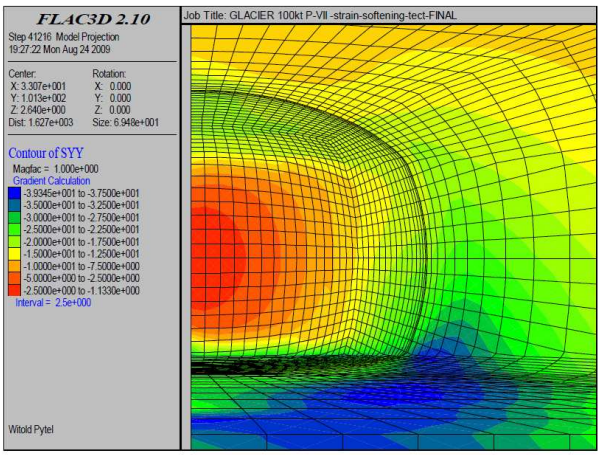

Figure 4.2. An example of stress simulations for the Glacier cavern in anhydrite [70]. Presented contours are given in [MPa] units.

The geomechanical studies showed that any contact zone between different geological layers, in particular between the salt and anhydrite layers, dramatically reduces the stability of the large chamber, so the only safe location is inside a thick homogeneous layer. Although salt layers are characterized by very low natural radioactivity, the creeping process is very fast. It would cause large displacements of the walls, bottom and roof of the chamber in short time periods and more than 3 m in 50 years. Deep locations located more than 1000 m b.s., are better in a sense of the reduction of cosmic radiation induced background; however, usually such locations are close to mining activities, which may induce seismicity.

After studying three possible sites in anhydrite and one in the salt layer (see the list on the previous page), the location (4.) in anhydrite at a depth of 639 m b.s. (1400 m w.e.) was found to be the best option for the 100 kton GLACIER detector cavern. The numerical calculations indicated that from a geomechanical point of view it is possible to excavate a large dimension chamber at this location and that viscoplastic properties of anhydrite rock are insignificant at this depth. This is a 115 m thick, homogeneous layer of good quality anhydrite rock in a calm area far from mining activities. The stability of the chamber could be additionally improved by bolting. Another big advantage of this location is a large P-VII shaft

in the near distance. Figure 4.3 depicts the project of the GLACIER cavern with safety chambers, galleries and technical infrastructure combined with the existing mine infrastructure and large P-VII shaft, resulting from the geomechanical studies within the LAGUNA project.

The cavern for the LENA scintillator detector has also been considered. The LENA design assumed a tall cylindrical detector tank 100 m in height and 30 m in diameter, placed very deeply underground, therefore the detector cavern could not be contained in a single geological layer. The horizontal version of the LENA cavern was feasible.

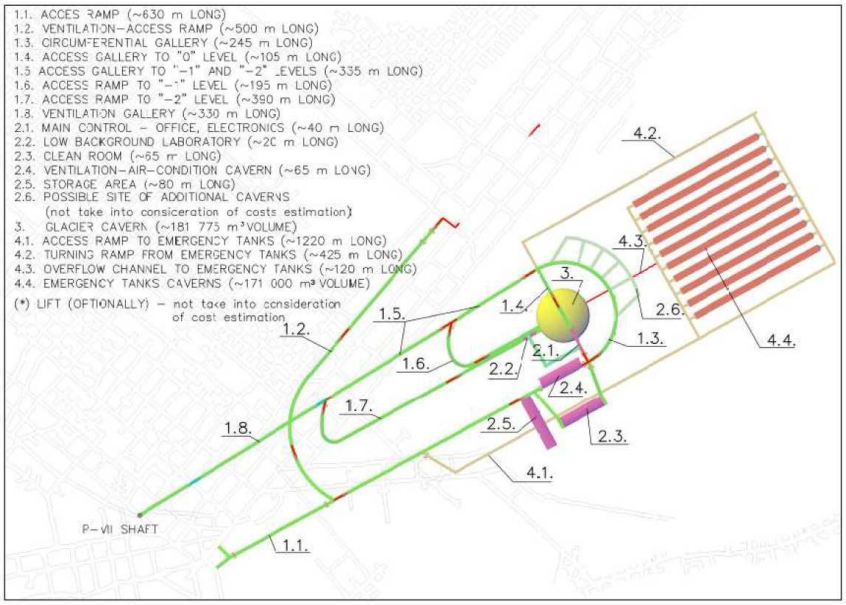

Figure 4.3. The project of the Glacier cavern with safety chambers and technical infrastructure combined with the existing mine infrastructure near the P-VII shaft in anhydrite at 639 m below surface.

4.3. Measurements of the natural radioactivity in the SUNLAB location

In this section the main results from the measurements of the natural radioactivity in the Sieroszowice salt deposit, performed within the cooperation of the H. Niewodniczański Institute of Nuclear Physics (IFJ PAN) in Kraków, Silesian University in Katowice and National Centre for Nuclear Research (NCBJ), branch in Łódź, are presented. The measurements have been performed in the P1 salt cavern located 950 m below the surface in the Polkowice-Sieroszowice

mine. The measurements took place in 2005 [73] and 2014 [74]. Additionally, the alpha spectroscopy measurements of anhydrite and salt rock samples from the Polkowice-Sieroszowice mine were performed at the IFJ PAN and the results were also presented in [73].

4.3.1. In-situ measurements

The radioactivity background in underground P1 salt chamber, originating from natural radionuclides, was measured using portable gamma-ray germanium spectrometry workstations. In 2004 it was the Ortec Industries setup, which consistsed of a HPGe detector (specification: 30% efficiency, Ge cristal 59 mm long and 58.6 mm in diameter). The spectrum of the detected gamma rays is presented in Figure 4.4. The following concentrations of natural isotopes were determined: ^{226}Ra (from ^{238}U series) equal to 3.1 ± 0.3 Bq/kg (average from ^{214}Pb and ^{214}Bi peaks), ^{232}Th equal to 0.7 ± 0.2 Bq/kg (average from ^{212}Pb and ^{228}Ac peaks) and ^{40}K equal to 9.2 ± 1.7 Bq/kg. The integrated background counting rates in the energy range of $40 - 2700$ keV were equal to 2.30 ± 0.02 [CPS/(keV kg)] (CPS means counts per second).

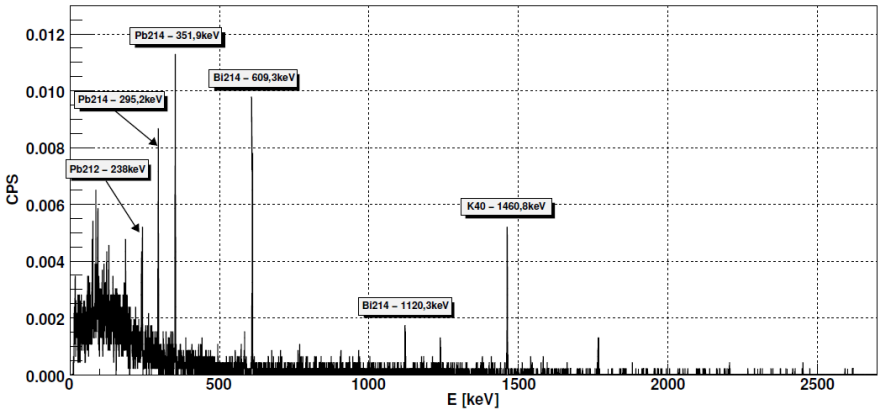

Figure 4.4. The gamma spectrum measured in the P1 salt cavern in the Polkowice-Sieroszowice mine [73].

Measurements with the same setup were performed by a group from the University of Silesia in the following underground laboratories in Europe within the European project ILIAS: Laboratoire Souterrain de Modane (LSM) Frejus in France, Laboratori Nazionali del Gran Sasso (LNGS) Assergi in Italy and the Boulby Underground Laboratory in the UK [75]. The results presented in Table 4.1 show that the natural radioactivity in the P1 salt cavern is 10-30 times lower than in other European underground laboratories.

Integral counting rates 40-2700 keV	[CPS/keV kg]
LSM Frejus	66.06 (0.03)
LNGS Gran Sasso	57.68 (0.02)
Boulby	23.83 (0.05)
Sieroszowice (2004)	2.30 (0.02)

Table 4.1. Integrated gamma background counting rates measured in the European underground laboratories [75].

The second round of measurements was performed in 2014 and 2015 with two different Germanium spectrometers, namely a low-background high-purity Germanium detector (HPGe) manufactured at IFJ PAN in Kraków and a commercially available portable coaxial Germanium spectrometer with reverse cathode (REGe), Canberra Industries Inc.

The specification of the low-background HPGe detector is as follows: the Germanium monocrystal mass is about 600 g, 56 mm in diameter and 53 mm in height, giving 25% relative efficiency; 2.1 keV FWHM at 1.33 MeV ^{60}Co line, no lead shield was used in the underground setup and the detector was placed 60 cm above the cavern's floor. The gamma spectrum obtained by the low-background spectrometer after a 24 hour measurement is presented in Figure 4.5.

The specification of the portable REGe spectrometer is as follows: the Germanium crystal of 40% efficiency, 61 mm in diameter and 63 mm in length, resolution of 2.08 keV and the Peak-to-Compton ratio of 57/1 at 1.33 MeV ^{60}Co line. The portable spectrometer was used in two configurations: with a 2.5 cm thick lead shield-collimator and a bare detector without shielding. The detector was placed a few centimeters above the cavern's floor. The results of a 24-hour measurement are presented in Figure 4.6.

The use of two detectors in different configurations gave the possibility to make several checks and compare the results. The main findings are: within the energy range of 50 to 2700 keV, the gamma-ray count rates varied from 5.93 $s^{-1}kg^{-1}$ to 6.32 $s^{-1}kg^{-1}$ for the low-background and portable detectors, respectively; the gamma flux of 0.124(2) $cm^{-2}s^{-1}$ was observed by the portable HPGe; the high purity portable HPGe detector measured the Uranium/Actinium/Thorium ratio as being equal to 0.602(120)/0.016(2)/0.023(2) and with the shielding applied the ratio was measured as being equal to 0.122(7)/0.019(1)/0.016(2). The compari-

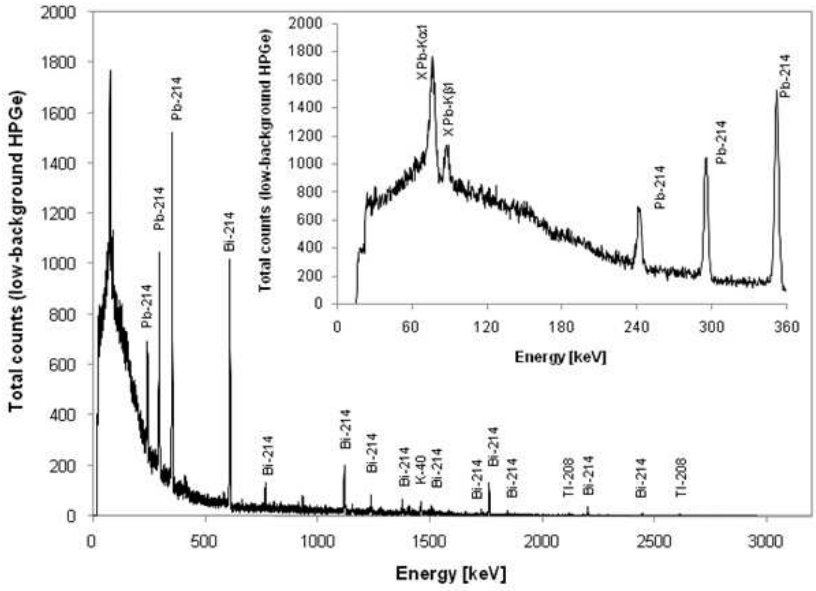

Figure 4.5. The gamma spectrum measured in the P1 salt cavern in the Polkowice - Sieroszowice mine for 24 hours by the low-background HPGe spectrometer without shielding [74]. The inset shows a zoom of the low-energy part of the spectrum up to 360 keV.

son of the spectra registered by the portable REGe detector and the constructed low-background HPGe spectrometer demonstrates that the internal impurities within the detector setup itself (visible in the Canberra REGe detector) in the environment with a very low-level of natural radioactivity, as it is in the P1 salt cavern, are the main sources of the background signal influencing the registered spectra.

The in-situ measurements of radon concentration in air were performed using AlphaGUARD PQ2000 ionization chambers within the measurements performed in the Sieroszowice mine in 2004. The radon concentration was measured in five locations: three of them were situated near the P1 cavern entrance, one in the middle, and one near the wall opposite the entrance. The measurements were performed during normal operation of the mine, i.e. the standard ventilation system was on. The results showed that most of the radon in the salt cavern comes with the air introduced by ventilation. In the well-ventilated place near the cavern entrance the radon level was 45 Bq/m^3, while inside the cavern with still air the level was 15 Bq/m^3. Unlike in natural caves or coal mines, the radon concentrations in the Polkowice-Sieroszowice mine are similar to radon levels observed in open air , i.e. the radon presence is caused mainly by the regularly working

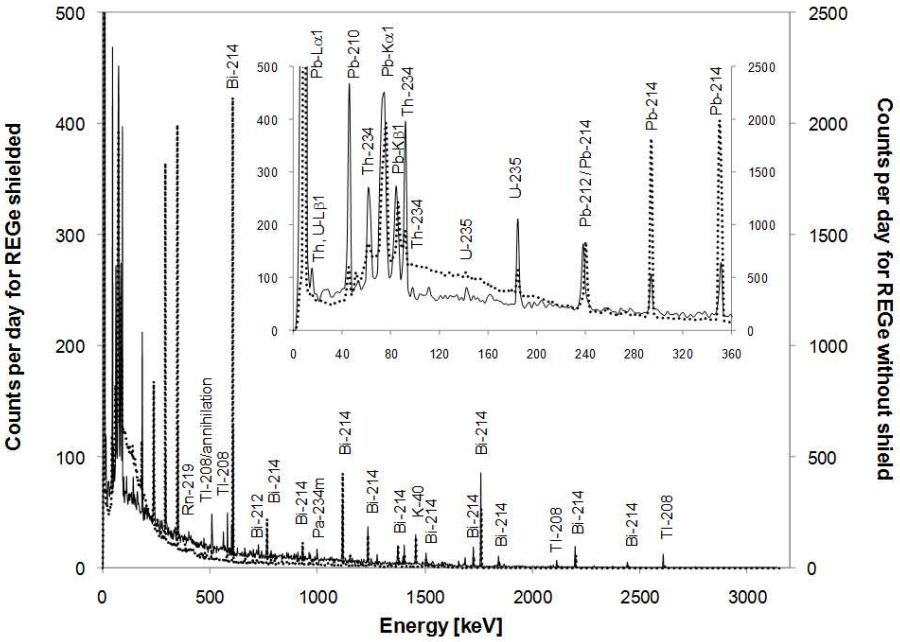

Figure 4.6. The gamma spectrum measured in the P1 salt cavern in the Polkowice - Sieroszowice mine for 24 hours by the portable spectrometer (REGe) with 2.5 cm lead shielding (solid line) and without shield (dotted line) [74]. The inset shows a zoom of the low-energy part of these spectra up to 360 keV. The scaling factor of vertical axes is equal to 5 and corresponds to the ratio of ^{40}K peak counts for unshielded vs. shielded detector

ventilation system. The salt layer seems to be a good protection against radon exhalation from deeper geological structures.

4.3.2. Spectroscopy measurements of rock samples

Several samples of salt rock and anhydrite from the Polkowice-Sieroszowice mine were analysed for natural radioactivity in 2004 and in 2006, both series of measurements being performed at IFJ PAN. The measurements were done using a low background gamma spectrometry with muon-veto shield and by alpha spectrometry (Silena Alpha quattro spectrometer) preceded by the radiochemical procedure.

The results of the measurement are presented in Table 4.2. All salt rock samples from the Polkowice-Sieroszowice show a very low concentration of radioactive traces. They are within an order of magnitude in agreement with the result of the extrapolation from the time of the deposit formation without significant contamination afterwards. Even the anhydrite rock has a much lower radioactivity

level than usually other measured rock samples.

Summarising, the values of Thorium and Uranium concentrations are very low (less than 1 Bq/kg) and much smaller than those for a typical rock (e.g. for granite about 20-30 Bq/kg). Both alpha and gamma spectrometric measurements also show that the salt deposit in the Polkowice-Sieroszowice region is characterised by a very low potassium content, which is positively surprising because Potassium is a common admixture in NaCl salt deposits.

	salt rock [Bq/kg]	anhydrite [Bq/kg]
^{238}U	0.0165 ± 0.0030	0.82 ± 0.10
^{234}U	0.0225 ± 0.0030	0.76 ± 0.09
^{232}Th	0.008 ± 0.001	0.52 ± 0.15
^{230}Th	-	1.26 ± 0.24
^{40}K	4.0 ± 0.9	-

Table 4.2. The results of alpha and gamma spectroscopy measurements of rock samples from the Polkowice-Sieroszowice mine [73].

4.3.3. Dose measurements

Kerma (kinetic energy released per unit mass) in the P1 salt cavern was measured using high sensitive thermoluminescent MCP-N (LiF: Mg, Cu, P) detectors. The measurement was performed by the Laboratory of Individual and Environmental Dosimetry at IFJ PAN and the readout and annealing conditions were applied according to standards. Because of the expected low background, detectors were exposed for 243 days (24.03.2005 - 22.11.2005). They were packed in badges, additionally covered in foil to avoid any contact with salt dust which is thermoluminescent. The dosimeters were hanged on the walls of the salt cavern in many places. The result is as follows: the average dose rate is 1.8 nGy/h. For comparison, a typical dose measured in Krakow 1 m above ground is at a level of 65 nGy/h. The dose measurement result is consistent with the results of other natural radioactivity measurements presented above, confirming a very low level of natural radioactivity in the salt rock of the Polkowice-Sieroszowice mine.

4.4. Simulations of the cosmic ray background for the SUNLAB location

The Earth atmosphere with a rate of about one thousand per square metre per second is hit by cosmic ray particles. In a very wide energy range these are mainly protons with some alpha particles and less than one percent of heavier nuclei. The primary cosmic rays interact with atom constituents of the atmosphere and produce cascades and secondary particles, such as hadrons, photons, neutrinos and charged leptons. The origin of primary cosmic rays and the evolution and composition of atmospheric cascades have been studied for tens of years. To avoid the background coming from the cosmic radiation, the experiments studying rare events such as neutrino interactions or searching for proton decays are performed in underground laboratories to use natural rock as shielding. Still, very penetrating particles are present even in deep underground locations. Muons are the most penetrating component of cosmic rays, besides neutrinos, which is due to their long lifetime and small cross section for interactions. Therefore, muons give the dominant background signal from cosmic radiation in deep underground laboratories. Yet, unlike neutrinos, they are easy to detect because they are charged.

The cosmic muon penetration and survival depend on the rock density and underground depth of the detector cavern. The standard rock density is defined as $\rho = 2.65\text{g/cm}^3$; however, the rock above the salt deposit in the Sieroszowice region is less dense and its average density is $\rho_{Sieroszowice} = 2.30\text{g/cm}^3$. The P1 salt cavern depth is 950 m b.s., and this level was assumed in cosmic muon simulations for the low background SUNLAB laboratory. This depth is equivalent to 825 m of standard rock or is 2100 m water equivalent.

The MUSUN is a fortran - based simulation package dedicated to the simulation of the cosmic muon transportation through geological structures [76]. The MUSUN based simulations performed for my master thesis [77] gave the expected muon flux $I_\mu = 1.23 \times 10^{-7} cm^{-2} s^{-1}$. The energy and angular distributions of cosmic muons at a depth of 950 m, corresponding to 825 m s.r., are shown in Figures 4.7 and 4.8. The mean muon energy at this depth is $\langle E_\mu \rangle = 247.30$ GeV, and the mean vertical angle is $\theta = 31.52°$.

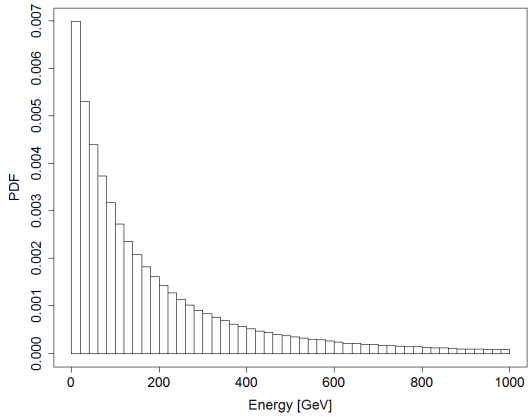

Figure 4.7. The expected muon energy spectrum at a depth of 950 m below the Earth's surface in the SUNLAB location corresponding to 825 m of standard rock. The energy spectrum is presented as a probability density function (PDF). The simulated MC sample used for the analysis was 10 000 events.

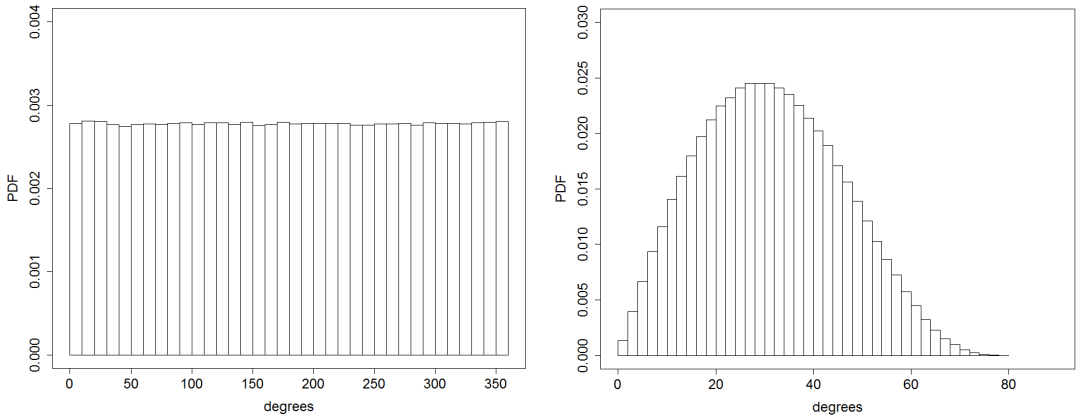

Figure 4.8. The expected muon azimuthal angle ϕ (left) and vertical angle θ (right) distributions at a depth of 950 m below the surface in the SUNLAB location corresponding to 825 m of standard rock. The distributions are presented as probability density functions. The simulated MC sample used for the analysis was 10 000 events.

Chapter 5

Software tools

In this chapter the software used for the studies presented in this thesis is described. All the examples given to illustrate the structure of the simulation programs come from the code developed by the author. The simulations of the neutrino oscillations and calculations of the sensitivities for the long baseline experiment at SUNLAB have been done using the GLoBES program. The simulations concerning interactions with matter, such as the neutrino beam production and observation of the signal in the far detector, have been performed using Geant4 and FLUKA software packages. A considerable part of the calculations was carried out with the help of the cloud computer system Cracow Cloud One (CC1) at IFJ PAN [78].

5.1. GLoBES

The software used in this thesis to perform the analysis of sensitivities for the discovery of the CP violation in the neutrino sector (presented in Chapter 8) is the General Long Baseline Experiment Simulator, i.e. GLoBES (v3.1(2010)) [79]. This modern open source software package has been used in most of the simulation studies concerning neutrino oscillation experiments, in particular the accelerator long baseline ones. In this thesis it has been used to describe the whole process of neutrino oscillations for SUNLAB, from the source at CERN to the signal observation in the far detector. The description of the experiment settings at an abstract level has been done using the GLoBES dedicated language AEDL (Abstract Experiment Definition Language). GLoBES also provides the C-library and a number of functions to compute many features, such as expected event rates, systematic errors and $\Delta\chi^2$ for oscillation parameters. However, in order to obtain the results of the oscillation experiment performance using GLoBES several external input data are needed. The most important ones are the neutrino flux and the detector response.

5.1.1. Neutrino flux specification

Let us start with the neutrino source description. For the simulated neutrino beam the neutrino fluxes of all neutrino flavours, belonging to either the signal or background components, have to be delivered by the user. The neutrino beam structure is quite complicated and specific for each experiment, depending on the target and focusing system design. The oscillation probabilities studied in this thesis are $P(\nu_\mu \to \nu_e)$ in appearance mode and $P(\nu_\mu \to \nu_\mu)$ in disappearance mode; $P(\overline{\nu}_\mu \to \overline{\nu}_e)$ and $P(\overline{\nu}_\mu \to \overline{\nu}_\mu)$ for the antineutrino beam accordingly. This means that an interesting signal always comes from ν_μ for neutrino mode or from $\overline{\nu}_\mu$ for antineutrino mode. Other neutrino beam components, like $\overline{\nu}_\mu$ ν_e, $\overline{\nu}_e$ (ν_μ $\overline{\nu}_e$, ν_e for antineutrino mode), are parts of the background.

For the GLOBES simulation, one has to prepare a file containing the neutrino and antineutrino energy spectra for both signal and background in a correct normalization at a distance of 100 km from the neutrino beam source, specific for a given experiment.

To handle different sources and simulation of flux files with different original normalization, the user of the GLOBES can use an additional factor $@norm$ to make sure that the final factor for event rate calculation for each GLOBES experiment is well defined. The normalization factor for the event rate calculation in GLOBES is defined as follow:

$$@norm = (1/5.2)(\mathrm{GeV}/\Delta_E)(\mathrm{cm}^2/A)(L/\mathrm{km})^2(\tau/m_u) \times 10^{-38}\,, \qquad (5.1)$$

where Δ_E is a width of the energy bin of 0.1 GeV, A is a unit area of 10^6 cm^2, L is a distance from the source equal to 100 km, (τ/m_u) is the number of target nuclei per unit target mass, which for liquid Argon is $(\tau/m_u) \sim 1\ \mathrm{kton}/1.66 \times 10^{-27}\ \mathrm{kg} \sim 6 \times 10^{32}$. Hence, in my GLOBES simulation $@norm = 1.1596 \times 10^{-7}$.

In the flux file the data is given as the number of neutrinos per A and Δ_E at a distance L. The cross section files are given for ν interaction with a single nucleon. The dedicated simulation has been performed to prepare these flux input files for the long baseline experiment at SUNLAB. The detailed description of the neutrino beam simulation is given in Chapter 6.

5.1.2. Detector response

The description of the detector response in the AEDL language for the simulation of a given neutrino oscillation experiment is the second important input. Details can be found in the online manual of GLoBES [79], here only the basic objects necessary for further discussion are described. The dedicated study concerning the detector response and energy resolution for the experiment at SUNLAB has been performed and is presented in Chapter 7.

In order to describe and experiment, two types of objects need to be defined: CHANNEL and RULE. CHANNEL is a link between oscillation physics and the detector response. It specifies the projection of the specific neutrino flavour produced by the source into the observed neutrino flavour in the far detector. For example, the $\nu_\mu \rightarrow \nu_e$ appearance signal channel is characterised by the information from the flux file for ν_μ, the oscillation probability for ν_μ to appear as ν_e, the ν_e cross section and detection properties, e.g. energy resolution. This channel for the experiment at SUNLAB is described as follows:

```
      channel(#appearance) <
@channel = #Sunlab_SPSflux.dat: +: muon: electron: #CC: #EN
>
```

This description in the AEDL language should be interpreted as follows: the information about the ν source should be taken from the file `Sunlab_SPSflux.dat` prepared for SUNLAB studies based on the SPS accelerator as a proton driver; the initial flavour is muon neutrino (`+: muon:`, for antineutrino would be `-: muon:`); the final flavour after the oscillation is electron neutrino (`electron:`); cross section values should be taken from the `CC.dat` file corresponding to Charge Current exchange cross section on nucleon; energy resolution is defined by `EN` variable.

The cross section files for CC and NC interactions are the standard files distributed together with the GLoBES2010 installation package. The description of the energy resolution can be done in two ways: automatic, for example using polynomial function $\sigma(E) = \alpha \cdot E + \beta \cdot \sqrt{E} + \gamma$ with $\alpha,\ \beta,\ \gamma$ being parameters; or manual, using directly the output of a detector Monte Carlo simulation and defining energy smearing matrices, sometimes called migration matrices, individually for each channel. Based on the channels, the expected event rates in the far detector are computed. One needs to define CHANNEL for each signal and

background reaction in both neutrino and antineutrino modes.

RULE is built out of CHANNELS and consists of "signal" and "background", which are weighted with efficiencies. Each rule implements independent systematics. The information in the rules specifies how the χ^2 is computed based on the event rates given by the channels. Within each rule, the event rates for different channels are added before calculating the sensitivity expressed by the χ^2 value.
An example of the RULE structure:

```
      rule(#NuE_appearance) <
@signal = 0.9 @ #appearance
@background = 0.80@#nu_e_beam : 0.005@#NC_bckg :  0.005@#nu_mu_disappearance
@signalerror = 0.10: 0.001
@backgrounderror = 0.05: 0.001
@sys_on_function = chiSpectrumTilt
@energy_window = 0.3 : 10.0
>
```

This description in the AEDL language should be interpreted as follows. The ν_e appearance channel (`#appearance`) will be used as a signal. The other channels, i.e. intrinsic ν_e beam contamination (`#nu_e_beam`), neutral current interaction (`#NC_bckg`) and ν_μ wrongly identified as ν_e (`#nu_mu_disappearance`) will be taken as a background. The numerical factor in the signal and background scales the event rate calculated for a specific channel to be taken during the sensitivity calculations. For example, `0.005@#nu_mu_disappearance` means that 0.5% of muon neutrino interactions will be misidentified and therefore will become a background for the χ^2 calculation. Similarly, the `0.005@#NC_bckg` means that 0,5% of all NC interactions are assumed to be wrongly reconstructed as ν_eCC interactions. A priori electron neutrinos present in the beam cannot be distinguished from electron neutrinos appeared from the oscillation; however, the detailed beam simulation shows that this background can be slightly reduced and `0.80@#nu_e_beam` means that 80% and not 100% of electron neutrinos present in the beam will contribute to the background. The signal error and background error variables have two components, e.g. `@signalerror = 0.05: 0.001`: The first one is an error of the normalization, here 5%. The second one refers to the energy calibration error of the signal, here 0.1%. The `@sys_on_function` and `@sys_off_function` commands specify the treatment of the systematics used for the χ^2 calculation, i.e. the systematics being switched on or switched off. GLoBES offers several ways of

systematic treatment, `chiSpectrumTilt` means that both the total event rate and shape of the spectrum are included in the sensitivity calculation. In this study only the mode with the systematics on and full spectrum analysis has been used. The energy window (`@energy_window = 0.3 : 10.0`) is given in GeV and defines the energy range to be used for the sensitivity calculations.

A set of RULES defines an EXPERIMENT. For the accelerator based experiment, discussed here, four rules have been created: ν_e appearance and ν_μ disappearance used as signals in both neutrino and antineutrino modes.

5.2. Simulation of particle interactions with matter.

Several simulations concerning interactions with matter have been performed within the framework of this thesis. In this section a short description of the Geant4 and FLUKA packages used for these simulations is presented.

5.2.1. GEANT4

Geant4 [80] is an open source toolkit for simulating the passage of particles through matter. It has been designed and implemented in an object-oriented technology in C++ programming language. It includes a range of functionalities such as tracking for a large set of particles and handling complex geometry designs. The physics models adapted in Geant4 include electromagnetic, hadronic and optical processes over a wide energy range. This toolkit is the result of the work of a worldwide collaboration of physicists and software engineers. Originally Geant had been developed at CERN for particle physics experiments, and then its use has been expanded into nuclear physics, accelerator design, space engineering, medical physics and other domains of science.

In this thesis Geant4 has been used for neutrino beam simulation described in Chapter 6. Proton interactions on a graphite target, meson production and propagation, magnetic horn shapes, finally the neutrino flux have been simulated using the GENEBES program of A. Longhin [81] based on Geant4 and dedicated to neutrino beam simulations.

5.2.2. FLUKA

FLUKA, similarly to Geant4, is a general purpose tool for calculations of particle transport and interactions with matter. Thanks to a very high accuracy

in the simulation of the interactions with matter for about 60 different particles in a wide energy range (up to 20 TeV for hadrons), FLUKA is commonly used in specific applications, such as simulations of accelerator shielding, target design, calorimetry, dosimetry, cosmic rays, radiotherapy etc. FLUKA is characterised by preserving correlations and by being predictive in the regions where experimental data are not available. However, the model parameters are fixed for all projectile-target combinations and energies and cannot be modified by the user.

Important for this thesis is the fact that the ICARUS simulation program is based on FLUKA. A dedicated Fortran77 routine, called ICA-FLUKA, was prepared to simulate neutrino and other particle interactions in liquid Argon. The detailed T600 LArTPC detector geometry description was also developed by the ICARUS collaboration using FLUKA. The ICA-FLUKA Monte Carlo tool was very well tuned and checked by the collaboration using data collected with the T600 detector during its tests in Pavia in 2001 and in the Gran Sasso Underground Laboratory in the years 2010 - 2013.

The FLUKA output file, containing neutrino events in the T600 detector in the `.flufz` format, can be visualised and analysed using the ICARUS collaboration reconstruction software. ICA-FLUKA and the reconstruction software have been used in this thesis to simulate a set of neutrino interactions in order to make the LArTPC detector characterisation and description for GLoBES more accurate. A more detailed description of this work is given in Chapter 7

5.3. Other software tools and packages.

The ROOT, R and Mathematica software tools have been used in this thesis for data analysis and visualization, calculations and plotting.

ROOT [82] is a data analysis framework well known and widely used in particle physics. Its compatibility with Geant4 is an additional advantage. Thanks to a tree-root filesystem ROOT is able to handle large sets of data.
R [83] is a language and software environment for statistical computing, popular in the scientific community. R provides a wide variety of statistical methods (linear and nonlinear modelling, classical statistical tests, time-series analysis, classification) and graphical techniques.
Mathematica 10.0 (Student Edition) [84] has been used mostly to calculate and

visualise the sensitivity levels for the CP violation discovery potential, described in detail in Chapter 8.

Chapter 6

Simulations of the neutrino beams for GLoBES

The definition of the neutrino source is the first step on the way to simulate the neutrino oscillations in a long baseline experiment. In the case of the SUNLAB laboratory in Poland, like for other locations studied in LAGUNA, the natural choice of the origin of the neutrino beam is CERN. Therefore, in this study the neutrino beams based on proton accelerators at CERN are considered. The distance from CERN to SUNLAB is 950 km, which defines the first oscillation maximum - the most interesting region to perform the $\nu_\mu \rightarrow \nu_e$ appearance study - as corresponding to the neutrino energy of 1.92 GeV. For the δ_{CP} study access to the second oscillation maximum would also be interesting, so a wide-band beam which covers neutrino energies down to about 400 MeV should be considered.

The simulation of such a beam is described in this chapter. It is based on the GENEBES program prepared by Andrea Longhin [81] within the framework of the EUROnu and LAGUNA projects. As a result, the neutrino and antineutrino flux at a distance of 100 km is delivered in a format suitable for the input to the GLoBES package.

6.1. The neutrino beam setup

As discussed earlier, a conventional neutrino beam is derived from the decays of charged π and K mesons, which are created in proton - nucleus interactions when a proton beam strikes a thick nuclear target. By a precise selection and monitoring of the π and K mesons, including their charges, neutrinos and antineutrinos can be selected and their energy spectra adjusted. The intensity of the neutrino beam and the quality of this adjustment depend on the proton driver properties and performance, the components and shape of the target as well as the design of the meson focusing system, usually based on the Van der Meer idea of magnetic horns.

In this study two separate cases of proton accelerators are considered. The first one is HP-PS2 (High Power-Proton Synchrotron) [85], a concept for the replacement of the CERN PS accelerator. As was mentioned before, this concept was studied within the LAGUNA project as a proton driver for the neutrino beam. In this thesis HP-PS2 served mainly for validation of the simulation program and understanding the beam production processes, because it has already been known that this upgrade is no longer considered by CERN.

The second case considered in this study is based on the existing, and very well understood SPS accelerator (Super Proton Synchrotron) currently under operation, but only after the realisation of the LHC Injectors Upgrade project (LIU) [86]. The LIU upgrades will result in an increase in the SPS proton beam power up to 750 kW. In addtion, the beam will have to be adjusted to the neutrino beam production, which is significantly different in the cycle structure from the beam prepared for the LHC. This will correspond to 7×10^{13} protons extracted from the SPS every 6 seconds. The main limitations on a higher proton intensity in SPS are beam losses in the beam injector chain. In this thesis the upgraded SPS proton beam has been used in the neutrino beam simulation and in the optimization of the focusing system.

The characteristics of both proton accelerators used in this studies are summarized in Table 6.1.

	HP-PS2	SPS
proton kinetic energy	50 GeV	400 GeV
extraction cycle (sec)	1.2	6
protons per cycle	25×10^{13}	7×10^{13}
p.o.t. per year	3×10^{21}	1×10^{20}
max power	2.4 MW	0.75 MW
E_{tot} (GeV $\times$ p.o.t/yr)	15×10^{22}	4×10^{22}

Table 6.1. Characteristics of the proton accelerators used in the beam simulation as proton drivers: HP-PS2 [85], [87] and SPS [88].

The wide band neutrino beam for the long baseline experiment analysed in this thesis is similar to the NuMI neutrino beam - Neutrinos at the Main Injector [89] [90] at Fermilab, sometimes called in the literature 'NOvA-like'. This model has been chosen because it is a relatively modern, well-tested setup. It consists of a one metre thick graphite target, a focusing system of two thin magnetic

horns named horn and reflector, and a hundred metres long meson decay tunnel.

The parameters characterising the beam line setup, which are used in the simulation program and in the optimization process, are summarized in Table 6.2. These are: the longitudinal position of the target - T_{DZ}, the horn-reflector distance DZ, the current circulating in the magnetic horns - I_h, the diameter - R_{DT} and length - L_{DT} of the cylindrical decay tunnel.

parameter	value
T_{DZ}	113 - 115 m
DZ	10 m
I_h	1000 A
R_{DT}	4m
L_{DT}	100m

Table 6.2. Parameter values used in the Geant4 simulation for the beam line setup.

The target was modelled as a cylinder 1.0 m long, 4 mm in diameter of graphite with a density $\rho = 1.85$ g/cm^3. The majority of π and K mesons produced in the proton - target interactions enter the focusing system composed of two cylindrically symmetric magnetic horns. The two magnetic horns are used as lenses, as was described in Section 3.2 and illustrated in Figure 3.1. The horn focuses particles of one charge, e.g. those positively charged, and defocuses, rejecting the particles of the opposite charge. In the horn particles with lower momenta are focused stronger, so the particles correctly charged but with too low momenta may not reach the reflector and will be rejected from further focusing. The reflector bends the trajectories of particles which passed the horn and entered it to obtain a parallel narrow beam by giving additional focusing to high momentum particles and by protecting the low momentum particles from over-focusing. The mesons that pass the reflector are directed into a decay tunnel. The intersections of cylindrically symmetric magnetic horns are presented in Figure 6.1. The target in Figure 6.1 (left), represented by a black thick horizontal line, is in the optimal position $T^*_{DZ} = 0$ m, corresponding to $T_{DZ} = 114$ m, where $T^*_{DZ} \equiv T_{DZ} - position\ of\ the\ horn$.

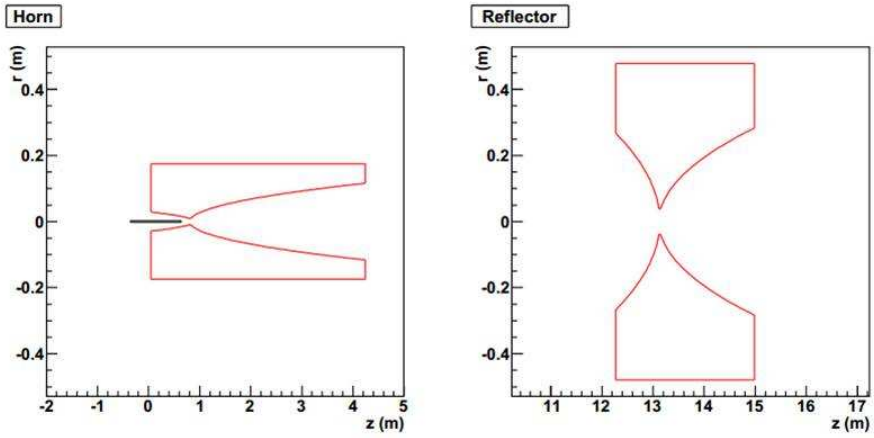

Figure 6.1. The shape of the horn and reflector used in a simulation program for a baseline 950 km; in the T^*_{DZ} frame.

6.2. Basic assumptions and description of the beam simulation program

The interactions of protons with the target nuclei are simulated using the QGSP hadronic package of GEANT4. Secondary mesons are followed until their decays into neutrinos. As described above, the geometry of the beamline (target, focusing horns, decay tunnel) is based on the NuMI beamline scheme and the critical parameters (DZ, R_{DT}, L_{DT}, T_{DZ}, I_h) are to be set by the user. The simulation has been performed in two modes, Positive Horn Focusing (PHF) for a ν_μ beam and Negative Horn Focusing (NHF) for a $\overline{\nu}_\mu$ beam. This is achieved by switching the horn current into the opposite direction ($I_h \rightarrow -I_h$) and therefore choosing the oppositely charged mesons to enter the decay tunnel.

The problem of finding whether the produced neutrino will reach the far detector, i.e. the simulation of the neutrino beam kinematic behaviour, is not simple and can be simulated diversely. It strongly depends on the choice of the beam energy spectrum. The mesons with higher energies are naturally produced more forward. Thus, the beams of relatively high energy neutrinos are naturally more intense close to the beam axis. The kinematic-scaling problem is solved using the probability of reaching the detector as a weight applied to every meson decay. The discussion of this solution and the probability estimation can be found in [91]. The probability P_π of neutrino ν_μ originated from a pion decay to reach the far detector, which is used as weight in the simulation program, is given by the following formula:

$$P_\pi = \frac{1}{4\pi}\frac{A}{L^2}\frac{1-\beta^2}{(\beta\cos(\alpha)-1)^2}\ , \tag{6.1}$$

where L is a distance to the detector (here 100 km); A - detector surface (here 100 m^2); α - meson's polar angle; β - meson's Lorentz boost (p/E).

As mentioned in the previous chapter, to simplify the comparison of different beam setups, a distance of 100 km is usually chosen as the distance at which the neutrino beam flux is calculated. The same is done in this thesis. This is why also in Equation 6.1 L is assumed as equal 100 km and A is equal 100 m^2. From the 100 km distance to the far detector site distance the flux is proportionally scaled as $\sim 1/L^2$.

The optimization performed for the LAGUNA ([92], [61]) was done for all seven sites (at distances of 130 km, 630 km, 665 km, 950 km, 1050 km, 1570 km, 2300 km), but with the HP-PS2 proton synchrotron only. The resulting neutrino fluxes are presented in Figure 6.2. At that time, the goal was to maximise the sensitivity for $sin^2(2\theta_{13})$ measurement since θ_{13} was not known and it was not possible to exclude its very small value. The main conclusions from the optimization procedure and resulting neutrino beams were as follows:
1. The maximum of the neutrino flux should be in the energy range corresponding to the first oscillation maximum region, because this gives the biggest effect on the sensitivity for the determination of unknown oscillation parameters. The coverage of the second oscillation maximum helps, however, the first oscillation region is dominant.
2. The strongest impact on the neutrino flux maximum position has the target vs horn position parameter (T_{DZ}). The target positioned upstream gives higher energy neutrinos.
3. Other parameters such as the distance between the horn and the reflector or the decay tunnel geometry do not have such a strong impact. The initial rough optimization is sufficient and the detailed optimization is not required.

The neutrinos with an energy of about 2 GeV which are close to the 1st oscillation maximum for SUNLAB are mostly generated by pions with an energy of about 6 GeV, for which the decay length is about 300 m. However, a shorter decay tunnel reduces the ν_e background coming from decaying muons. The 100 m long decay tunnel was chosen in the study [61] as the most optimal for a 950 km

baseline. The optimization performed for the neutrino beam study in this thesis confirmed the above conclusions, so these assumptions remained unchanged.

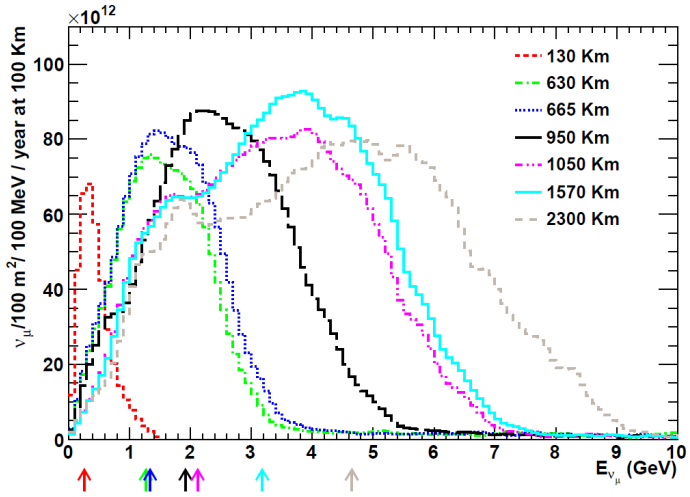

Figure 6.2. Neutrino fluxes per 100 m^2 at a distance of 100 km optimized for all 7 sites considered for LAGUNA and normalised to one year of running at the HP-PS2 with power of 2.4 MW [61]. The arrows depict the first oscillation maximum for each site.

In the proposed long baseline experiments based on superbeams the beam energy spectrum is wide in order to cover a wide range of possible scenarios and values of the δ_{CP} parameter. Nevertheless, the crucial part of the spectrum is the region near the oscillation maximum of the interesting oscillation channel. This is why the neutrino beam energy spectra are differently optimized for different baselines.

As was discussed in Section 2.2, for the electron neutrino appearance experiment aiming at the mass hierarchy determination and δ_{CP} measurement all the effects which have an impact on the oscillation behaviour should be taken into account. Thus, the choice of the neutrino energy corresponding to the first oscillation maximum which is made assuming no matter effects and $\delta_{CP} = 0$ is not fully correct. However, this approach is commonly used as the most natural choice before measuring the neutrino mass hierarchy and δ_{CP}. The neutrino energy corresponding to the first oscillation maximum for the ν_e appearance and calculated this way is 4.67 GeV for the Pyhäsalmi baseline of 2300 km baseline, 1.92 GeV for the SUNLAB baseline of 950 km, and 2.4 GeV for the DUNE baseline of 1300 km.

6.3. Simulations based on the High-Power PS2 project

The studies for SUNLAB based on the High-Power PS2 project assumed a proton energy of 50 GeV and a total exposure of 3×10^{21} protons on target per year. The goal of this part of the simulation was to correctly understand the simulation program and to reproduce the neutrino fluxes obtained previously within the LAGUNA project. The Polkowice-Sieroszowice site is the primary goal for studies presented in this thesis. However, the Pyhäsalmi site was the leading proposition for the far site in the LAGUNA-LBNO project. Thus, the neutrino fluxes for both these sites were reproduced in order to be compared.

The GENEBES simulation software was successfully installed in the CC1 [78] infrastructure at IFJ PAN. The simulated fluxes for SUNLAB and Pyhäsalmi based on the 100 000 p.o.t Monte Carlo samples are presented in Figure 6.3. They are consistent with those coming from [61] and presented in Figure 6.2.

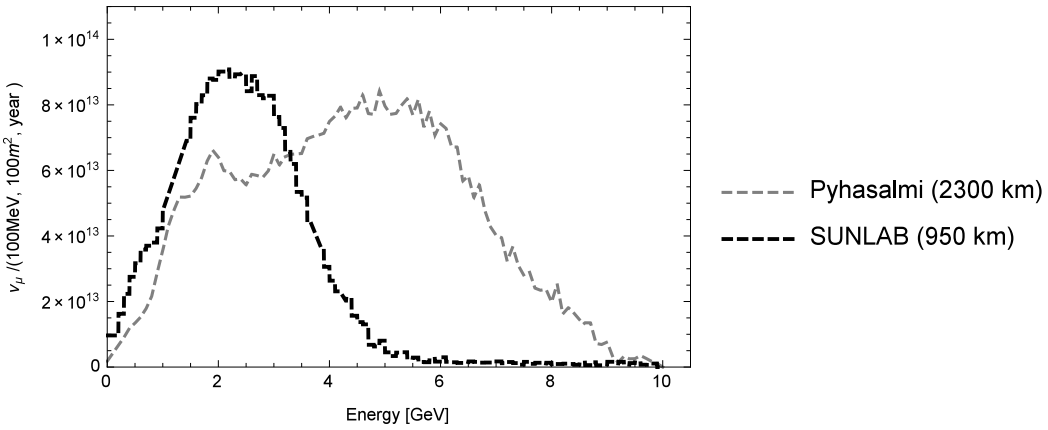

Figure 6.3. Neutrino fluxes at a distance of 100 km from the HP-PS2 accelerator simulated for the SUNLAB and Pyhäsalmi sites.

The neutrino beam is not a 100% pure ν_μ beam. Even if the secondary mesons are very well focused and selected, other neutrino flavours appear in the beam. In Figures 6.4 and 6.5 the beam composition simulated within the framework of this thesis is presented for the SUNLAB location and for the Pyhäsalmi mine. For reference, the beam composition for the Pyhäsalmi mine from [93] is shown in Figure 6.6. This figure depicts the neutrino beam as it will appear at the far detector site after travelling 2300 km, assuming no oscillations.

In summary, the reproduction of the fluxes using the HP-PS2 proton beam was a successful test of the applied simulation program.

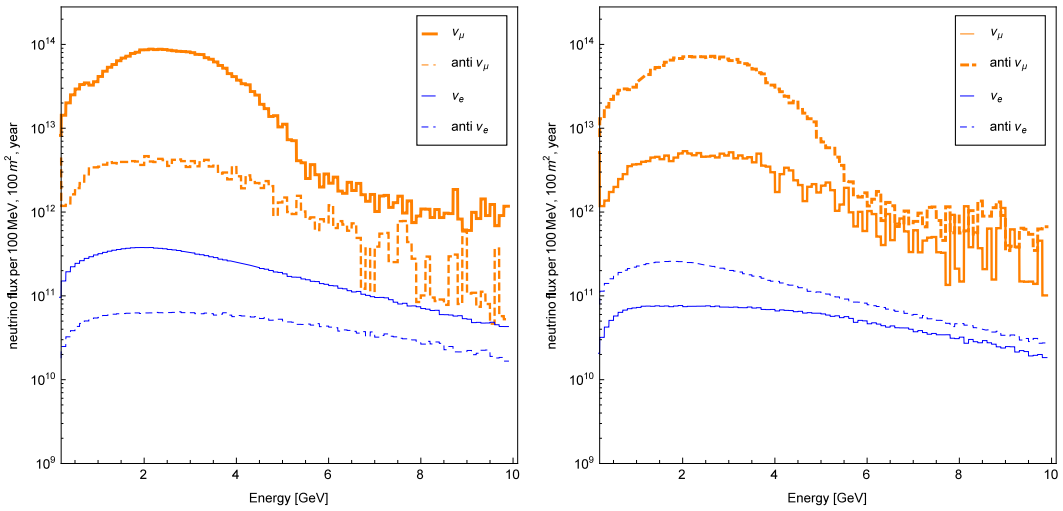

Figure 6.4. Neutrino (left panel) and antineutrino (right panel) flux simulated for the SUNLAB site using 50 GeV protons and assuming one year of running and the HP-PS2 power of 2.4 MW.

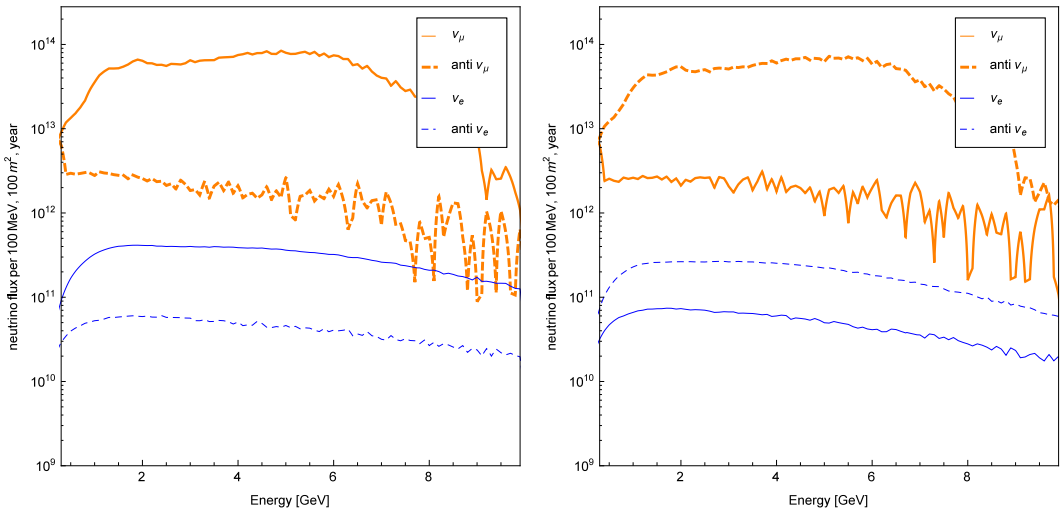

Figure 6.5. Neutrino (left panel) and antineutrino (right panel) flux simulated for the Pyhäsalmi site using 50 GeV protons and assuming one year of running and the HP-PS2 power of 2.4 MW.

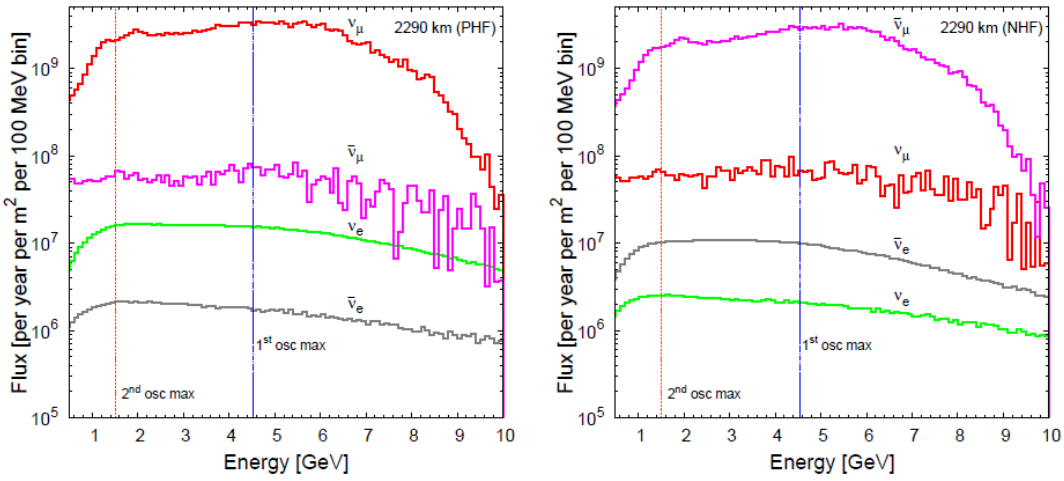

Figure 6.6. Neutrino (left panel) and antineutrino (right panel) beam composition simulated for the Pyhäsalmi site by the LAGUNA collaboration as to appear at the far detector site with no oscillation effect assumed. For comparison with Figure 6.5 the contents should be rescaled by a factor of 10^4. The HP-PS2 accelerator is assumed as a proton driver [93].

6.4. Simulations based on the SPS accelerator at CERN

Following the correct reproduction of the HP-PS2 study, the same MC simulation program was used for further studies based on the realistic approach assuming the use of protons from the upgraded SPS accelerator. This way the simulation of the neutrino beam for SUNLAB is based on the current plans for upgrade of the accelerator complex at CERN. The specifications for the upgraded SPS as a source of protons are given in Table 6.1.

The starting point of the program optimization for this new beam setup was the HP-PS2 beam setup, which had already been optimized in many details for oscillation studies with a baseline of 950 km. Then, the SPS parameters were introduced into the program, the source was substituted with 400 GeV protons and a beam power set to 0.75 MW. The shape, size and distance between the target, horn, reflector and decay tunnel remained unchanged as being optimized for choosing the mesons from a desired part of their energy spectrum in order to get the muon neutrino beam peaked at 1.92 GeV at SUNLAB. The simulated neutrino fluxes for all neutrino flavours at a 100 km distance after the decay tunnel are presented in Figure 6.7.

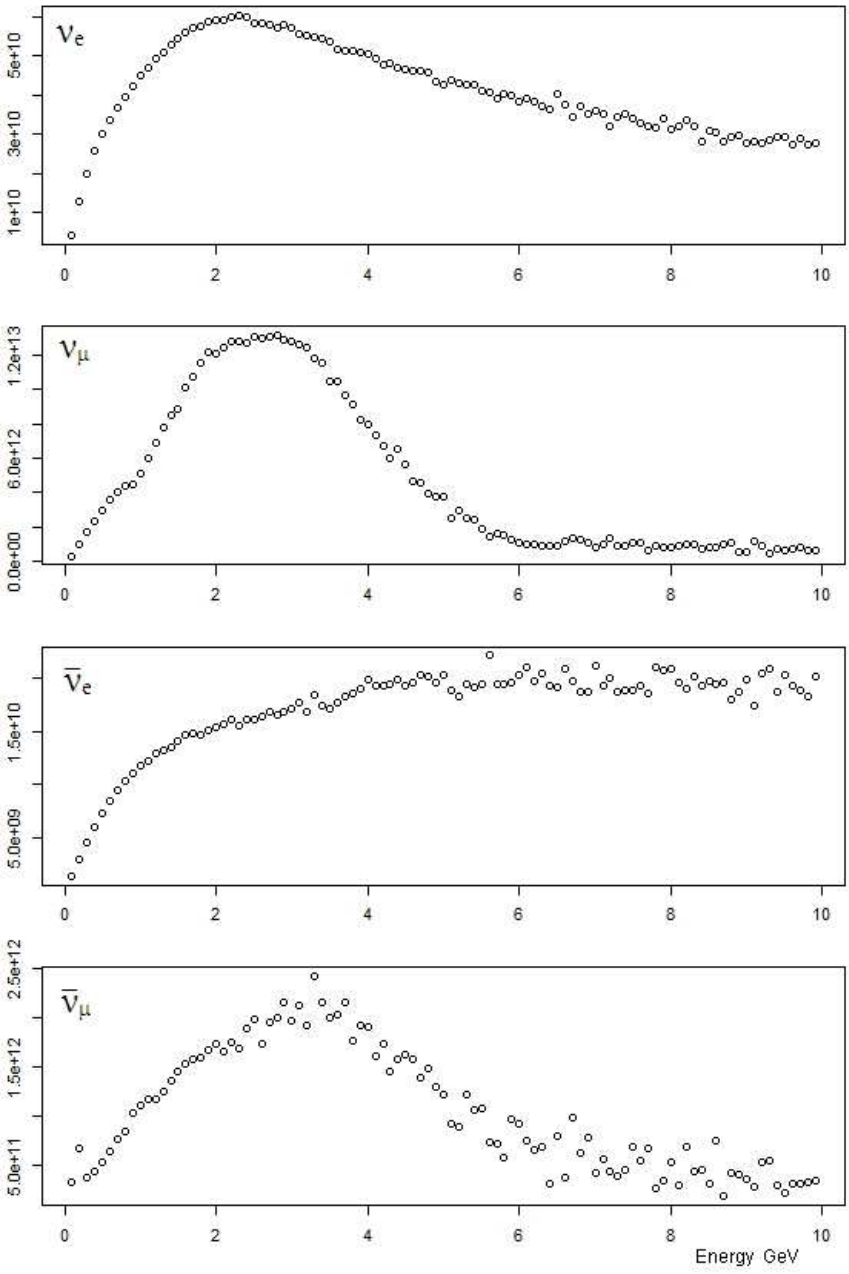

Figure 6.7. Neutrino fluxes for the standard focusing system and the primary beam of 400 GeV protons from the upgraded SPS accelerator.

The optimisation was aimed at obtaining the maximal flux at the energy corresponding to the $\nu_\mu \leftrightarrow \nu_e$ first oscillation maximum and the best possible flavour purity of the neutrino beam. Thus, two parameters, the purity and intensity of the muon neutrino flux, were taken as measures of the optimisation. Of course, the neutrino beam should be maximally intense and pure close to the first (1.92 GeV) oscillation maximum, but also as good as possible at the second

($\sim$ 0.4 GeV) oscillation maximum. To ensure this, the optimisation measures are calculated in the energy region from 0 to 3 GeV.

The first parameter - p - purity of the beam - is defined as :

$$p = \frac{N_{\nu_\mu}}{N_{\nu_\mu} + N_{\overline{\nu}_\mu} + N_{\nu_e} + N_{\overline{\nu}_e}} \ , \tag{6.2}$$

where N_x is the summed number of neutrinos with x-flavour in the selected energy range. The other parameter - I - intensity is the total number of ν_μ delivered to the 'detector' at 100 km:

$$I = N_{\nu_\mu} \ . \tag{6.3}$$

The optimisation based on the T_{DZ} parameter as the one with the biggest impact on the meson selection process was performed as follows. The position of the target was moved every 10 cm in a range of 2 meters starting from $T_{DZ} = 113$ m and ending at $T_{DZ} = 115$ m. For each position of the target the neutrino flux, intensity I and purity p were calculated based on 10 000 generated protons on target. The results are presented in Figure 6.8. The procedure was performed only for the PHF mode, as the NHF mode is almost fully symmetric within the applied model.

For each T_{DZ} value the analysis of the meson production on target was performed as an additional check of the correctness of the simulation program and for a better understanding of the optimisation process. The meson production analysis and its results are discussed in detail in Section 6.5.

The intensity I reaches its highest values between target positions $T_{DZ} =$ 114 , and 114.2. However, the highest values of purity are for the target moved upstream (113.5 - 114.0) and go down rapidly with the target moving inside the horn, i.e. for positions greater than 114.1. As an illustration of the effect, the ν_μ fluxes at the two peripheral ($T_{DZ} = (113\text{m}, 115\text{m})$) and the optimal ($T_{DZ} = 114$) target positions are shown in Figure 6.9. The best solution for the meson focusing characterized by high levels of both the purity and intensity corresponds to the central position $T_{DZ} = 114.0$ ($T^*_{DZ} = 0$) of the target and this position was chosen for further simulations.

The final beam fluxes and compositions for the PHF and NHF modes with the best meson focusing setup, obtained for the MC simulation sample of 500 000

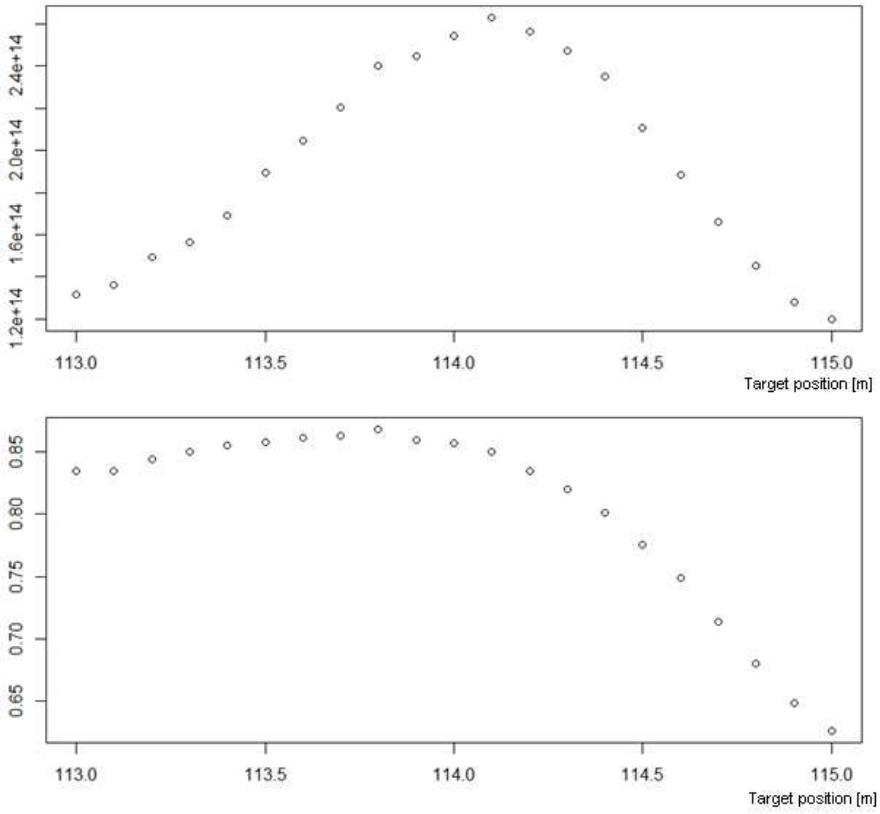

Figure 6.8. Intensity (upper panel) and purity (lower panel) of the beam as a function of the target position T_{DZ}.

MC generated protons and scaled to one year of the SPS running with a power of 0.75 MW, are presented in Figure 6.10. These fluxes are used as an input for the CP violation studies with GLoBES, presented in Chapter 8.

6.5. Meson production and selection

The secondary mesons produced in the proton interactions with the graphite target are an intermediate step on the way to the neutrino beam production. The energy spectrum and intensity of the resulting neutrino beam strongly depend on the number of produced mesons and selection of their energy range; additionally, the beam purity depends on the correctness of the meson charge selection. The analysis of the secondary mesons presented below concerns the optimisation process performed for the 950 km baseline.

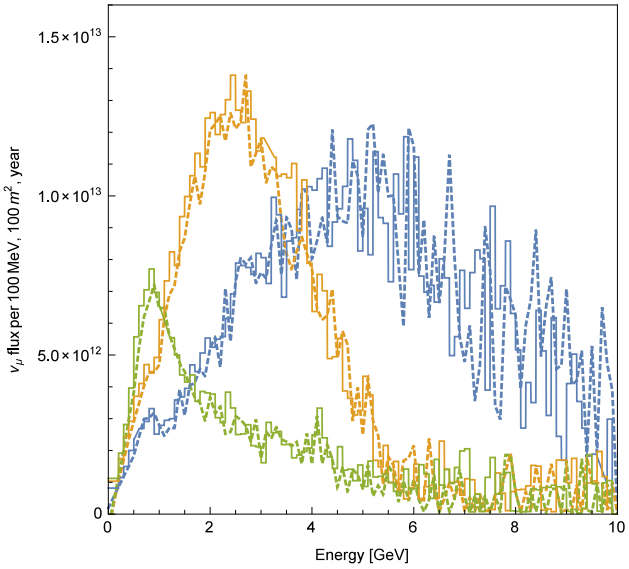

Figure 6.9. Muon neutrino flux distributions as a function of neutrino energy for 400 GeV protons at three target positions T_{DZ} = 113, 114, 115 m. Normalization is for one year of the SPS running with a power of 0.75 MW. Solid lines are for the neutrino (PHF) mode, dashed lines for the antineutrino (NHF) mode.

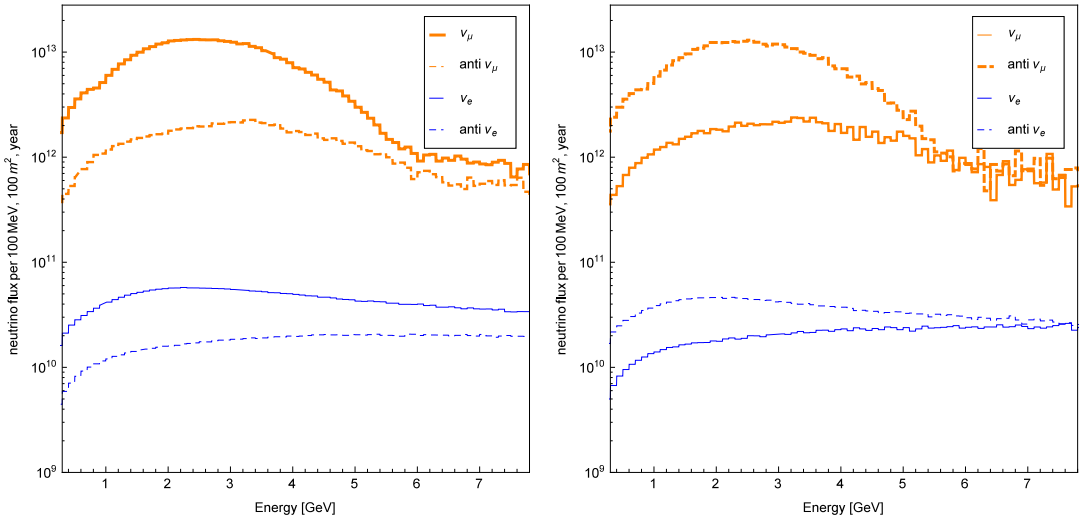

Figure 6.10. The unoscillated signal and background neutrino fluxes optimized for the SUNLAB site using 400 GeV protons (left:PHF mode, right:NHF mode). Normalization is for one year of the SPS running with a power of 0.75 MW.

6.5.1. Pion and Kaon production on the graphite target

Two Monte Carlo samples of 10 000 protons each, with energies E_p = 50 GeV and E_p = 400 GeV, interacting with the 1 m thick graphite target were

produced. The most important mesons for the neutrino production are pions and kaons. The average multiplicity of mesons produced in a single proton - target interaction is: $\langle N_{meson} \rangle = 8.2$ for 50 GeV protons and $\langle N_{meson} \rangle = 25.8$ for 400 GeV protons.

The pion and kaon production rates for the proton-target interactions are shown in Figure 6.11 and are summarized in Table 6.3 for $E_p = 50$ GeV and $E_p = 400$ GeV. As it can be seen, at both energies there is around 10% bigger production of π^+'s than π^-'s ($N_{\pi^+}/N_{\pi^-} = 1.10$). This gives a positive effect on the neutrino beam, for which π^+'s are the main source of muon neutrinos. The lower production of π^-'s, which are the main source of antineutrinos, gives a negative effect on the antineutrino beam flux.

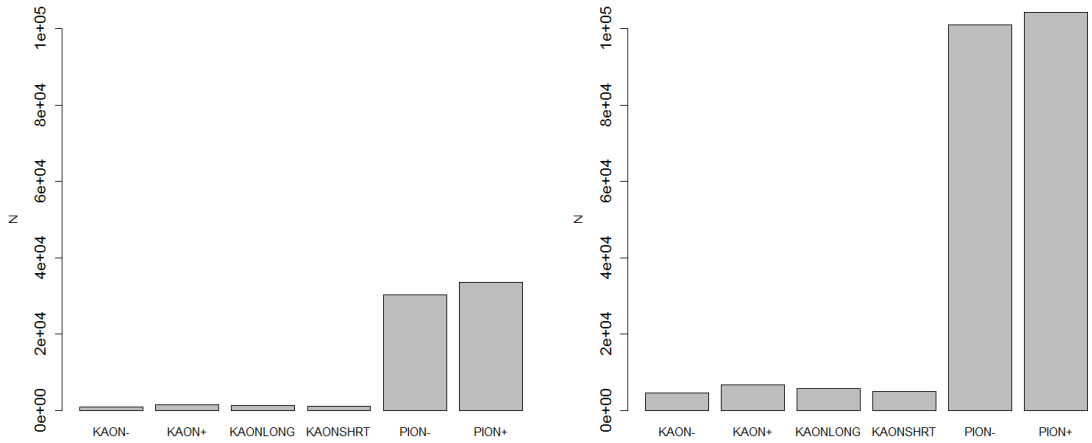

Figure 6.11. Meson production on the target for MC samples of 50 GeV protons (left) and 400 GeV protons (right), $T_{DZ} = 114$.

meson type	K^-	K^+	K_L	K_S	π^-	π^+
50 GeV proton beam	0.012	0.023	0.017	0.015	0.44	0.49
400 GeV proton beam	0.02	0.029	0.024	0.022	0.44	0.46

Table 6.3. Meson production rates on the target for the MC samples of 50 GeV and 400 GeV protons. The total production of pions and kaons is normalized to one.

6.5.2. Meson selection by the target-horn position and horn-reflector focusing system

The focusing system can be operated in the Positive Horn Focusing (PHF) mode for choosing positively charged mesons and producing the neutrino enhanced

beam as a result, or in the Negative Horn Focusing (NHF) mode with negatively charged mesons chosen and the antineutrino-enhanced beam produced. The relative target-horn position is crucial for the mesons selection by the focusing system. Table 6.4 illustrates the influence of this position on the fractions of π and K mesons, produced in the proton-target interactions, which pass to the decay channel. Results are given for the PHF mode and three characteristic target positions. The $T_{DZ} = 114$ target position gives the highest fraction of π^+'s passing to the decay tunnel and this is the position chosen as optimal.

meson type	N.of mesons leaving target	N.of mesons entering tunnel	**fraction**	target position T_{DZ}
PION+	102142	22630	0.2216000	113
PION-	99378	8585	0.0863900	
KAON-	4594	545	0.1186000	
KAON+	6660	1286	0.1931000	
KAON L	5494	1178	0.2144000	
PION+	104289	28084	0.2693000	114
PION-	101011	11259	0.1115000	
KAON-	4621	623	0.1348000	
KAON+	6692	1403	0.2097000	
KAON L	5636	1250	0.2218000	
PION+	104259	18752	0.1799000	115
PION-	100531	14730	0.1465000	
KAON-	4501	680	0.1511000	
KAON+	6625	1014	0.1531000	
KAON L	5395	1160	0.2150000	

Table 6.4. Fractions (column 4) of mesons (column 1) entering the decay tunnel after selection throughout the focusing system for three characteristic target positions (column 5). The number of mesons produced in the beam-target interactions (column 2) and the number of mesons entering the decay tunnel after selection (column 3) are also given. Information is based on the MC sample for the 400 GeV protons.

The meson compositions selected by the optimized focusing system for the baseline 950 km and the PHF mode are presented in Figure 6.12 for two energies of primary protons: 50 GeV and 400 GeV. It is visible that for primary protons of the lower energy the selection of the desired positively charged pions in the PHF mode

is more effective than for mesons originating from protons of the higher energy.

The comparison between the meson composition for the NHF and PHF modes using the MC sample of 400 GeV protons is shown in Figure 6.13. The slight overproduction of positively charged pions is visible.

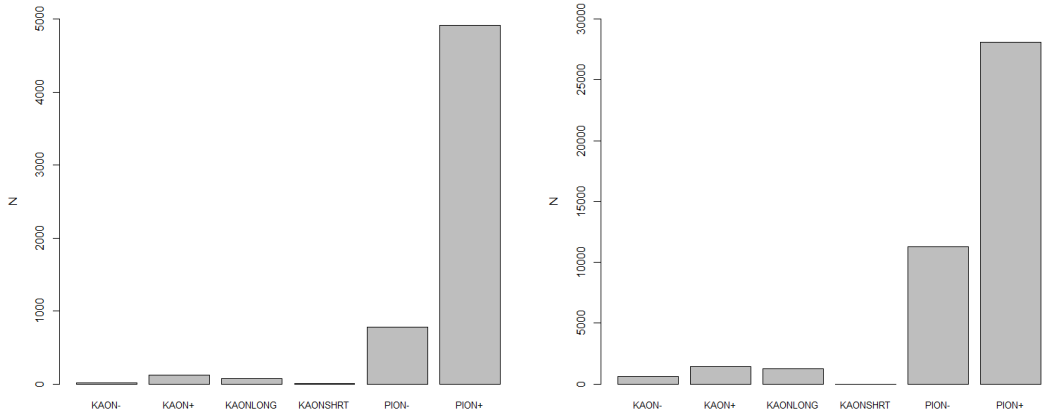

Figure 6.12. Mesons selected by the focusing system for the MC sample of 50 GeV protons (left) and for the MC sample of 400 GeV protons (right). The neutrino beam and the optimal target position at $T_{DZ} = 114$ are assumed.

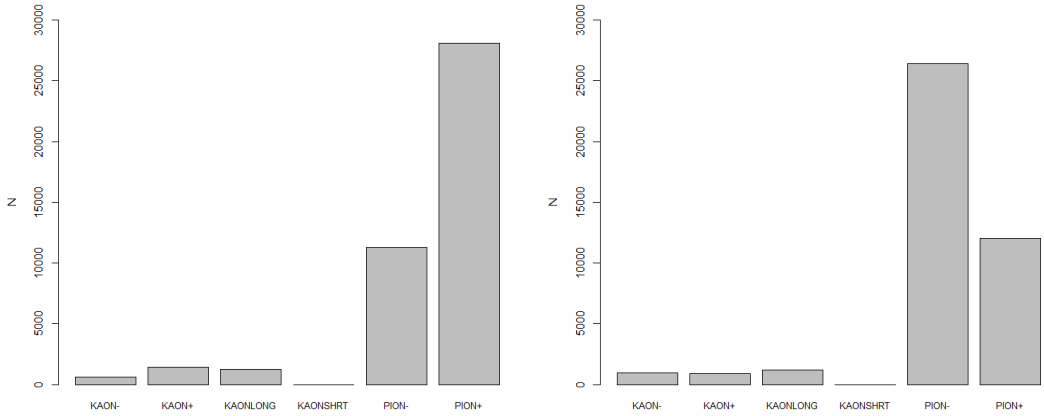

Figure 6.13. Mesons selected by the focusing system for the NHF mode (left) and for the PHF mode (right), for the MC sample of 400 GeV protons and for the optimal target position at $T_{DZ} = 114$.

meson type		K^-	K^+	K_L	K_S	π^-	π^+
50 GeV proton beam	PHF	0.002	0.02	0.01	0	0.13	0.83
400 GeV proton beam	PHF	0.01	0.03	0.03	0	0.26	0.66
400 GeV proton beam	NHF	0.02	0.02	0.03	0	0.64	0.27

Table 6.5. Mesons selected by the focusing system for the MC samples of 50 GeV and 400G eV protons for $T_{DZ} = 114$. The total production of pions and kaons is normalized to one.

Table 6.5 and Figures 6.14 and 6.15 summarize the optimisation process of the target positioning for the SPS scenario. Table 6.5 summarizes the composition of mesons entering the decay tunnel after leaving the optimized focusing system for 50 GeV protons and the PHF beam mode, and for 400 GeV protons and both beam modes. The efficiency of choosing the positive charge, which is a measure of the intensity I for the PHF mode for each tested target position (T_{DZ}), is presented in Figure 6.14. Additionally the correctness of choosing the positive pions vs negative pions for the PHF mode, being a measure of the purity p, is presented in Figure 6.15.

One can see that in the case of the 400 GeV proton beam, even for the target optimal position, only less than 30% of pions produced on the target enter the decay tunnel after the selection by the focusing system. The charge selection is also far from being ideal for the 400 GeV proton beam because the fraction of correctly selected pions is only about 65%. For the 50 GeV proton beam, the purity is much higher and reaches about 83%. This shows that the proton driver suitable for the low energy neutrino beam should be optimised for the acceleration of a low energy, but very intense proton beam.

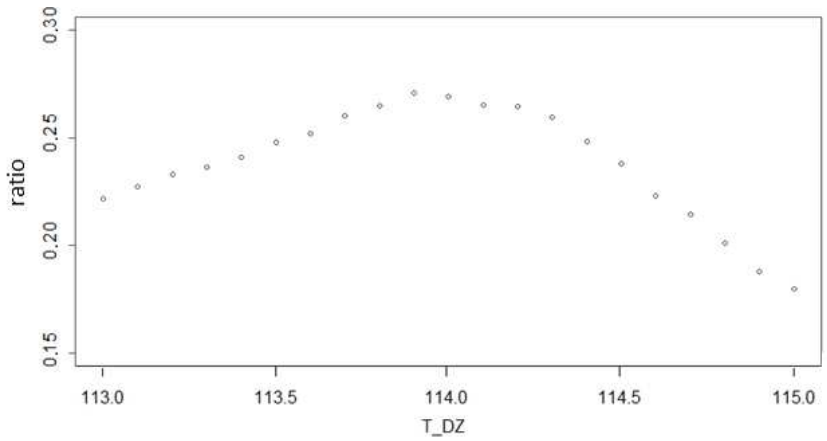

Figure 6.14. The ratio of π^+'s chosen by the focusing system to the total number of π^+'s produced on the target as a function of the target position (T_{DZ}).

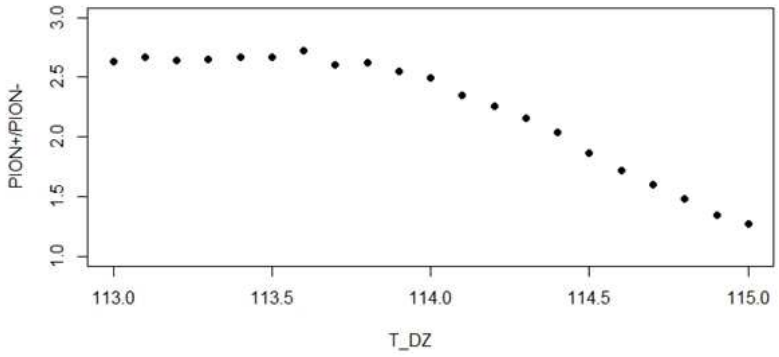

Figure 6.15. The ratio of π^+'s to π^-'s chosen by the focusing system as a function of the target position (T_{DZ}) for the MC sample of 400 GeV protons.

Chapter 7

The detector description for GLOBES

The parametrisation of the detector performance has a significant impact on sensitivity studies of the oscillation experiment. The detector type, here LAr-TPC, has a strong influence on the studied energy range and identification of signal and background events in the long baseline experiment. The experience gained within the ICARUS experiment is adapted for this detector description. The input for the GLOBES based sensitivity simulation includes detector performance, i.e. energy resolution and detection efficiencies, signal processes and background sources. The input values were chosen conservatively to reflect the performance that can be realistically achieved for the proposed LAr-TPC detector used for studies of the ν_μ disappearance channel and the ν_e appearance channel. The first section of this chapter contains a description of the parameters used as inputs, while the next sections contain descriptions related to the LAr-TPC performance.

7.1. Liquid Argon Time Projection Chamber - inputs for GLOBES

The far detector in the simulation described in this thesis is assumed to be a LAr-TPC single phase detector. The concept of the liquid Argon Time Projection Chamber detector was shortly described in Section 3.1. Thanks to the ICARUS experiment, the information about the detector performance is known from the analysis of the experimental data and is not only based on simulations. Additionally, the ICA-FLUKA based Monte Carlo simulation program is well tuned to the detector response, which makes it a good tool for additional studies. However, one should mention that the CNGS beam was optimised for the ν_τ appearance study with the mean neutrino energy of 17 GeV, so the ICARUS detector has collected higher energy data than are expected at the SUNLAB experiment. Therefore, some issues such as momentum reconstruction of not fully-contained long muon tracks will be a smaller problem for the SUNLAB experiment because of a much

lower energy neutrino beam and a much bigger detector.

The detector characteristics used as inputs in the sensitivity calculations with GLOBES are shown in Tables 7.1 and 7.2. Two detector masses assumed in the GloBES CP violation sensitivity simulations, presented in Chapter 8, are 20 kton in the initial phase of the experiment and 100 kton in the final phase of the experiment. However, the detector mass is the scaling factor of exposure and in the first approximation it does not have a big impact on the event reconstruction quality. Therefore, the same tables are used for both mass values.

In the GLOBES analysis for SUNLAB both signal channels are included, the ν_e appearance and ν_μ disappearance, so the parametrisation of signal and background treatment is given for both signal channels. For the ν_e appearance channel three types of background are taken into account as being possible to occur in the LAr-TPC detector: the NC events, $\nu_\mu CC$ events wrongly identified as electron events and $\nu_e CC$ events originating from an intrinsic beam contamination with ν_e neutrinos. For the ν_μ disappearance channel the main source of background are the NC events, while the atmospheric ν_μ neutrinos can be easily distinguished by the beam timing and direction.

Characteristics	
signal	ν_e appearance (ν_e CC)
background	ν_μ CC; NC; intrinsic ν_e ($\nu_e CC$)
mass	20 and 100 kton
energy threshold	300 MeV
signal detection efficiency	90% for e
energy resolution :	$0.15\sqrt{E/GeV}$ $e^{\pm}$; $0.20\sqrt{E/GeV}$ $\mu^{\pm}$,
CC events	
NC events	Migration Matrix
background efficiency:	
NC (ν_μ NC)	0.5%
from mis-id muons (ν_μ CC)	0.5%
intrinsic ν_e	80%
systematic error for signal	5%
systematic error for background	5%

Table 7.1. Input for GLoBES for the ν_e appearance signal.

Characteristics	
signal	ν_μ disappearance (ν_μ CC)
background	NC
mass	20 and 100 kton
energy threshold	300 MeV
signal detection efficiency	100% for μ
energy resolution:	$0.20\sqrt{E/GeV}$ for $\mu^\pm$
CC events	
NC events	Migration Matrix
background efficiency:	0.5%
ν_μ NC	
systematic error for signal	5%
systematic error for background	5%

Table 7.2. Input for GLoBES for the ν_μ disappearance signal.

The systematic errors are simply assumed to be 5%; it means that the total normalization of both the signal and background is allowed to vary by 5% during the sensitivity calculations. This assumption was made following the other oscillation studies for long baseline experiments [64], [93], [94].

7.2. Signal and Background event identification

The quality of the event type identification is essential for the analysis of the detector performance. Events are divided into three groups: NC, $\nu_e CC$ and $\nu_\mu CC$ based on the interaction type and neutrino flavour and then classified as signal and background events depending on the specific analysis. The LAr-TPC detector is not magnetized, therefore event characteristics are the same for both the PHF and NHF beam modes. Thanks to good spacial resolution in the LAr detectors, event identification can be made by using the event topology, electromagnetic activity and energy losses by ionization of charged particles leaving an interaction vertex. Examples of the $\nu_e CC$ and $\nu_\mu CC$ events for a neutrino energy $E_\nu = 400$ MeV, corresponding to the second oscillation maximum region at SUNLAB for $\nu_\mu \rightarrow \nu_e$ and simulated using the ICA-FLUCA generator, are presented in Figure 7.1.

7.2.1. ν_e appearance channel - signal and background characteristics

SIGNAL $\nu_e CC$ ($\overline{\nu}_e CC$)

The characteristic feature of the $\nu_e CC$ event is an electron leaving the interaction primary vertex and developing an electromagnetic cascade. The position of the interaction vertex is defined thanks to other particles leaving the same vertex. In the case of quasi-elastic neutrino interactions the position of the primary vertex can only be defined if a short track corresponding to the recoil proton is visible in the vicinity of the electromagnetic cascade. The detection efficiency of electron events is assumed to be 90%.

Background (ν_μ CC; νNC; intrinsic ν_e ($\nu_e CC$))

The most difficult background, by its nature identical to the ν_e signal, is due to the interactions of electron neutrinos and antineutrinos contaminating the ν_μ beam. In the simulated neutrino beam the total $\nu_e + \overline{\nu}_e$ contamination is at the 1% level. The only way to control the impact of this source of background is a good knowledge of the neutrino beam by its precise simulation and monitoring. Here, the error is assumed at the 80% level, which means that 80% of ν_e interactions from the beam contamination will enter the signal sample.

The $\nu_\mu CC$ events may be wrongly identified as $\nu_e CC$ owing to the hadronic production of electromagnetic cascades close to the primary vertex coupled with a muon track identified as a pion or electromagnetic activity on this muon track. This is very unlikely and in the analysis the 0.5% chance of misidentifying a muon neutrino interaction as an electron neutrino event is assumed.

The νNC is a leading background component for the low energy part of the detected electron neutrino spectrum. The characteristic feature of the NC interaction is an undetectable neutrino leaving the interaction vertex. The π^0 production at the primary vertex may lead to wrong identification of an NC interaction as a $\nu_e CC$ event. Several checks can be done to enhance the π^0 versus electron neutrino event identification. Two of them are very efficient. The first method is to check the starting point of the electromagnetic cascade because of the conversion of the photon from the π^0 decay. For the π^0 decays the cascade is usually separated from the primary vertex as a radiative length in liquid Argon is 14 cm. This method requires the identification of the primary vertex through the presence of charged particle(s) leaving it. The second method is based on the analysis of the deposited energy dE/dx for initial segments of the cascade and distinguishing between a single minimum ionizing particle (electron from $\nu_e CC$) and a double

minimum ionizing particle for the first e^+e^- pair from the photon conversion (for π^0 from NC). Distinguishing between a π^0 and an electron is excellent in the liquid Argon TPC, as was demonstrated by the ICARUS experiment. The false positive classification error of $NC\pi^0$ as electron event is estimated as $\eta_{\pi^0 NC} = 0.01$ [95]. It means that only 1% of the $NC\pi^0$ sample is wrongly classified as electron event. Therefore, in this study the chance for classifying the event from full NC sample as a signal $\nu_e CC$ event is assumed conservatively as 0.5%.

7.2.2. ν_μ disappearance channel - signal and background characteristics

SIGNAL $\nu_\mu CC$ ($\overline{\nu}_\mu CC$)

The characteristic feature of the $\nu_\mu CC$ interaction is a long straight muon track, leaving the primary interaction vertex among other particles. Depending on the energy and position in the detector, the muon is stopping, decaying or leaving the detector. Some electromagnetic activity on the muon track such as delta rays and bremsstrahlung radiation is possible, but it can be easily identified. The criterium for classifying a long, high energy and not fully contained track as belonging to the muon and not to the charged pion is the fact that no hadronic interaction is observed along at least 2.5 m of this track, starting from the interaction vertex. The detection efficiency of a muon event is assumed to be 100%.

Background νNC

The νNC interaction with charged $\pi^\pm$ mesons in the final state ($NC\pi^\pm$) can become a background for $\nu_\mu CC$ if any of these charged pions is misidentified as a muon. Based on the ICARUS study, the false positive classification error η_π is estimated to be $\eta_\pi = 0.016$ [95]. It means that in ICARUS $1,6\%$ of the NC sample is wrongly identified as $\nu_\mu CC$. Therefore, taking into account smaller neutrino energy range and better event containment in the case of the larger detector the background at the 0.5% level of the total NC sample is assumed.

7.3. Energy reconstruction in LAr-TPC

Thanks to the good liquid Argon properties, the LAr-TPC is an excellent, homogeneous and totaly active calorimeter. The energy of a particle traversing the detector is mostly converted into ionization electrons which are then drifted and read out on wires. The collected charge, converted to a digital signal, must be calibrated, including physical effects such as absorption, Fermi motions, charge recombination and detector effects, e.g. electronic noise. Such a corrected signal is a good measure of the energy deposited by the incoming particle. The fast

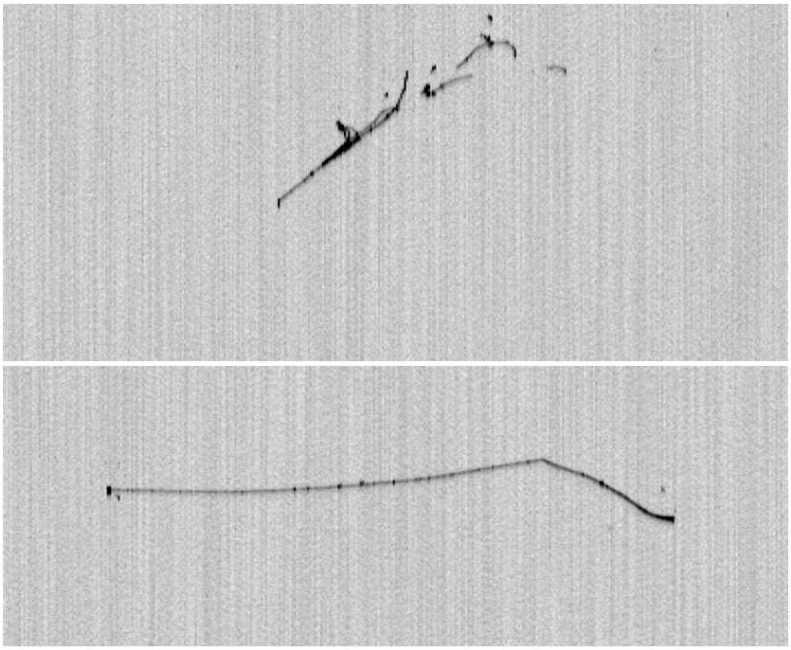

Figure 7.1. Examples of the simulated quasi elastic neutrino interactions in the T600 detector for the neutrino energy $E_{\nu\ Truth} = 400$MeV. The upper panel presents an electron neutrino CC interaction with a single electron leaving the interaction vertex and developing into an electromagnetic cascade. The bottom panel shows a muon neutrino CC interaction fully contained with a single, long muon track leaving the interaction vertex.

scintillation signal emitted by the excited argon molecules can be registered by PMTs and used as a trigger signal. The energy threshold for the event detection strongly depends on the readout electronics. The efficiency greater than 99% has been found by the ICARUS collaboration for an energy deposit in the detector $E_{dep} > 300$ MeV within the detailed trigger study [96].

For a better understanding of the neutrino energy reconstruction in LAr-TPC, the analysis based on simulated events was performed using the MC ICA-FLUKA generator. In the ICARUS experiment the MC samples were prepared for the CNGS beam with an average energy $E_{mean} = 17$ GeV. This MC simulation included all the detector features, full calibration and signal smearing effects. However, ICA-FLUKA was not prepared to be used with a different neutrino flux than CNGS, while for the SUNLAB study the expected energy spectrum covers a much lower energy range. Therefore, the dedicated sample covering the lower energy range (0-4 GeV) was prepared, composed of the monoenergetic $\nu_e CC$, $\nu_\mu CC$, NC events at the energies of 0.5 GeV, 1GeV,1.5 GeV, 2 GeV, 2.5 GeV, 3 GeV, 3.5

GeV, 4 GeV. Each sample contained 100 events. Figure 7.2 depicts the spectrum of the reconstructed neutrino energy deposited in the LAr-TPC detector for each interaction type, while in Figure 7.3 the dependence of the reconstructed energy on the true incoming neutrino energy is presented. In the case of ideal energy reconstruction the bin counts would agree with dotted lines in Figure 7.2 and would be placed on diagonals in Figure 7.3.

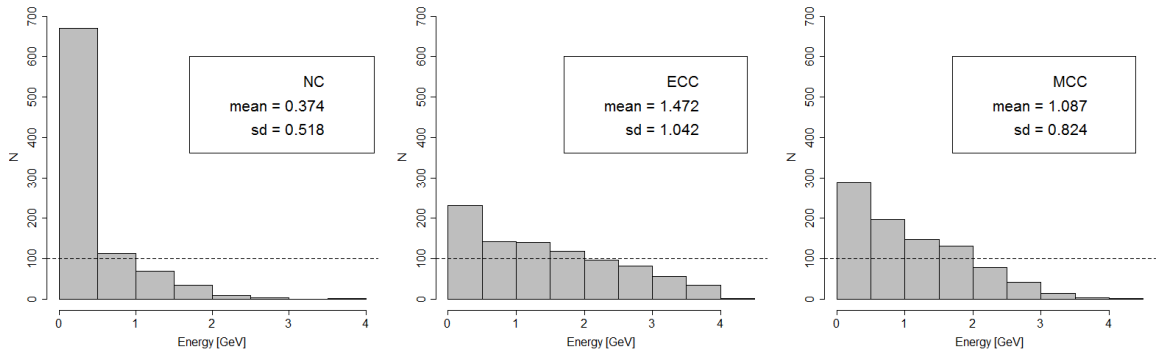

Figure 7.2. Deposited energy spectrum in the LAr-TPC detector presented as the number of events for each 0.5 GeV energy bin for the simulated samples of NC (left panel), $\nu_e CC$ (middle panel) and $\nu_\mu CC$ events (right panel). Dotted lines mark hundred events generated for each bin.

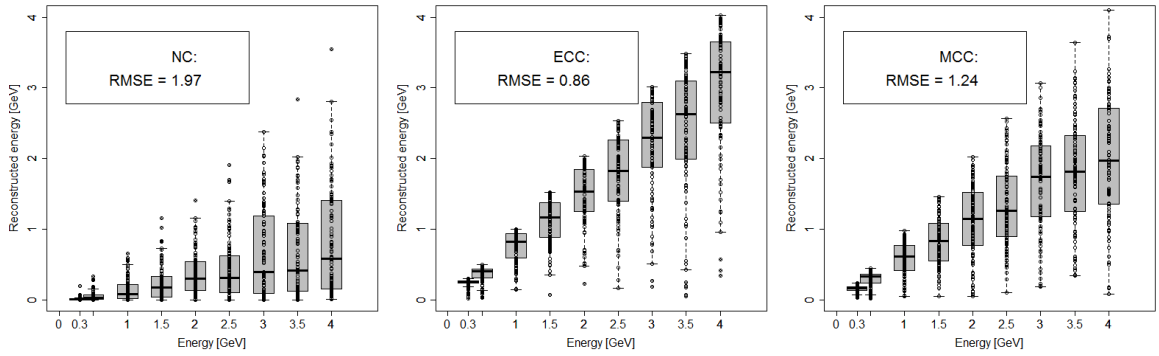

Figure 7.3. The reconstructed neutrino energy as a function of the true neutrino energy for NC (left), $\nu_e CC$ (middle) and $\nu_\mu CC$ (right) interaction samples. Black dots represent single events while lower and upper bands of the boxes corresponds to the first and third quartiles of the reconstructed energy distribution.

The dependence of the energy reconstruction on the interaction type is visible. For the NC sample, the measured deposited energy is much lower than the incoming neutrino energy, which is due to the fact that a final state neutrino leaves the detector and usually takes a big part of the initial energy. The best is the neutrino energy reconstruction for the $\nu_e CC$ events, mostly owing to the

fact that the electron, which is usually the most energetic particle in the final state, easily develops an electromagnetic cascade and is often fully contained. The neutrino energy reconstruction of the $\nu_\mu CC$ events is much better than for the NC events, but is also underestimated mostly owing to the limited containment of the detector. In particular, muons are lose their energy predominantly through the ionisation process, so approximately 5 metres are required to contain the muon with energy of 1 GeV. As a consequence the muon deposited energy reconstruction will be better for larger detectors planned for the future experiments. In addition, magnetized muon trackers placed behind the LAr-TPCs are planned to improve the momentum reconstruction of high energy muons leaving the liquid argon. The muon momentum reconstruction is not included in this analysis and it is a topic of a separate study. It is worth noting that in a certain range the muon momentum reconstruction in LAr-TPC is possible even without a magnetic field by the measurement based on the multiple Coulomb scattering.

As an additional illustration of the quality of energy reconstruction, the Root Mean Square error (RMSE) value as a function of the neutrino reconstructed energy is shown in Figure 7.4 for the same MC samples. In the case of the ideal energy reconstruction the value of RMSE would equal zero.

Figure 7.5 shows a monoenergetic sample of 2 GeV neutrinos corresponding to the first oscillation maximum for ν_e CC signal, and for the three considered interaction types. A considerable energy underestimation and smearing for the CC and NC events are clearly visible.

Two ways of taking into account the energy resolution are foreseen in the GLoBES simulation program: the migration matrices and automatic smearing using a defined smearing function.

7.3.1. Migration Matrix approach for energy smearing

Based on the discussion above, one can observe that in order to simulate the LAr-TPC detector response the true neutrino energy for $\nu_e CC$ and $\nu_\mu CC$ events should be smeared based on the reconstructed energy visible in the detector using a suitable function.

The situation is diametrically different in the case of NC events. The smearing behaviour of the NC events is much more complicated and needs a special transition matrix containing the smearing coefficients. Such matrices are

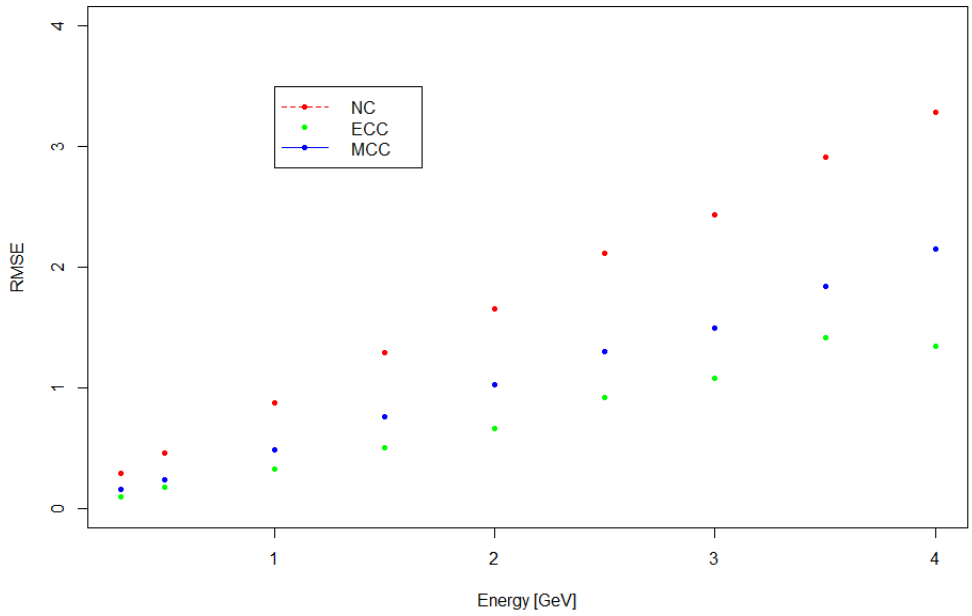

Figure 7.4. Root Mean Square Error for NC (red), $\nu_e CC$ (green) and $\nu_\mu CC$ (blue) events as a measure of the quality of the neutrino energy reconstruction for different types of neutrino interactions and energies.

sometimes called Migration Matrices.

The simulated sample described in the previous subsection was too small to be used in the creation of $E_{true} \rightarrow E_{reco}$ transition matrices for NC interactions. For technical reasons, it was very difficult to produce larger samples. Another reason was a much worse containment in the case of the ICARUS detector than the one expected for SUNLAB. Therefore, the Migration Matrices prepared by the LBNE collaboration (now LBNF-DUNE) and kindly provided by Lisa Whitehead were used [97]. This solution was also used by several long baseline experiment study groups [93], [94], [98].

7.3.2. Energy resolution functions

The automatic energy smearing used for $\nu_e CC$ and $\nu_\mu CC$ events is based on the function $\sigma(E) = \alpha \cdot E + \beta \cdot \sqrt{E} + \gamma$, where the smearing function parameters are assumed: for $\nu_e CC$ $\alpha = \gamma = 0$, $\beta = 0.15$, and for $\nu_\mu CC$ $\alpha = \gamma = 0$ and $\beta = 0.20$. The assumptions are conservative and it was shown in published studies that one can expect a better resolution for both electron and muon events in the LAr-TPC detector [99], [100], [39] [101].

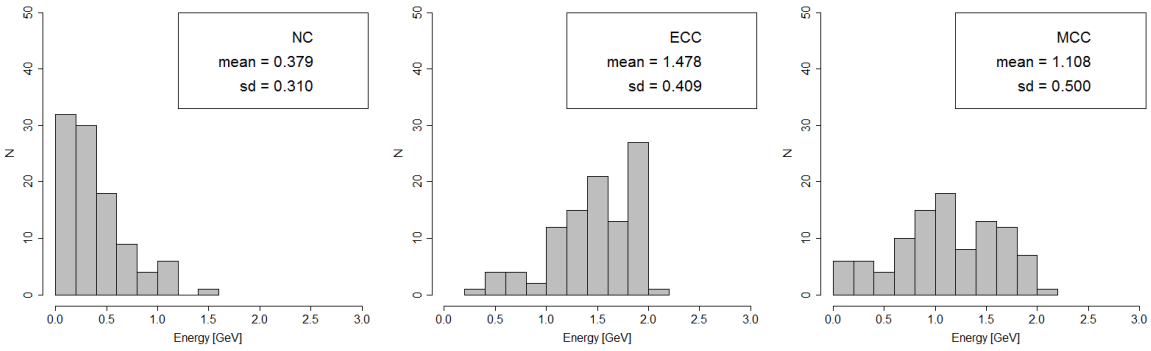

Figure 7.5. Reconstructed energy spectra for NC, $\nu_e CC$ and $\nu_\mu CC$ events for the monoenergetic 2 GeV sample.

Chapter 8

Results of the oscillation simulations for SUNLAB using GLoBES

The capabilities of SUNLAB, hosting a huge LAr-TPC as a far detector of the long baseline experiment, to determine the δ_{CP} parameter are presented in this chapter. The discussion is based on the expected event rate and sensitivity for excluding the CP conserving scenario, which is often called the 'CP-violation discovery potential'. This is the last phase of the simulation of the long baseline oscillation experiment at SUNLAB, following the neutrino beam simulation presented in Chapter 6 and the detector description presented in Chapter 7. The sensitivity calculation for the δ_{CP} determination at SUNLAB, discussed in this chapter, is based on a χ^2 minimization method. For comparison, the results of the LBNE and LAGUNA-LBNO studies concerning the CP-violation discovery potential are also presented.

8.1. Basic assumptions

The standard set of the oscillation parameters used in the δ_{CP} sensitivity calculations is:

$$\theta_{12} = 0.601,\ \theta_{13} = 0.162,\ \theta_{23} = 0.785,\ \ \Delta m^2_{21} = 0.0000762,\ \Delta m^2_{31} = 0.0024\ ,$$

where values of mixing angles are given in radians and Δm^2 values in eV^2. These are the central values of the oscillation parameters determined by the global fits presented in Section 1.4.4. For θ_{23} the maximal mixing is assumed as the one favoured by the atmospheric and T2K data.

The Earth density is an important factor for incorporating matter effects in the simulations of the oscillation process. The Preliminary Reference Earth model (PREM) [102], which is a one-dimensional model providing the average description of the Earth properties as a function of its radius, has been applied.

A single phase ICARUS type LAr-TPC is assumed in two detector mass scenarios: 20 kton in the initial phase of the experiment and 100 kton in the final phase of the experiment. Ten years of running is assumed for each stage resulting in Exposure = 20 kt $\times$ 10 yr $\times 10^{20}$p.o.t. = 2×10^{22} [p.o.t. $\times$ kt] for the initial stage and Exposure = 10×10^{22} [p.o.t. $\times$ kt] for the final phase.

The neutrino mass hierarchy is assumed to be known and results are presented for both scenarios - Normal (NH) and Inverted (IH) Hierarchies. If not stated otherwise, the operation time is equally divided between the neutrino (PHF) and antineutrino (NHF) beam modes.

The majority of the analysis results for SUNLAB are presented for the first stage of the experiment. The sensitivity for the CP-violation discovery potential is presented for both stages of the experiment.

8.2. Event rates

Figures 8.1 and 8.2 portray the expected signal and background event spectra for the ν_e appearance and ν_μ disappearance as a function of the reconstructed neutrino energy. The spectra are calculated assuming $\delta_{CP} = 0$ and the standard set of values of the oscillation parameters. The total exposure is equally divided between the PHF and NHF beam modes, therefore the exposure for each mode is Exposure = 1×10^{22} [p.o.t. $\times$ kt], which corresponds to 5 years of running with a 20 kton LAr-TPC detector. The detection efficiency and background rejection capabilities of the LAr-TPC detector are included according to Tables 7.1 and 7.2.

In Figure 8.1 the total expected $\nu_e CC$ event rate is marked with a black line. This total event rate consists of the signal $\nu_e CC$ events shown by a red dashed line and the three sources of background: the intrinsic ν_e beam contamination, ν_μCC events with mis-identified muons and NC events with electrons from the π^0 decay all marked with the remaining three lines. For both mass hierarchy scenarios and for both PHF and NHF modes the signal to background ratio is very good in the first oscillation maximum region. However, a high level of the NC background in the low energy region drastically limits the impact of the second oscillation maximum in the oscillation analysis. In the higher energy region, for the reconstructed energy $\gtrsim$ 5 GeV, the background from the intrinsic ν_e beam contamination becomes dominant. For the antineutrino beam mode, the expected event rates are much smaller than for the neutrino mode as a result of the approx-

imately three times smaller cross section for $\overline{\nu}$'s interactions. The Earth matter effects in the ν_e appearance neutrino channel (PHF) for the NH case cause the enhancement of the expected event rate, as compared to the expected event rate for the IH case. Similarly, for the $\overline{\nu}_e$ appearance channel (NHF), the matter effects in the IH case cause the enhancement of the predicted event rate as compared to the NH case. This behaviour illustrates the A_{CP} asymmetry discussed in Section 2.2.

In Figure 8.2 the $\nu_\mu CC$ signal is shown by a black solid line. The background coming from the NC sample is very small, but it is visible that it may degrade the analysis in the region of the oscillation minimum especially for the antineutrino beam.

Figures 8.1 and 8.2 present the signal event rates for a specific, conserving CP value of $\delta_{CP} = 0$. It is interesting to see how the signal event rate varies as a function of δ_{CP}. This dependence on the δ_{CP} value for the whole range of δ_{CP} values $(0, 2\pi)$, calculated for the ν_e and $\overline{\nu}_e$ appearance channels and for both mass hierachies, is presented in Figure 8.3. One can see a relatively strong dependence for the neutrinos. The opposite behaviour of the neutrino and antineutrino curves illustrates the A_{CP} asymmetry. This asymmetry is bigger for the NH than for IH.

Another check concerns the expected event rates for SUNLAB and the Pyhäsalmi site assuming neutrino beams based on the HP-PS2 and SPS proton accelerators discussed in Chapter 6. The results are presented in Figure 8.4, assuming 5 years of running with a 100 kton LAr-TPC in the PHF mode with a normal mass hierarchy. This corresponds to the total exposure 5×10^{22} p.o.t. $\times$ kt for SPS (400 GeV protons) and 15×10^{23} p.o.t. $\times$ kt for HP-PS2 (50 GeV protons). The intense HP-PS2 based neutrino beam gives the expected event rate an order of magnitude higher than the SPS based one, which would be a great asset for the δ_{CP} study. The long distance to Pyhäsalmi site offers better access to the second oscillation maximum.

8.3. CP-violation discovery potential

The potential to discover the CP-violation (CPV), if it happens, is measured by the experiment ability to exclude the CP-conserving values, i.e. $\delta_{CP} = 0, \pi$ at an assumed confidence level. By definition, this measurement becomes more difficult for the δ_{CP} values close to 0 and π. Therefore, the CP-violation may not

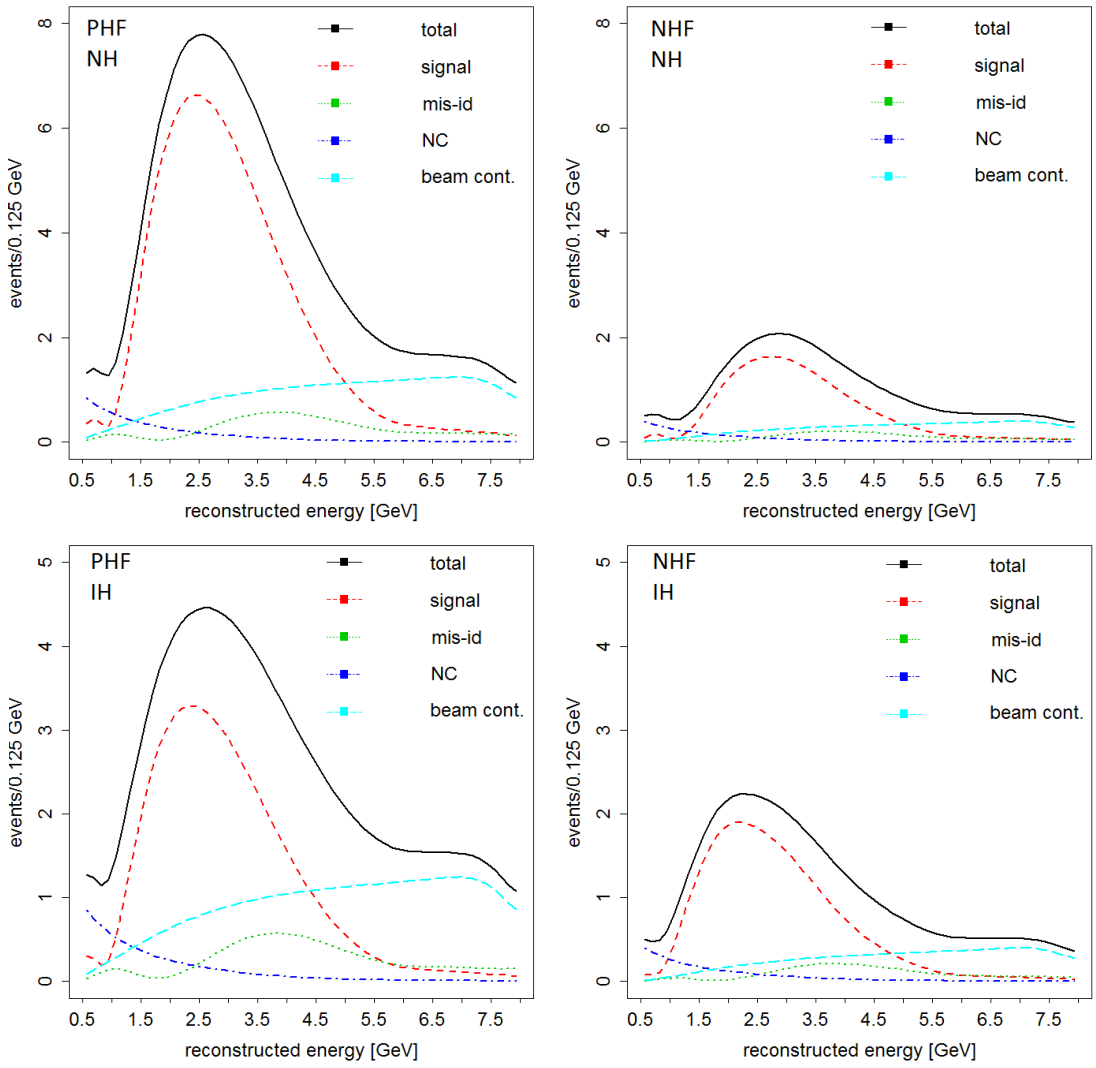

Figure 8.1. Expected event rate spectra of the signal $\nu_e CC$ and background contributions ($\nu_e CC$ beam contamination, misidentified muons $\nu_\mu CC$ and NC) for the appearance channel $\nu_\mu \rightarrow \nu_e$ at SUNLAB. The assumed exposure is Exposure$= 1 \times 10^{22}$p.o.t. $\times$ kt for each of the PHF (left panels) and NHF (right panels) beam modes. Standard values of the oscillation parameters, $\delta_{CP} = 0$ and the known mass hierarchy (NH - upper panels, IH - lower panels) are assumed.

be possible to discover if it is very small.

The sensitivity for such a discovery is evaluated by minimizing the χ^2 for a fit based on the predicted event rates for the assumed 'true' and 'test' values of δ_{CP} for the chosen oscillation channels [79]. The 'true' parameters are chosen by Nature, the 'test' refers to the δ_{CP} values at which the likelihood is calculated with respect to the 'true' value. For the accelerator long baseline experiments the ν_e

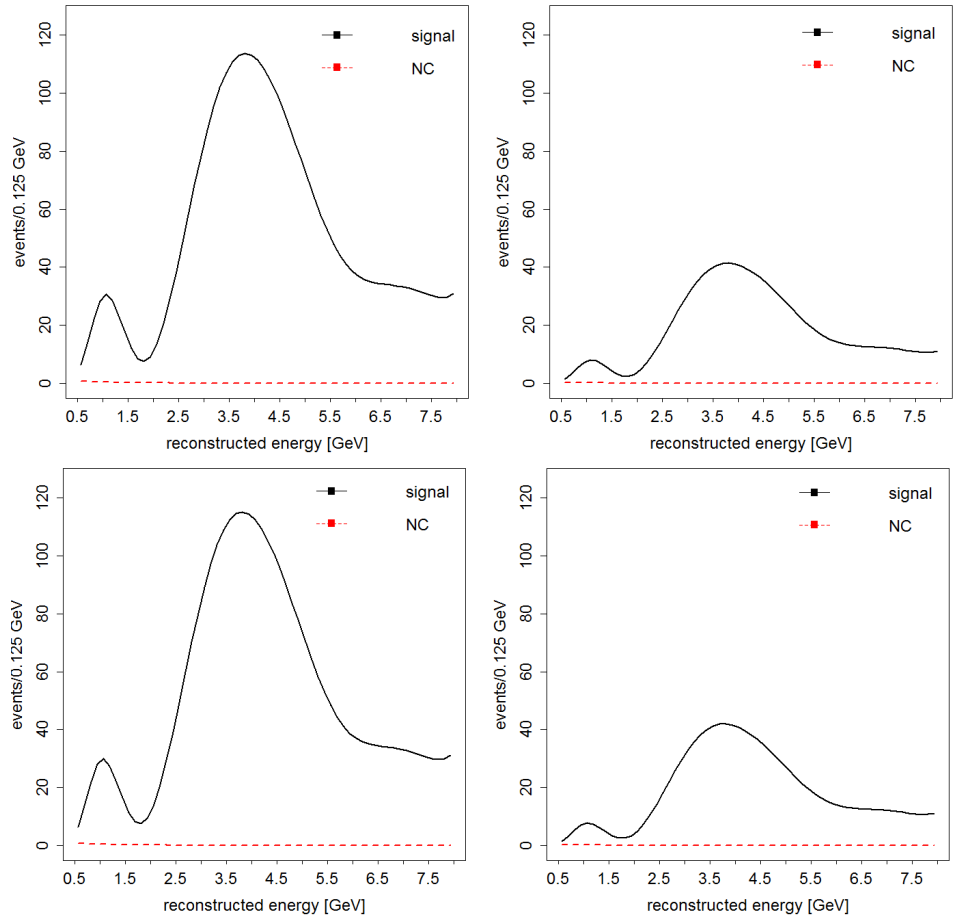

Figure 8.2. Expected event rate spectra of the signal $\nu_\mu CC$ and the background NC contributions for the disappearance channel $\nu_\mu \rightarrow \nu_\mu$ at SUNLAB. The assumed exposure is Exposure$= 1\times10^{22}$p.o.t. $\times$ kt for each of the PHF (left panels) and NHF (right panels) beam modes. Standard values of the oscillation parameters, $\delta_{CP} = 0$ and the known mass hierarchy (NH - upper panels, IH - lower panels) are assumed.

appearance and ν_μ disappearance channels are considered and χ^2 has the following form:

$$\chi^2 = \chi^2_{\nu_e app} + \chi^2_{\nu_\mu disapp} + \chi^2_{syst} \ , \tag{8.1}$$

where the $\chi^2_{\nu_e app}$ term corresponds to the ν_e appearance channel, the $\chi^2_{\nu_\mu disapp}$ contains information from the ν_μ disappearance channel, the χ^2_{syst} term contains 5% signal and background normalization errors.

In order to evaluate the hypothesis that $\delta_{CP} = 0$ *or* π, the $\Delta\chi^2$ was calculated in the following way:

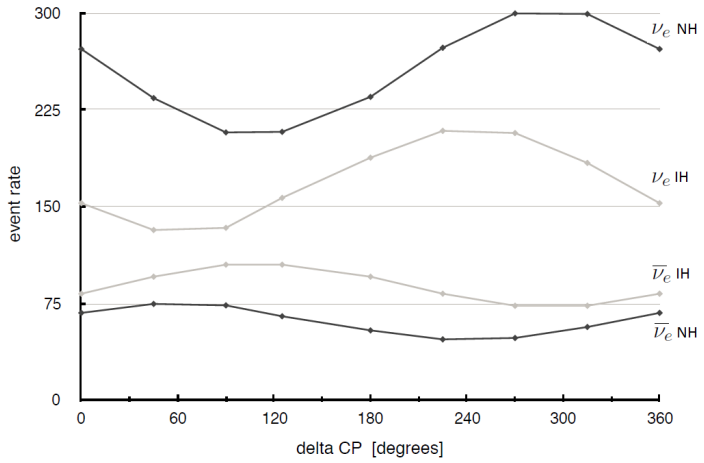

Figure 8.3. Expected total signal event rates ($\nu_e CC$) calculated for the $\nu_\mu \rightarrow \nu_e$ appearance channel as a function of the δ_{CP} parameter for both hierarchies and both neutrino and antineutrino modes. The assumed exposure is 1×10^{21} p.o.t. $\times$ kt for each of the beam modes. Detector effects are included according to Table 7.1

.

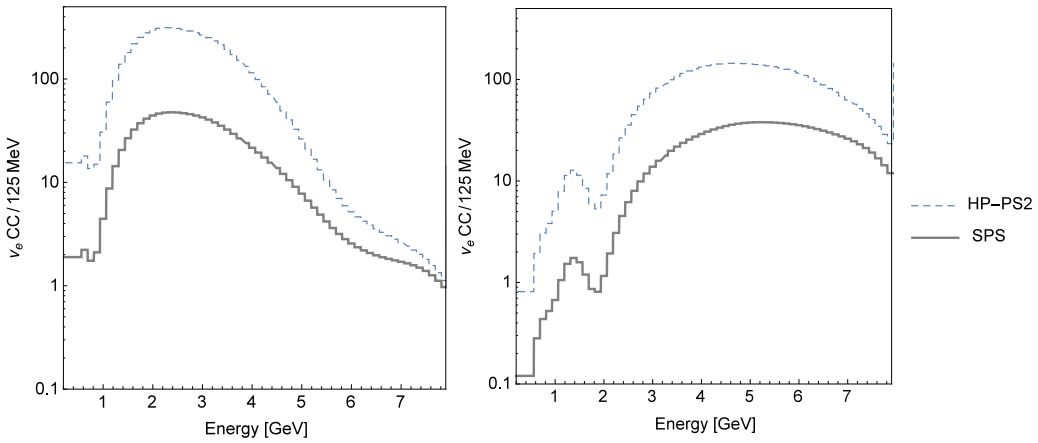

Figure 8.4. Expected signal event rate spectra for the $\nu_\mu \rightarrow \nu_e$ appearance at SUNLAB (left) and Pyhäsalmi site (right). The neutrino beams for two proton driver scenarios are assumed, the SPS with Exposure$= 5 \times 10^{22}$ p.o.t. $\times$ kt and the HP-PS2 with Exposure $= 15 \times 10^{23}$ p.o.t. $\times$ kt. No detector effects are included. Standard oscillation parameters and $\delta_{CP} = 0$ are assumed .

$$\Delta\chi^2 = \chi^2_{\delta_{CP}\, fix} - \chi^2_{\delta_{CP}\, vary}\ , \tag{8.2}$$

where the $\chi^2_{\delta_{CP}\, fix}$ corresponds to the minimized χ^2 value from Eq. (8.1) at a fixed δ_{CP} value, while for $\chi^2_{\delta_{CP}\, vary}$ δ_{CP} varies over the full range of values ($\delta \in -\pi, \pi$). Mass hierarchy is assumed to be known in the calculations, either

inverted or normal. The $\Delta\chi^2$ is calculated with marginalisation over all oscillation parameters except δ_{CP}, so the $\Delta\chi^2$ fit has one degree of freedom (1 dof). The CP violation hypothesis will be accepted at a given confidence level (CL) when the value of $\Delta\chi^2$ is below the chosen critical value. For example, for χ^2_{1dof} the $CL = 99.7\%$, equivalent to 3σ for the Gaussian distribution, corresponds to $\Delta\chi^2 = 9$, and $CL = 99.99\%$, equivalent to 5σ, corresponds to $\Delta\chi^2 = 25$.

The sensitivity plots for the CP violation discovery at SUNLAB, calculated using the GLoBES package, are presented in Figures 8.5 - 8.7. The $\Delta\chi^2$ value calculated for the true $\delta_{CP} \in (-\pi, \pi)$ value and assuming the standard oscillation parameters is shown in each plot as a function of the true δ_{CP}. The left panels of the figure are for NH while the right panels are for IH. Horizontal lines depict the $\Delta\chi^2$ critical values for 1σ, 2σ, 3σ of the CP violation discovery potential.

Two neutrino and antineutrino beam sharing scenarios: 50% PHF + 50% NHF and 40% PHF + 60% NHF were tested; the latter to partially compensate for a smaller cross section for antineutrino interactions. As presented in Figure 8.5, the 50% PHF + 50% NHF scenario gives a better sensitivity for the CPV determination, so only this scenario was used in other checks.

Both the ν_e appearance and ν_μ disappearance channels are included in the analysis. Even though the ν_μ disappearance channel does not have a direct impact on the δ_{CP} measurement (Section 1.3.3), it helps to improve the precision of the atmospheric parameters. The small, but visible positive effect on the sensitivity for the CPV determination is presented in Figure 8.6.

Figure 8.7 depicts the CP-violation discovery potential for the SUNLAB experiment in the initial and final phases. For the initial phase of the experiment, the CP-violation discovery potential at 2σ level covers 51% of the δ_{CP} parameter range and reaches 3σ level in the case of NH for CPV close to maximal violation. The final phase of the experiment can give the coverage of δ_{CP} parameters of 58% for NH and 60% for IH at 3σ level and reaches 5σ in both cases for 20% of δ_{CP} range for regions of δ_{CP} close to the maximal violation.

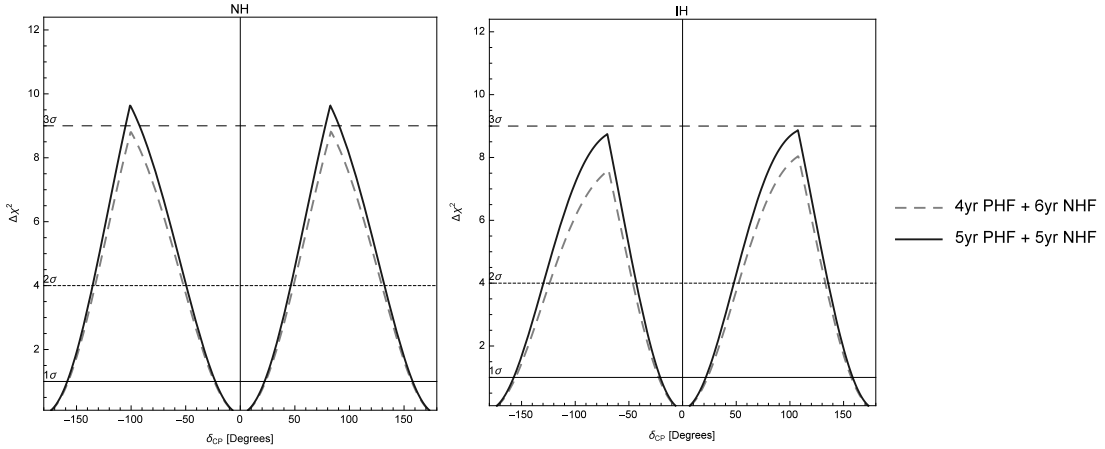

Figure 8.5. The $\Delta\chi^2$ contours representing the sensitivity for the CP-violation discovery potential for SUNLAB as a function of the true value of δ_{CP}. The initial phase of the experiment, standard oscillation parameters and NH (left panel) or IH (right panel) mass hierarchy are assumed. Two scenarios of beam time sharing are presented: 50% PHF + 50% NHF and 40% PHF + 60% NHF.

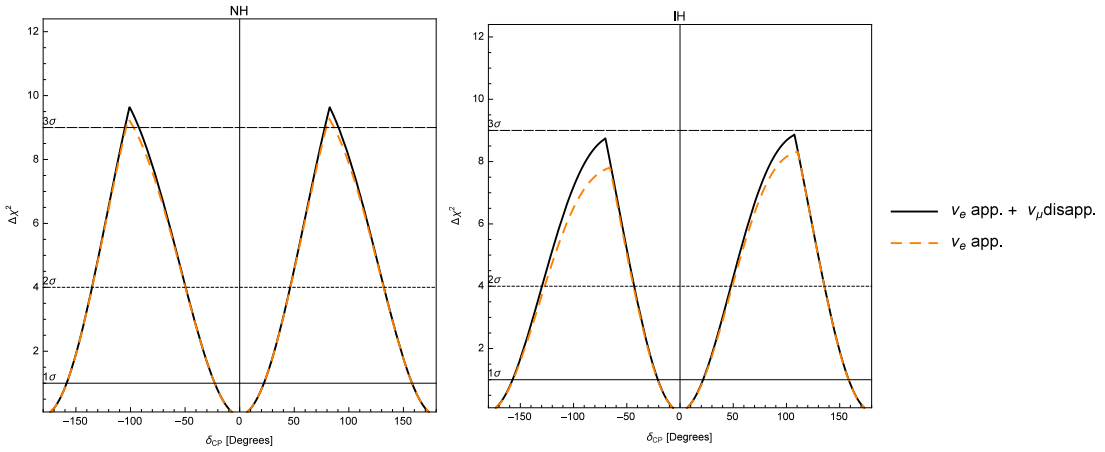

Figure 8.6. The $\Delta\chi^2$ contours as a function of the true value of δ_{CP}, representing the sensitivity for the CP-violation discovery potential for SUNLAB including the information from the ν_μ disappearance channel (solid line) and without this information (dashed line). The initial phase of the experiment, standard oscillation parameters and NH (left panel) or IH (right panel) mass hierarchy are assumed.

8.3.1. CP-violation discovery potential for LBNE and LAGUNA-LBNO

The CP violation discovery potential for LBNE and LAGUNA-LBNO at the Pyhäsalmi site is presented in this section for comparison with the results

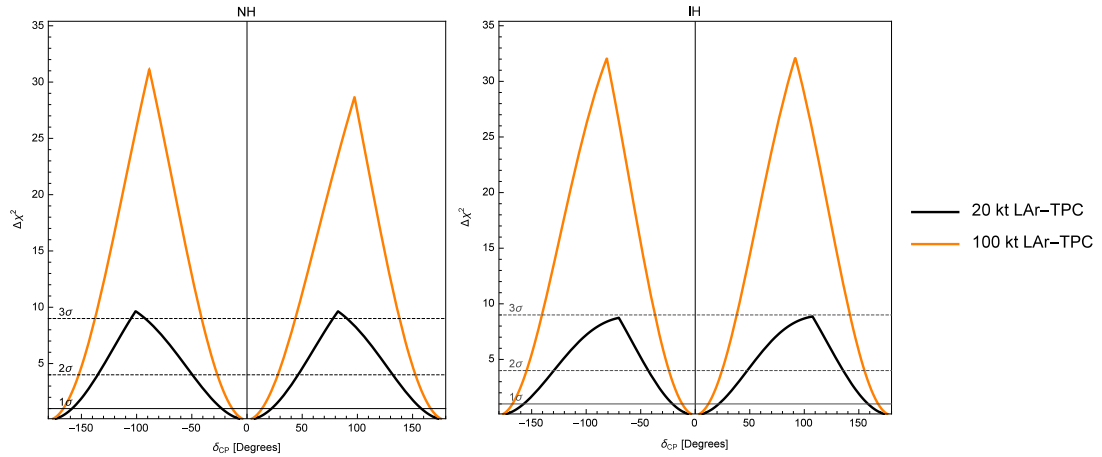

Figure 8.7. The $\Delta\chi^2$ contours representing the sensitivity for the CP-violation discovery for SUNLAB as a function of a true value of δ_{CP} assuming NH (left panel) and IH (right panel) as known; calculated for the experiment initial phase $\text{Exposure}_{20kt} = 2 \times 10^{22}$ and the experiment final phase $\text{Exposure}_{100kt} = 10 \times 10^{22}$.

obtained for SUNLAB.

For LBNF-DUNE a very detailed analysis concerning the sensitivity of the future experiment for the δ_{CP} measurement is currently being performed by the DUNE collaboration. However, the physics potential studies for LBNE, which was the initial name of the Fermilab based long baseline neutrino oscillation experiment, were available earlier and could be used for comparison [56]. The assumption concerning the first phase of the LBNE experiment was to use a 10 kt LAr-TPC detector in a six-year run with 1.2 MW beam power, corresponding to Exposure$= 9 \times 10^{22}$ p.o.t. $\times$ kt. The χ^2 contours illustrating the CP-violation discovery potential for this experiment and for the combination of LBNE, T2K and NOvA are presented in Figure 8.8. One can see that in combination with T2K and NOvA, LBNE would determine the leptonic CP violation with a precision of 3σ or greater for 40% of δ_{CP} values and for the maximal CP violation it would reach the statistical significance of about 5 standard deviations.

The initial phase of the LAGUNA-LBNO experiment was assumed for 12 years of running with a 20 kton LAr-TPC detector using a 400 GeV SPS beam. For the final phase a 70 kton detector mass was assumed and 12 years of running. The LAGUNA-LBNO also considered as an interesting option of the experiment with two independent neutrino beams, one from CERN and the other from the Protvino accelerator complex in Russia. Figure 8.9 presents the sensitivity contours for the

determination of the CP violation from the LAGUNA-LBNO study [65]. The initial phase of the LAGUNA-LBNO with one beam from SPS only corresponds to Exposure $= 3 \times 10^{22}$ p.o.t. $\times$ kt and would determine the CP violation at the 3σ level for about 38% of δ_{CP} values. The Protvino beam would give an additional exposure of 8×10^{22} p.o.t. $\times$ kt; therefore, the sensitivity for the CPV determination of such a double beam setup is higher and reaches the 5σ level for 27% of δ_{CP} values.

An additional interesting conclusion from the LAGUNA-LBNO study is discussed in [103]. Assuming conservative expectations on the systematic errors and 10 years of running with a 70 kton detector exposed to the neutrino beam based on CERN SPS, a significance for CP violation above the 3σ level will be reached for 40% of the δ_{CP} values under the assumption that $sin^2 2\theta_{13}$ will be known with a precision of 2.5% from reactor experiments.

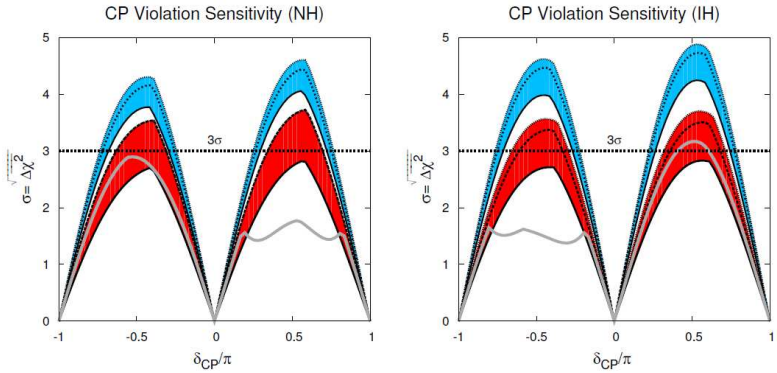

Figure 8.8. Sensitivity contours for the determination of the CP violation from [56]. The red band shows the sensitivity that is achieved by a typical experiment with the LBNE 10-kt detector alone, where the width of the band shows the range of sensitivities obtained by varying the beam design and the signal and background uncertainties. The cyan band shows the sensitivity obtained by combining the 10-kt LBNE with T2K and NOvA, and the gray curves are the expected sensitivities for the combination of NOvA and T2K. Exposure is 9×10^{22} p.o.t. $\times$ kt

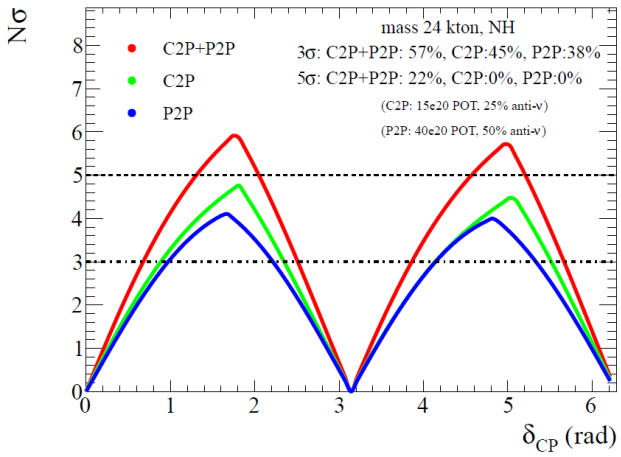

Figure 8.9. Sensitivity contours, expressed in σ's for the determination of the CP violation for LAGUNA-LBNO from [65]. Plot is obtained assuming a 20 kton far detector and Normal Hierarchy. Exposure is 3×10^{22}p.o.t. kt for the SPS based neutrino beam and 8×10^{22} p.o.t. $\times$ kt for the Protvino based neutrino beam

Chapter 9

Effect of the natural radioactivity and cosmic muon background

The knowledge of all sources of background is necessary for every experiment. Studies of rare phenomena, such as interactions of neutrinos from various sources and searches for proton decays or dark matter particles, are usually performed in underground laboratories and background sources specific for this environment have to be taken into account. These are the cosmic radiation background, decreasing with an increasing depth, and the background due to natural radioactivity in the form of photons and neutrons emitted by the surrounding rock and the detector construction material.

The large LAr TPC at SUNLAB would carry out a vast research programme, but its part concerning the accelerator long baseline experiment for the determination of the CP violation is very specific from the point of view of the above two kinds of background. The correlation between the neutrino events registered in the far detector and the precise time of the neutrino beam pulse and direction reduce the cosmic radiation background almost completely. In turn, the energy range of accelerator neutrinos at SUNLAB is much higher than the energies of neutrons and photons from radioactive nuclides. Therefore, these two sources of background were not considered as additional contributions to the systematic error for the determination of the CP violation.

However, for completeness and to supplement the information given in Chapter 4, some issues concerning these two sources of background are discussed in this chapter.

9.1. Natural radioactivity

The natural radioactivity measurements performed in the Polkowice- Sieroszowice mine and presented in Section 4.3 show that this kind of background is extremely low at SUNLAB. In particular, thanks to the alpha spectroscopy mea-

surements of salt and anhydrite rock samples, using tables from [104] it was possible to estimate the concentration of Uranium ~ 3 *ppb* and Thorium ~ 2 *ppb* in the salt rock, as well as the concentration of Uranium ~ 60 *ppb* and Thorium ~ 400 *ppb* in the anhydrite rock. Uranium and Thorium traces are the source of low energy neutrons which can mimic low energy neutrinos or candidates for dark matter particles.

Based on the simulation studies performed for the Boulby underground laboratory [105], whose salt rock is characterised by a similar concentration of radioactive nuclides as the anhydrite in the Polkowice-Sieroszowice mine, the approximation of the total neutron production rate in the anhydrite is $\sim 1{\times}10^{-7}\ cm^{-3}s^{-1}$. The energies of (α, n) neutrons do not exceed 6 MeV. The simulation results from the neutron production energy spectrum from U and Th traces in the salt rock at Boulby are presented in Figure 9.1 coming from [105].

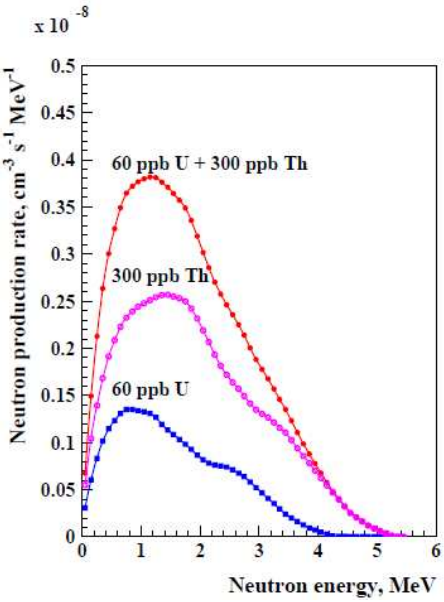

Figure 9.1. Neutron energy spectrum from U and Th traces in rock at Boulby as calculated with modified SOURCES program [105]. Contributions from 60 ppb U (lower curve), 300 ppb Th (middle curve) and the sum of the two (upper curve) are shown.

It is clear that neutrons at such a low intensity and energies do not influence the long baseline experiment at SUNLAB.

9.2. Cosmic muon background

The muon component of cosmic rays is very penetrable. The GeV-range muons lose roughly 2 MeV/(g/cm^3) on ionisation when traversing the rock, i.e. a 100 GeV muon can penetrate 50000 g/cm^3 or 0.5 km water equivalent. As shown in Section 4.4, the expected muon flux in SUNLAB at a depth of 950 m is $I_\mu = 1.23 \times 10^{-7}\text{cm}^{-2}\text{s}^{-1}$ and the muon average energy is $\langle E \rangle = 247.30$ GeV.

Low energy muons passing through matter lose their energy almost entirely through ionisation of the medium, but above the critical energy, which for muons in liquid Argon is $E_c = 483$ GeV, radiative processes become dominant in their energy loss. The analysis of radiative processes of high energy muons passing through the LAr-TPC detector [77] shows that photons, electrons and positrons are usually produced at very small angles with respect to muon tracks (90% at an angle smaller than 10° angle) and have low energies. It happens rarely that the irradiated energy is very high, even a few hundreds of GeV, but also in such cases the electromagnetic cascade is associated with a muon track and it can be easily identified as a background event.

The muons passing through rock and the detector material can produce fast neutrons, e.g. in the capture of slow μ^- by nuclei. This can be a potentially serious problem in underground experiments, because such fast neutrons can enter the fiducial volume of the detector and interact with Argon nuclei without being correlated with the parent muon. Fast neutrons can also produce π^0s which are an important background for $\nu_e CC$ interactions. However, the muon-induced processes are strongly depth-dependent. In addition, the study of the muon induced background for underground laboratories [106] gives the value of the mean energy of the muon-induced neutrons for a depth of 2100 m.w.e., similar to 950 m in the Polkowice-Sieroszowice mine, as $\langle E_n \rangle = 80$ MeV. It means that in practice this kind of background does not influence the long baseline experiment at SUNLAB.

Summary

The study presented in this thesis concerns the Sieroszowice Underground Laboratory SUNLAB hosting a large LAr-TPC far detector of a long baseline neutrino oscillation experiment with a neutrino beam from CERN. The proposed SUNLAB location in the Polkowice-Sieroszowice mine in the Lower Silesia province in Poland is characterized by great underground infrastructure, good geological conditions and an extremely low level of natural radioactivity.

The determination of the SUNLAB capabilities to discover the CP violation in the neutrino sector was the main goal of this study. In order to achieve this, a neutrino beam was simulated assuming the upgraded SPS accelerator at CERN as the source of the primary proton beam. The beam line setup was optimized to get the most intense neutrino flux at the energy of 1.92 GeV, corresponding to the first oscillation maximum for the ν_e appearance oscillation channel at the CERN-SUNLAB distance of 950 km. Additionally, the parametrisation of the LAr-TPC detector response was developed. In particular, the discussion of the signal and background processes for the ν_e appearance was based on the experience gained in the ICARUS experiment.

Based on these inputs the study of the sensitivity for determining the CP-violating phase was performed for several operation scenarios of the long baseline experiment at SUNLAB, such as time sharing between the neutrino and antineutrino beam, treatment of ν_μ disappearance channel and two detector mass scenarios. The conclusions are that for ten years of running with the initial detector of 20 kton mass, the discovery of the CP violation at about 3 σ level is possible if the CP violation is close to maximal. For the final phase of the experiment with a 100 kton detector and ten years of data taking, the 3 σ sensitivity is reached for about 60% of δ_{CP} values and the 5σ sensitivity is reached for regions of δ_{CP} close to the maximal violation.

The results demonstrate good SUNLAB capabilities to discover the CP violation for neutrinos, but some limitations have to be mentioned. The energy of the 400 GeV proton beam from SPS is too high to produce an intense and pure neutrino beam optimized for the energy of about 1.9 GeV. In turn, it practically excludes the use of the second oscillation maximum and the two-stage optimisation of the neutrino beam, with the first stage oriented towards the determination of the mass hierarchy and the second stage for the determination of the CP violation. This is why the study was performed assuming that the hierarchy is known, i.e. that it will be measured by other experiments. Finally, the systematic effects were included only at the level of 5% uncertainty of the signal and background normalisations. A more detailed analysis will be needed if there is a chance for approval of the long baseline experiment with a far detector at SUNLAB.

The comparison of the results obtained for SUNLAB with those from other long baseline projects with liquid Argon far detectors is not simple, because each study is based on its own assumptions and software. However, one observation is valid for every project - the total exposure should be as big as possible, i.e. one should maximise the neutrino beam intensity, detector mass and running time. The maximum power of 0.75 MW and the energy of 400 GeV of the SPS proton beam impose serious limitations on the neutrino beam intensities for the European sites. However, the neutrino energy of 4.67 GeV, corresponding to the first oscillation maximum at Pyhäsalmi, makes it easier to obtain a relatively high intensity neutrino beam as compared to the neutrino energy of 1.9 GeV for SUNLAB. This is why also the second oscillation maximum can be used more effectively at Pyhäsalmi than at SUNLAB, and one can apply the two-stage approach to the beam optimisation, starting with the determination of the neutrino mass hierarchy and then the CP violation. If successfully constructed, the neutrino beam for LBNF-DUNE, based initially on the 1.2 MW and finally on 2.4 MW proton beam power, will be the first neutrino superbeam ever constructed. This will be a great advantage for the neutrino oscillation studies at LBNF-DUNE.

Acknowledments

I would like to express my sincere gratitude to my supervisor
Prof. Agnieszka Zalewska for her continuous support, patience and immense knowledge.

I would like to thank the rest of our neutrino group - my friends: Monika, Ania, Dorota, Tomasz, Krzysztof, Marcela and Paweł for discussions, encouragement and great atmosphere in the office.

I must also acknowledge the ICARUS collaboration: the experiences gained during my stays at LNGS, work with the detector itself and on the analysis software are priceless. My sincere thanks also goes to Dr Andrea Longhin, who gave me access to his neutrino beam simulation code together with detailed patient instructions and kind conversations.

This research would not have been possible without the financial support of Polish National Science Centre grant *Preludium* UMO-2011/03/N/ST2/01971.

Bibliography

[1] M. Haranczyk, Neutrino 2014 2-7.06.2014, Boston USA; http://neutrino2014.bu.edu/files/2013/08/Neutrino-2014-Poster-contributions-book.pdf.

[2] M. Haranczyk, NNN15 conference; 28-31.10.2015 Stony Brook USA; https://indico.bnl.gov/contributionDisplay.py?contribId=114sessionId=6confId=1282.

[3] M. Haranczyk, J.Phys. Conference Series 689 (2016) 012019, *Simulations of the Long Baseline Neutrino Experiment for the Sieroszowice Underground Laboratory (SUNLAB).*

[4] S. Schael et al., (ALEPH, DELPHI, L3, OPAL, SLD, LEP Electroweak Working Group, SLD Electroweak Group, SLD Heavy Flavour Group), Phys.Rept. 427 (2006) 257.

[5] K. Olive et al., (Particle Data Group), Chin. Phys. C 38 (2014) 090001.

[6] S. Mertens, (KATRIN collaboration), Physics Procedia 61 (2015) 267 , 13th TAUP conference.

[7] P. Ade et al., (PLANCK collaboration), Astron. Astrophys. 571 (2014) A16.

[8] C. Spiering, Eur. Phys. J. H 37 (2012) 515.

[9] J.N. Bahcall and M. Pinsonneault, Phys.Rev.Lett. 92 (2004) 121301.

[10] J.N. Bahcall, A.M. Serenelli and S. Basu, Astrophys. J. Lett. 621 (2005) L85.

[11] V. Castellani et al., Phys.Rept. 281 (1997) 309.

[12] F. Reines and C. Cowan, Nature 178 (1956) 446.

[13] B. Pontecorvo, Sov. Phys. JETP 6 (1957) 429.

[14] Z. Maki, M. Nakagawa and S. Sakata, Prog. Theor. Phys. 28 (1962) 870.

[15] L. Wolfenstein, Phys. Rev. D 17 (1978) 2369.

[16] R. Davis Jr, D.S. Harmer and K.C. Hoffman, Phys. Rev. Lett. 20 (1968) 1205.

[17] J.N. Bahcall and R. Davis Jr, Science 191 (1976) 264.

[18] P. Anselmann et al., (GALEX collaboration), Physics Letters B 285 (1992) 376.

[19] J. Abdurashitov et al., (SAGE collaboration), Physics Letters B 328 (1994) 234.

[20] K.S. Hirata et al., (Kamiokande collaboration), Phys. Rev. Lett. 63 (1989) 16.

[21] Q.R. Ahmad et al., (SNO collaboration), Phys. Rev. Lett. 89 (2002) 011301.

[22] K. Eguchi et al., (KamLAND collaboration), Phys. Rev. Lett. 90 (2003) 021802.

[23] T. Araki et al., (KamLAND collaboration), Phys. Rev. Lett. 94 (2005) 081801.

[24] S.P. Mikheev and A.Y. Smirnov, Sov. J. Nucl. Phys. 42 (1985) 913.

[25] G. Alimonti et al., (Borexino collaboration), Nucl. Instrum. Meth. A600 (2009) 568.
[26] G. Bellini et al., (Borexino collaboration), Phys. Rev. Lett. 107 (2011) 141302.
[27] G. Bellini et al., (Borexino collaboration), Nature 512 (2014) 383.
[28] O. Smirnov et al., (Borexino collaboration), Phys. Part. Nucl. 46 (2015) 166.
[29] D. Casper et al., Phys. Rev. Lett. 66 (1991) 2561.
[30] K. Hirata et al., Phys. Lett. B 280 (1992) 146.
[31] Y. Fukuda et al., (SuperKamiokande collaboration), Phys. Rev. Lett. 81 (1998) 1562.
[32] Y. Ashie et al., (Super-Kamiokande collaboration), Phys. Rev. D 71 (2005) 112005.
[33] M.H. Ahn et al., (K2K collaboration), Phys. Rev. D74 (2006) 072003.
[34] P. Adamson et al., (MINOS collaboration), Phys.Rev.Lett. 110 (2013) 171801.
[35] K. Elsener et al., The CERN neutrino beam to Gran Sasso (NGS). Conceptual technical design, http://proj-cngs.web.cern.ch/proj-cngs/, 1998.
[36] N. Agafonova et al., (OPERA collaboration), Phys. Lett. B 691 (2010) 138.
[37] C. Rubbia, Nucl. Phys. B Proceedings Supplements 48 (1996) 172.
[38] C. Rubbia, M. Haranczyk and e. al., JINST 6 (2011) P07011.
[39] M. Antonello et al., (ICARUS collaboration), Eur. Phys. J. C 73 (2013).
[40] K. Abe et al., (T2K collaboration), Phys. Rev. Lett. 107 (2011) 041801.
[41] K. Abe et al., (T2K collaboration), Phys.Rev.Lett. 112 (2014) 061802.
[42] Y. Abe et al., (Double CHOOZ collaboration), Phys. Rev. Lett. 108 (2012) 131801.
[43] F.P. An et al., Phys. Rev. Lett. 108 (2012) 171803.
[44] F.P. An et al., (Daya Bay collaboration), Phys. Rev. Lett. 115 (2015) 111802.
[45] S.B. Kim et al., (RENO collaboration), Phys. Rev. Lett. 108 (2012) 191802.
[46] M.C. Gonzalez-Garcia, M. Maltoni and T. Schwetz, J. High Energy Phys. 2014 (2014) 11.
[47] S. Adrian-Martinez et al., (ORCA-KM3NeT collaboration), preprint arXiv:1601.07459 (2016), *Letter of Intent for KM3NeT2.* .
[48] M. Aartsen et al., (IceCube-PINGU Collaboration), preprint arXiv: 1401.2046 (2014), *Letter of intent: The precision IceCube next generation upgrade (PINGU).*
[49] S.K. Agarwalla et al., Nucl. Phys. B 798 (2008) 124.
[50] K. Abe et al., (HyperKamiokande collaboration), preprint arXiv:1109.3262 (2011), *Letter of Intent: The Hyper-Kamiokande Experiment*.
[51] M. Blennow et al., J. High Energy Phys. 1403 (2014) 028.
[52] M. He et al., (JUNO collaboration), Nucl. Part. Phys. Proceedings 265 (2015) 111.
[53] S.B. Kim, (RENO collaboration), preprint arXiv:1412.2199 (2014), *New results from RENO and prospects with RENO-50*.
[54] A. Rubbia, Acta Phys. Pol. B 41 (2010) 1727.
[55] J. Borne et al., Acta Phys. Pol. B 41 (2010) 1733.

[56] C. Adams et al., FERMILAB-PUBL-14-022, preprint arXiv:1307.7335 (2013), *The long-baseline neutrino experiment: exploring fundamental symmetries of the universe*.

[57] M. Wurm et al., Astropart. Phys. 35 (2012) 685.

[58] A. Ereditato and A. Rubbia, Nucl. Phys. B - Proceedings Supplements 139 (2005) 301 .

[59] M. Haranczyk et al., Acta Phys. Pol. B 41 (2010).

[60] A. Ferrari, A. Guglielmi and P. Sala, Nucl. Phys. B - Proceedings Supplements 145 (2005) 93 , Neutrino Oscillation Workshop 2004.

[61] A. Longhin, preprint arXiv:1206.4294 (2012), *Optimisation of neutrino beams for underground sites in Europe*.

[62] J. Norem et al., *Muon Collider Task Force Report*, https://mctf.fnal.gov/annual-reports/mctf-report-207.doc.

[63] P. Zucchelli, Phys. Lett. B 532 (2002) 166.

[64] A. Stahl et al., CERN-SPSC-2012-021, SPSC-EOI-007 (2012), *Expression of Interest for a very long baseline neutrino oscillation experiment (LBNO)*.

[65] S.K. Agarwalla et al., preprint arXiv:1412.0804 (2014), *The LBNO long baseline oscillation sensitivities with two conventional neutrino beams at diferent baselines*.

[66] CERN Council, The European Strategy for Particle Physics, Update 2013 s/106 (May 7 2013), 2013.

[67] M. Antonello et al., (LAr1-ND, ICARUS-WA104, MicroBooNE), preprint arXiv:1503.01520 (2015), *A Proposal for a Three Detector Short-Baseline Neutrino Oscillation Program in the Fermilab Booster Neutrino Beam*.

[68] R. Acciarri et al., (LBNF-DUNE collaboration), preprint arXiv:1601.02984 (2016), *Long-Baseline Neutrino Facility (LBNF) and Deep Underground Neutrino Experiment (DUNE) Conceptual Design Report*.

[69] A. Zalewska et al., Acta Phys. Pol. B 41 (2010) 1803.

[70] W. Pytel et al., Interim Report for SUNLAB (LAGUNA Design Study), http://laguna.ethz.ch:8080/Plone/deliverables/laguna-legacy-deliverables.

[71] J. Slizowski et al., Advances in High Energy Physics 2013 (2013).

[72] A. Rubbia et al., LAGUNA (Grant Agreement No. 212343) - Deliverables, http://laguna.ethz.ch:8080/Plone/deliverables/laguna-legacy-deliverables.

[73] J. Kisiel et al., Acta Phys. Pol. B 41 (2010) 1803.

[74] K. Polaczek-Grelik, M. Haranczyk and e. al., JRNC (2015) 1.

[75] D. Malczewski, J. Kisiel and J. Dorda, JRNC 298 (2013) 1483.

[76] V. Kudryavtsev, Comput. Phys. Commun. 180 (2009) 339.

[77] M. Haranczyk, *Procesy tla dla pomiarow oddzialywan neutrin w podziemnym laboratorium w Sieroszowicach*, www.neutrino.ifj.edu.pl, Master Thesis, Jagiellonian Univ. 2009.

[78] Cracow Cloud One CC1, http://cc1.ifj.edu.pl/pl/.

[79] P. Huber, M. Lindner and W. Winter, Comput. Phys. Commun. 167 (2005) 195, http://www.mpi-hd.mpg.de/personalhomes/globes.

[80] S. Agostinelli et al., Nucl. Instr. Meth. A 506 (2003) 250 , http://geant4.cern.ch.

[81] A. Longhin, private communication.

[82] https://root.cern.ch.

[83] R. Core Team, *R: A Language and Environment for Statistical Computing*, http://www.R-project.org/, 2014.

[84] WolframResearch, Mathematica, Version 10.0, 2014, http://www.mathematica.pl/.

[85] CERN PS2 working group, http://paf-ps2.web.cern.ch/paf-ps2/.

[86] LIU - LHC Injectors Upgrade Project, https://espace.cern.ch/liu-project/default.aspx.

[87] A. Rubbia, preprint arXiv:1003.1921 (2010), *A CERN-based high-intensity high-energy proton source for long baseline neutrino oscillation experiments with next-generation large underground detectors for proton decay searches and neutrino physics and astrophysics*.

[88] E. Shaposhnikova, LAGUNA - LBNO General meeting at CERN 2012 .

[89] G. Bock et al., (NuMI Beam), Technical Design Handbook, http://www-numi.fnal.gov/numwork/tdh/tdh-index.html, 2004.

[90] P. Adamson et al., Nucl. Instr. Meth. A 806 (2016) 279.

[91] A. Cazes, *Study of the CNGS beam and muon identification with the OPERA experiment.*, PhD Thesis, Paris Univ., VI-VII, 2004.

[92] S. Di Luise, A. Longhin and A. Rubbia, PoS ICHEP2012 (2013) 386.

[93] S. Agarwalla, T. Li and A. Rubbia, J. High Energy Phys. 2012 (2012) 1.

[94] T. Akiri et al., (LBNE collaboration), preprint arXiv:1110.6249 (2011), *The 2010 interim report of the long-baseline neutrino experiment collaboration physics working groups*.

[95] D. Dequal et al., (ICARUS collaboration), *Final update of 2010 - 2012 CNGS data processing*, ICARUS-TM 15-0X June 19, 2015.

[96] M. Antonello, M. Haranczyk and e. al., (ICARUS collaboration), JINST 9 (2014) P08003.

[97] L. Whitehead, private communication.

[98] M. Ghosh et al., J. High Energy Phys. 2014 (2014) 1.

[99] A. Menegoli, (ICARUS collaboration), *ICARUS T600: status and perspectives for sterile neutrino searches at FNAL*, NNN15 conference, 2015.

[100] A. Rubbia et al., (ICANOE collaboration), *A proposal for a CERN-GS long baseline and atmospheric neutrino oscillation experiment*, INFN/AE-99-17, CERN/SPSC 99-25, SPSC, 1999.

[101] M. Ghosh, S. Goswami and S.K. Raut, Eur. Phys. J. C 76 (2016) 1.

[102] A.M. Dziewonski and L. Anderson, Phys. Earth Planet. Inter. 25 (1981) 297 .

[103] L. Agostino et al., (Laguna-Lbno Consortium), 566 (2014) 012002.

[104] G. Heusser, Annual Review of Nuclear and Particle Science 45 (1995) 543.
[105] E. Tziaferi et al., Astropart. Phys. 27 (2007) 326 .
[106] D.M. Mei and A. Hime, Phys. Rev. D 73 (2006) 053004.